IACMI/R004-2019/5.02

# THERMOPLASTIC COMPOSITE COMPRESSED GAS STORAGE (CGS)


Author: Lee Silverman
Date: 10/2/2019

**Final Technical Report**
**004-2019-5.02**

**Approved for Public Release.**
**Distribution is Unlimited.**

The Institute for iacmi Advanced Composites Manufacturing Innovation
THE COMPOSITES INSTITUTE
U.S. DEPARTMENT OF ENERGY

Materials Science and Technology
Division Advanced Manufacturing
Office

# Thermoplastic Composite Compressed Gas Storage (CGS) Tanks

Principle Investigator: Lee Silverman

Organization: E.I. DuPont de Nemours and Company, Inc.

Address: 200 Powder Mill Road, Building 323/306B

Phone: 302-695-4350

Email: lee.a.silverman@dupont.com

Co-authors:
Kaushik Mallick, Steelhead Composites, Golden, Colorado, 80401
Jared Stonecash, University of Dayton Research Institute, Dayton, Ohio, 45469
Leonard Poveromo, Composites Prototyping Center, Plainview, New York, 11803

Date
Published:
October 2,
2019

Prepared by
Institute for Advanced Composites
Manufacturing Innovation
Knoxville, Tennessee 37932
managed by
Collaborative Composite Solutions, Inc.
for the
US DEPARTMENT OF ENERGY
under contract DE- EE0006926

# 1 TABLES

## 1.1 Table of Contents


1 TABLES ..... iv
1.1 Table of Contents ..... iv
1.2 List of Acronyms ..... v
1.3 List of Figures ..... v
1.4 List of Tables ..... vii
1.5 List of Appendices ..... viii
1.6 Acknowledgements ..... ix
2. EXECUTIVE SUMMARY ..... x
3. INTRODUCTION ..... 11
4. BACKGROUND ..... 11
4.1 Technical Approach and Rationale ..... 15
4.2 Pressure Vessel Type Selection ..... 16
4.3 Selection of Vessel Fabrication Method ..... 17
4.4 Polymer Matrix Development ..... 19
4.5 Continuous Fiber Reinforced Polymer UD Tape Production ..... 19
4.6 UD Tape Characterization ..... 20
4.7 AFP-Produced Ring and Cylinder Production ..... 21
4.8 Design and fabrication of a Type III fiber placed composite pressure vessel ..... 23
4.9 Pressure testing of the fiber placed composite pressure vessel ..... 31
4.10 Technoeconomic Analysis of Thermoplastic CPV GCS Vessels ..... 31
5. RESULTS AND DISCUSSION ..... 32
5.1 Carbon Fiber ..... 32
5.2 Polymer Characterization ..... 32
5.3 Unidirectional Tape Fabrication ..... 35
5.4 Unidirectional Tape Characterization ..... 36
5.5 AFP Condition Optimization ..... 51
4.8 AFP Vessel Fabrication – Fluted Envelope ..... 60
5.6 CPV Vessel Testing ..... 62
4.10 Technoeconomic Analysis ..... 69
4.11 Market Assessment ..... 74
6. BENEFITS ASSESSMENT ..... 74
7. COMMERCIALIZATION ..... 74

8. ACCOMPLISHMENTS ..... 75
9. CONCLUSIONS ..... 75
10. RECOMMENDATIONS ..... 76
11. REFERENCES ..... 77
APPENDICES ..... 78
Appendix 1. Testing and Evaluation ..... 78

## 1.2 List of Acronyms

| | |
|---|---|
| ADC | Automated Dynamics Corporation |
| AFP | Automated Fiber Placement |
| CGS | Compressed Gas Storage |
| CNG | Compressed Natural Gas |
| COM | Cost of Manufacture |
| CPC | Composites Prototyping Center |
| CPV | Composite Pressure Vessel |
| DSC | Differential Scanning Calorimeter |
| FEA | Finite Element Analysis |
| IACMI | Institute for Advanced Composite Manufacturing Innovation |
| PA | Polyamide |
| ROI | Return on Investment |
| SEC | Size Exclusion Chromatography |
| SME | Subject Matter Expert |
| TPU | Thermoplastic Polyurethane |
| UD | Unidirectional |
| UDRI | University of Dayton Research Institute |

## 1.3 List of Figures

Figure 1. Processing schemes for a) thermoset- and b) thermoplastic-based CPVs. ..... 12
Figure 2. Schematic of Automated Fiber Placement process. ..... 13
Figure 3. Primary roles and responsibilities for each team member organization. ..... 16
Figure 4. The Automated Fiber Placement (AFP) robot that was operated at CPC, a) the entire robotic system, and b) a close-up of the thermoplastic tape application head. ..... 18
Figure 5. Example of directly-fabricated rings as made with the AFP. ..... 22
Figure 6. Picture of the split-ring tester showing a) the test ring mounted in the fixture along with the placement of strain gauges, b) a close-up of an applied strain gauge, and c) the sample after failure. ..... 23
Figure 7. Assortment of spinformed liners for Type III vessels manufactured by Steelhead Composites. ..... 24
Figure 8. Different stages of overwrapping a traditional cylindrical vessel with domes using AFP (a) machine set-up (b) first hoop layer (c) ±45o layers (d) completed wrap with a final hoop layer. ..... 25
Figure 9. Comparison between conventional vessel design and modified design required to

enable current AFP operability. 26
Figure 10. Schematic showing the possibility of using existing AFP head at CPC to provide coverage at the polar ends of a vessel with conical domes. 27
Figure 11. New design for a liner with conical domes designed and fabricated by Steelhead Composites that enable AFP coverage at the polar ends. 27
Figure 12. Finite element model and mesh for the Type III composite pressure vessel using a liner with conical domes. 28
Figure 13. Contour plots of (a) local laminate angle of the composite plies and (b) maximum longitudinal fiber strain (%) 29
Figure 14. CNC control of the AFP head for composite overwrap required a build-from-scratch computer code that generates the (a) path controlling the machine G-code (b) hoop patterns (c) helical path that ensures full coverage without gaps and overlaps; (d) end view displaying a star pattern that is repeated for full coverage. 30
Figure 15. Stages of vessel wrapping for the lightly wrapped composite pressure vessel. 31
Figure 16. Zoltek carbon fiber spools showing a) tow breaks and b) fiber falling from spool end. 32
Figure 17. DSC of polymer formulation. 33
Figure 18. Melt flow index of proprietary blend compared to Nylon 6,6 using ASTM D 1238. 34
Figure 19. Shear rate dependence of matrix polymer using ASTM D 3835-16. 34
Figure 20. Molecular weight distribution of matrix polymer as compounded (blue), after tape fabrication (black), and after AFP ring fabrication (red). Internal Nylon 6,6 standard shown in green. 35
Figure 21. Example tape fracture with Panex 35 carbon fiber with polyamide. 38
Figure 22. Example tape fracture with MR 34-700 carbon fiber with polyamide. 38
Figure 23. Optical micrograph of tape surface on Roll 13. 39
Figure 24. Single layer tape tensile strength results for Rolls 11B and 13A. 40
Figure 25. Single layer tape tensile modulus results for Rolls 11B and 13A. 41
Figure 26. Tensile strength results for Rolls 11B and 13A at -65F. 41
Figure 27. Tensile modulus results for Rolls 11B and 13A at -65F. 42
Figure 28. Yarn grips used for tensile testing. Note that there is not a well-defined gauge length. 43
Figure 29. Weibull plot of failure strength as a function of the tape gauge length for materials tested at DuPont, blue – 2 inch, red – 4 inch, and green – 8 inch. 43
Figure 30. Tensile strength of Roll 11 tapes of quarter inch width. Each bar is data from the same tape taken at various portions along the roll. 44
Figure 31. Tensile strength of Roll 11 tapes of half inch width. Each bar is data from the same tape taken at various portions along the roll. 45
Figure 32. Weibull plot of failure strength as a function of tape width, red - half inch, blue - quarter inch. 45
Figure 33. Photomicrographs of polished cross-sections of UD tape. The tape thickness is 0.17mm. The dark blue material is tape used to prevent potting material intrusion into the tape during sample preparation. 47
Figure 34. Optical micrograph of tape fracture surface confirming the presence of unwetted fiber bundles. 47
Figure 35. Photomicrograph of a polished cross-section of 1mm thick plaque showing no residual porosity. 48

Figure 36. Explosive fracture resulting from tension testing of UDRI compression molded tape laminate. ..... 50
Figure 37. Optical microscopy of polished cross-section of UDRI compression molded laminate. ..... 51
Figure 38. Results of designed experiment - dependence of ring thickness in inches on process variables. ..... 54
Figure 39. Results of designed experiment - dependence of ring density in g/cc on process variables. ..... 55
Figure 40. Results of designed experiment - dependence of ring strength in ksi on process variables. ..... 56
Figure 41. IR Thermograph taken during the direct fabrication of the 1mm thick rings. ..... 59
Figure 42. Optical micrographs of polished cross sections of as-fabricated 5.75 inch ID rings, showing no residual voids after AFP process. The ring is 1mm thick. ..... 60
Figure 43. Optical micrographs of polished cross sections of as-fabricated 12 inch ID rings, showing no residual voids after AFP process. The ring is 1mm thick. ..... 60
Figure 44. As-fabricated dome on fluted vessel. ..... 61
Figure 45. Stages of fluted vessel wrapping including, in order of the process, application of the landing ply, the first hoop ply, the helical ply, and the second hoop ply. ..... 61
Figure 46. Close up of wrapped vessel, including the helical and hoop plies. ..... 62
Figure 47. Pressure vs hoop strain measured during the initial pressurization cycles, compared with FEA prediction. ..... 63
Figure 48. FEA prediction of pressure vs hoop strain, compared with test data at rupture pressure. ..... 65
Figure 49. Picture of the composite pressure vessel fabricated with (a) fiber reinforced thermoplastic composites, post rupture compared with the same for a vessel fabricated with (b) fiber reinforced thermoset composites ..... 66
Figure 50. Picture of low tension vessel after pressure testing. ..... 66
Figure 51. Pressure vs. strain behavior for low tension (black) and high tension (red) test vessels. ..... 67
Figure 52. Depiction of zero degree plies that could be made with AFP. ..... 68
Figure 53. Location of circumferential wafers to reinforce the dome while saving weight. ..... 68
Figure 54. Process flow for thermoset and thermoplastic Type III CPV systems. ..... 69
Figure 55. Tape tensile testing samples with bonded tabs. ..... 79
Figure 56. Mounted tensile specimen with extensometer. ..... 80
Figure 57. Two inch wide tape used in compression molding. ..... 81
Figure 58. Compression molded thermoplastic laminate test panels. ..... 81
Figure 59. Test setup for ASTM D2290 Split Ring Tension test, including locations of strain gauges. ..... 82
Figure 60. ASTM D2290 Split Ring Tension, with 5.75 inch ring after testing. ..... 83
Figure 61. Removing aluminum liner wall to extract test specimen, including a) cutting cylinder and aluminum mandrel, c) drilling through aluminum substrate, and d) removing composite ring. ..... 85
Figure 62. Short beam shear testing setup for curved specimens extracted from rings. ..... 86

## 1.4 List of Tables

Table 1. Benefits and drawbacks of CPV laydown systems. ..... 13

Table 2. Value propositions for thermoset- and thermoplastic-based CPVs in compressed gas storage (CGS). ..... 15
Table 3. Summarized tape tension results comparing Zoltek and MR carbon fibers. Different sample numbers represent different locations on the roll from which the tapes were harvested. ..... 37
Table 4. Fiber volume and void content for Roll 11B. ..... 39
Table 5. Fiber Volume and Void Content for Roll 13A. ..... 40
Table 6. Effect of gauge length on tape strength. ..... 42
Table 7. Short beam shear results from AFP ring made at 330C, 12 inches per second, and 200 pounds pressure. ..... 46
Table 8. Physical properties for ring used for fabrication of short beam shear samples. ..... 46
Table 9. Results of tensile testing for pressed UD plaque at UDRI. Each data point is for a separate sample cut from a single plaque. ..... 50
Table 10. ASTM D2290 tension results (RT dry) ..... 52
Table 11. ASTM D2290 tension results (RT dry) ..... 52
Table 12. ASTM D2290 tension results (RT dry). ..... 53
Table 13. Summary of physical properties for 5.75” diameter ring specimens. ..... 57
Table 14. Strength of rings as a function of diameter and initial form ..... 58
Table 15. Effect of tape tension on hoop strength of 12 inch diameter rings. ..... 59
Table 16. Summary of costs for various vessel type. Capital and investment costs: thousands of dollars. Fixed, variable and total costs: dollars per vessel ..... 70
Table 17. Fixed cost breakdown. Costs are listed in thousands of dollars per year. ..... 70
Table 18. Variable cost breakdown for materials, including waste due to the process. Cost is listed as dollars/vessel. ..... 70
Table 19. Required Unit operations. Where more than one unit required, 24/7 operation is assumed. Liners for Type IV vessels are purchased from external source ..... 73
Table 20. Underlying assumptions for Cost of Manufacture estimate. ..... 73
Table 21. Ring process condition matrix. ..... 84

## 1.5 List of Appendices

Appendix 1. Testing and Evaluation……..78

## 1.6 Acknowledgements

This project was sponsored by the U.S. Department of Energy, Office of Energy Efficiency and Renewable Energy, Advanced Manufacturing Office, under contract DE-EE0006926 with the Institute for Advanced Composites Manufacturing Innovation (IACMI).

The authors would like to acknowledge the work of many team members that made this work possible, from project guidance, to administration, to execution. This extended and talented team included:

DuPont: Jacob Dickinson, Janet Sawgle, Mary Strzlecky, Mark Weinberg, Bryan Sauer, Tim Harper, Ryan Martin, Charles Woodward, Zachary Dilworth and Doug King.

Michigan State University: Erik Stitt

University of Dayton Research Institute: Brian Rice

Composites Prototyping Center: Michael Murphy

IACMI: Dale Brosius, Lisa Fitzgerald, Erin Brophy, John Unser, and John Hopkins

Thank you all for your diligent and inspired efforts.

# 2. EXECUTIVE SUMMARY

This report summarizes the progress made on utilizing polyamide carbon fiber tapes for composite overwrapped pressure vessels (CPVs) using Automated Fiber Placement (AFP). This project is joint development project run through the Institute for Advance Composite Manufacturing Innovation (IACMI) with DuPont, Steelhead Composites, University of Dayton Research Institute, and the Composites Prototyping Center. Over the course of this program, the Team developed and/or demonstrated the materials and processes that are required to produce vessels for compressed gas storage, including polyamide matrix formulation, unidirectional polyamide/carbon fiber tape production, and automated fiber placement on a vessel liner. In addition, a cost of manufacture analysis was performed that compares Type III and Type IV vessels made with both thermoplastic and thermoset chemistries.

This report summarizes the myriad of technical advances made during this project, culminating with production and testing of an aluminum-lined Type III pressure vessel. Each step was optimized locally so as to produce the best material. The end result was a test vessel that, while demonstrating some of the benefits of thermoplastic matrix composites, did not perform as well as those produced by filament winding of carbon fiber/epoxy prepregs. This was most likely due to the Team's focus on local optimization rather than globally optimizing the entire process from beginning to end. Should further work be contemplated, a more focused effort on global optimization should be pursued.

# 3. INTRODUCTION

The current manufacturing process for compressed gas storage (CGS) tanks involves the formation of well-impregnated continuous fibers in an epoxy matrix followed by filament winding the resulting prepreg on a vessel liner. The final part is then produced by curing the composite material with heat. While this technique is acceptable for current generation of CGS tanks, it can lead to a high cost of manufacture, high energy use, long cycle time, and no or low recyclability of the epoxy-based thermoset composite parts. Although development of advanced thermoset based CGS tanks is ongoing, fiber reinforced thermoplastic compositesmay provide an all-around more attractive option to produce CGS tanks. Recyclability, especially if high volume applications in automobiles become common, is a key selling feature.

It was therefore the first goal of this project to use a thermoplastic polyamide polymer combined with carbon fiber in the form of unidirectional (UD) tape in conjunction with Automated Fiber Placement (AFP) to produce CGS tanks (e.g., 350 bar compressed natural gas (CNG), 700 bar hydrogen). Per the recommendation from Steelhead, the initial CPV target for this program was a 350 bar 30 L type III (i.e., aluminum lined) vessel. This vessel was selected because the small size and moderate pressure keeps the material and time requirements to produce vessels reasonable during development.

The second goal of the project was to estimate the cost of manufacture for pressure vessels made with this technology. For this combination of materials and processing to have a chance for commercialization, it must be cost competitive with the incumbent technology based on thermoset materials. Therefore, a technoeconomic assessment was performed.

# 4. BACKGROUND

The Institute for Advanced Composites Manufacturing Innovation, IACMI, is a partnership of industry, academic institutions, as well as federal, state, and local governments that are working together to benefit the nation's energy and economic security. This diverse public/private partnership validates manufacturing technologies that respond to private industry's need for faster and more cost-, material-, and energy-efficient composite manufacturing, including recycling at the end of product life. IACMI's research and development programs are driven by major industry participation with a focus on reducing technical risk and developing a robust supply chain to support a growing advanced composites industry. The goals of IACMI are:

1) Reducing production cost of finished carbon fiber composites for targeted applications (vehicles, wind, high-pressure gas storage at a minimum) by >25% in five years, on a pathway to reduction of cost >50% over ten years
2) Reducing the embodied energy of carbon fiber composites by 50% compared to 2015 technology on a pathway to 75% reduction in ten years.
3) Demonstrate that the technology is capable at a sufficient scale for >80% recyclability or reuse of fiber reinforced polymer composites in five years into useful components with projected cost and quality at commercial scale competitive with virgin materials on a pathway to 95% recyclability or reuse starting in ten years

The Team believed that this program as designed would reduce the cost of manufacture (COM) of CPVs because the toughness of the resin matrix and the flexibility of the laydown process will enable the use of less carbon fiber in the construction of the vessel. Since carbon fiber is the most expensive component of the materials system, reducing the amount of fiber required for a vessel will reduce the cost of the entire system. Reducing the weight will also make these vessels more attractive in mobile applications such as hydrogen storage tanks in fuel cell-powered vehicles, making thermoplastic systems even more attractive.

Thermoset-based Type III systems are prepared by first combining the carbon fiber with the thermoset matrix, subsequently using filament winding technology to wrap the prepreg around an aluminum vessel liner, and finally curing the assembly in a low temperature enclosure as shown in the flowchart in Figure 1a. Generally, prepreg can be purchased, made ahead of time, or it can be made in line with filament winding by routing the fiber tows through an oligomer-filled coating bath immediately prior to wrapping on the liner. The speed of impregnating the fiber tows with the resin is very fast due to the low viscosity of the low molecular weight oligomers, and as is discussed below, this is an advantage over thermoplastic systems. However, the system must be cured afterwards, and this additional step adds cost to the manufacturing process.

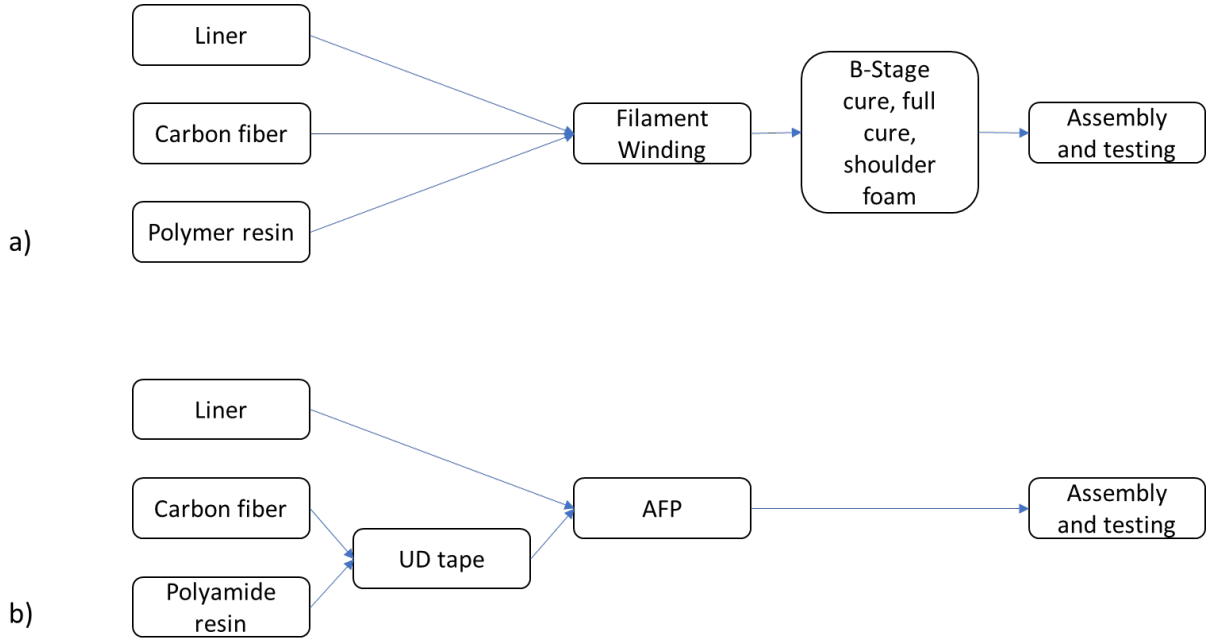


Figure 1. Traditional processing schemes for a) thermoset- and b) thermoplastic-based CPVs.

Thermoplastic-based systems generally use a different processing route. The heart of this process is Automated Fiber Placement (AFP). The process flow must be different, as shown in Figure 1b, due to the short residence time at elevated temperatures. Briefly, the AFP process melts the thermoplastic resin as the UD tape is being applied to the vessel after which it solidified as shown in Figure 2. The resulting structure is therefore complete after this one process, eliminating the need for curing. However, due to the very short amount of time above

the polymer melt temperature, there is very little time for the polymer to impregnate the fiber bundles. Thus, the material that is processed with AFP must be mostly, if not completely, free of voids prior to processing. Nearly void-free thermoplastic prepreg UD tape must, therefore, be produced prior to this process, and requires much time and effort.

For the sake of completeness, AFP can be used with thermoset systems as well. In this case the bubble-free thermoset prepreg tape cure is initiated by the laser, and the cure continues for some time after the laser exposure. The reader is directed to Automated Dynamics for more information on this topic.

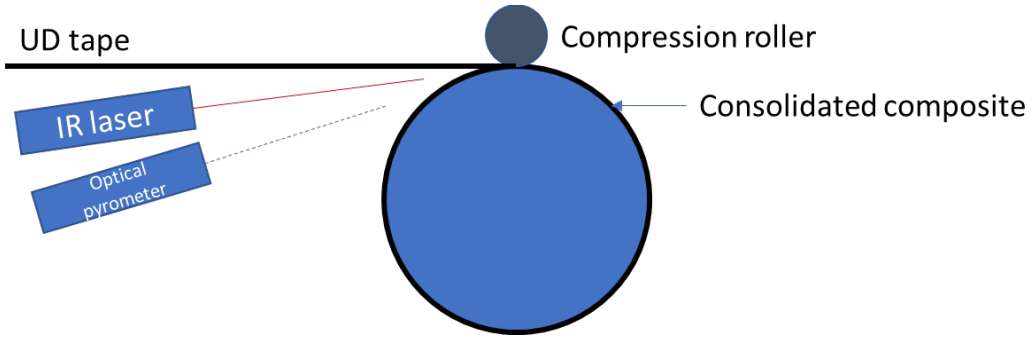


Figure 2. Schematic of Automated Fiber Placement process.

One advantage of the thermoset systems is that this technology has been practiced for decades, and therefore the filament winding patterns and equipment have been well optimized, leading to the benefits shown in Table 1. A typical filament winder is comprised of one controller, and three to five parallel spindles with associated fiber creels and inexpensive placement heads. Because of this arrangement, the cost of manufacture of Type III vessels is reduced relative to one-at-a-time AFP processing, as will be described later in this report.

Table 1. Benefits and drawbacks of CPV laydown systems.

| |
|---|
| Thermoset prepreg-based system<br>• Process – impregnate continuous carbon fibers with an epoxy resin matrix, filament wind on liner, cure with heat<br>• Benefits – inexpensive parallelized capital investment, well-known technology<br>• Potential downside – multiple steps, high energy cost, long cycle time, low recyclability |
| Thermoplastic UD tape-based system<br>• Process – impregnate continuous carbon fibers with polyamide matrix, AFP on liner<br>• Potential benefits – short cycle time, increased toughness, design flexibility, reduced weight, recyclability<br>• Potential downside – cost of capital, limited experience |

The manufacturing cost of thermoset CGS tanks is driven up by variability in the manufacturing process and brittleness of the reinforcing composite structure, which has led to a high tank burst

safety factor (2.25x or higher), i.e. the degree to which the tank must be over-designed. This high safety factor is driven by[7]:

1) Voids (3-5 volume %) in the composite structure due to air being trapped during winding, resulting in lowered mechanical performance of the composite reinforcing structure when compared with void free composites
2) Resin segregation within the composite layers if the tanks are not rotated during cure, thereby producing variability in the composite structure resulting in reduced mechanical properties when compared with unsegregated composites
3) Susceptibility of the composite structure to damage from impact (e.g., dropping) but having no observable indication of damage, thereby necessitating a high safety factor
4) Low intra- and inter-laminar shear strength of the thermoset based composite that inherently reduces the load bearing capability of the composite shell up to the design burst pressure

Other potential downsides to the thermoset-based process is that it must be done in multiple serial steps, increasing the time that it takes for one vessel to get through the entire process, and the need to heat a relatively large space in which the resin is cured on the rotating vessel liner. However, while it may take some time for a single vessel to make it through the entire process, this is rarely a problem because the batch process steps are run in parallel, leading to a high total throughput.

Two inherent advantages of thermoplastic versus thermoset composites are the lack of a thermoset resin curing step, which significantly increases cycle time for thermoset based composites, and the increased toughness of thermoplastic resins, such as polyamides (PA). The increased toughness of the thermoplastic matrix may allow CGS tanks to be designed with a lower safety factor (2.0 or lower) than what current codes and standards allow. The lower safety factor might be justified by the improved integrity of the composite structure, a potential increased strength translation of the carbon fiber reinforcement due to fewer voids and defects, and the ability of the thermoplastic composite reinforcement layer to absorb impacts better. This might be predicted result in a significant reduction in carbon fiber and its associated winding time, thereby significantly reducing the cost of materials and manufacture. It should be cautioned though, that standards modification would be an extremely long process. Nonetheless, enhanced toughness may result in modest reduction in the composite mass on the vessel due to manufacturers developing confidence that the thermoplastic composites will sustain impacts without major damage to the composite.

One significant drawback of thermoplastic resins is their high melt viscosities when compared with uncured thermoset resins, making fiber wet-out challenging. Thus, many thermoplastic applications have relied on low filament count carbon fiber tow (i.e, <12k), a slightly more expensive material than the heavier tow options. However, value may be captured at the end-of-life of thermoplastic based materials due to their greater recyclability as compared to thermoset matrix composites.

Another requirement of the thermoplastic systems is the high cost of capital associated with the AFP system. Current systems are expensive, as will be later explained, and the current generation of AFP robots operate on one spindle at a time. This lack of capital productivity is a challenge that needs to be overcome to prove that this technology has potential to displace some

of the more productive thermoset technology in the future.

The Team believes that there are applications where thermoplastic CPVs have the potential to displace thermoset systems in specific applications. The value propositions for thermoset- and thermoplastic-based systems are summarized below (Table 2). The low viscosity of the thermoset matrix prior to curing enables these systems to be more highly loaded with carbon fiber while maintaining low void levels. Assuming the same levels of defects, this leads to thermoset structures that are potentially stiffer and stronger than thermoplastic systems, in turn enabling the use of less composite on the outside of each vessel. In addition, because thermoset systems have been practiced commercially for a long time, the engineering of the vessel design along with the optimization of the processing equipment has led to high performance factors and high capital utilization rates. These factors will make thermoset technology difficult to displace. However, as stated before, the enhanced toughness of thermoplastics, along with the recyclability and the potential to use designs that are not available to filament winding machines, make thermoplastics an attractive option should the technology be proven out.

Table 2. Value propositions for thermoset- and thermoplastic-based CPVs in compressed gas storage (CGS).

| | Thermosets | Thermoplastics |
|---|---|---|
| Carbon fiber loading | + | - |
| Process maturity | + | - |
| Regulatory approved | + | - |
| Matrix toughness | - | + |
| Recyclability | - | + |
| Design flexibility | - | + |
| System cost | + | ? |

In light of the foregoing reasons and as previously stated, the overall objective of this project was the demonstration of an AFP-based process for the creation of thermoplastic continuous fiber reinforced polymer (CFRP) composite CPVs and the creation of a technoeconomic analysis that describes it. Together, these demonstrations should enable a data-based decision as to whether this technology can be competitive with thermoset-based systems in the current climate.

## 4.1 Technical Approach and Rationale

This program was designed to be a collaboration between the 4 primary partners (lead contacts in parentheses): Dupont (Lee Silverman), the University of Dayton Research Institute (Jared Stonecash), the Composites Prototyping Center (Leonard Poveromo), and Steelhead Composites (Kaushik Mallick). Although the team worked coherently and collaboratively in all phases of this work, the tasks for which each organization had primary responsibility is shown in Figure 3. DuPont was the overall project lead.

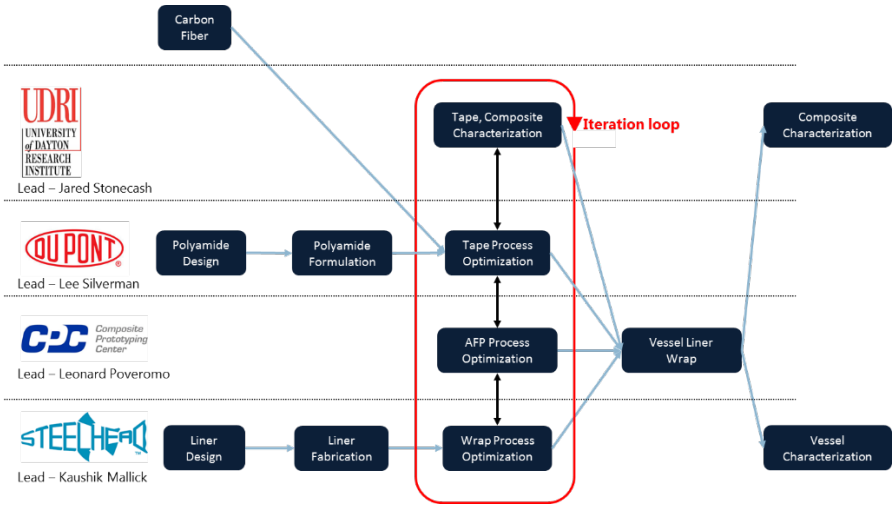


Figure 3. Primary roles and responsibilities for each team member organization.

The primary responsibilities of the team members were:

1) DuPont (Wilmington, DE) had a primary responsibility, aside from being the program leader, for the design and fabrication of the polyamide polymer matrix, and supply the UD tape made from that polymer.
2) The Composites Prototyping Center (Plainview, NY) housed and operated the Automated Fiber Placement (AFP) robot that was outfitted with an application head specifically suited for thermoplastic UD tapes. The AFP was supplied by Automated Dynamics, part of the Trelleborg Group.
3) The University of Dayton Research Institute (Dayton, OH) carried the primary responsibility for the characterization of the UD tapes and composites rings formed from them.
4) Steelhead Composites (Golden, CO) was responsible for the design and fabrication of the Type III vessel liner along with the design of the CPV wrap pattern, the modeling of the hybrid structure, and the testing of the fabricated pressure vessels.

## 4.2 Pressure Vessel Type Selection

Compressed gasses are ubiquitous in today's technological environment, and vessels to contain them are available in a variety of forms. These forms are:

Type I: All-metal construction, generally steel. Type I vessels are the least expensive.

Type II: Mostly steel or aluminum with a glass-fiber composite overwrap in the hoop direction. The metal vessel and composite materials share about equal structural loads.

Type III: Metal liner with full composite overwrap, generally aluminum, with a carbon fiber composite. The composite materials carry the structural loads.

Type IV: An all-composite construction featuring a polymer (typically high-density polyethylene, or HDPE) liner with carbon fiber or hybrid carbon/glass fiber composite. The composite materials carry the structural loads.

Type V: An all-composite construction without a liner, made entirely from a composite carbon fiber or hybrid carbon/glass fiber composite. The composite materials carry the structural loads and provide a leakproof enclosure for the gas.

At the outset of the program, the Team had to decide on what type of vessel to use as the focus of the investigation. Because this program is most concerned with compressed natural gas storage for vehicular transportation, one key selection criteria for vessel type is the weight of a 350 bar rated pressure vessel. However, since hydrogen storage is an oncoming technology, the Team kept in mind the importance of the hydrogen permeability, even though hydrogen vessels are rated at 700 bar.

In order of increasing vessel weight for a given pressure and volume capacity, the various types are ranked as shown below (lighter is better):

$$\text{Type I} > \text{Type II} > \text{Type III} > \text{Type IV} = \text{Type V}$$

where Type 1 is the heaviest. This ranking is directly related to the amount of high strength composite that is available to support the internal pressure, and since carbon fiber has a higher specific modulus and specific strength than aluminum, vessels that rely on carbon fiber for reinforcement are preferred. From this list, it can be readily seen that for a given pressure, Type IV and V vessels are the lightest. Conversely, systems that rely on carbon fiber are inherently more expensive than vessels that are based on metal. Therefore, in order of cost of manufacture,

$$\text{Type I} < \text{Type II} < \text{Type III} < \text{Type IV} = \text{Type V}$$

where Type I are the least expensive.

In order of increasing hydrogen permeability, the various types are ranked as shown below:

$$\text{Type I} = \text{Type II} = \text{Type III} < \text{Type IV} < \text{Type V}$$

Hydrogen permeability is minimized by the presence of metal in the liner. Given a thick enough layer of metal, the permeability drops below measurable values. Clearly, based on this ranking, Types I – III are the best suited.

Based on this reasoning, the Team decided to focus on Type III vessels with an aluminum liner. Type III vessels have a good combination of system cost, system weight, and hydrogen permeability. This type of vessel is also produced commercially by one of the partners in the program, Steelhead Composites, and the Team was therefore able to learn from the considerable experience of this Subject Matter Expert (SME).

## 4.3 Selection of Vessel Fabrication Method

As with any materials development, the properties of the finished product are a function of the microstructure of the material, which in turn is a function of the raw materials and the process that operates on them. In this program, we examined two potential processes from which one was selected. Following the process selection, the constraints on the raw materials were addressed.

Thermoplastic CFRP composites for compressed gas storage are fabricated using the following general scheme:

1) Preparation of the matrix polymer
2) Creation of an intimate mixture of the carbon fiber and the polymer in a unidirectional (UD) tape format
3) Creation of a shell of the UD tapes in a specific pattern to make a preform, often containing a metal liner (Type III)
4) Consolidation of the preform under pressure and at a temperature above the melting temperature of the system to form a dense composite

Often, the method of consolidation determines the processing time at elevated temperature and pressure. Consolidation of the structure is required to eliminate any residual voids in the precursor materials as well as fuse all the material together into one coherent mass of CFRP. The process is accomplished above the melting temperature, and subsequent movement of the polymer within and between the fiber tows vastly reduces the number of strength limiting flaws, such as small- or large-scale porosity, in the system.

For the present case of a Type III vessel with an aluminum liner, there are several possible ways to consolidate the structure. The first is to put the UD-Tape-wrapped vessel in a heated mold and apply pressure from the outside. In this process, the carbon fiber tape is compressed as the polymer is melted, and the resulting composite is smaller in diameter than the original tow laydown. This shrinkage is obligatory because the reduction/elimination of void space in the composite requires that the volume of the composite layer is decreased in this process. Due to the geometry of the system, the radial shrinkage of the composite necessitates circumferential shrinkage. This will lead to buckling of the carbon fiber because the fiber is wrapped around the circumference of the vessel, that in turn will result in a composite layer of lower modulus and strength than a well-aligned fiber system. For this reason, this process was not pursued.

An alternate processing scheme, Automated Fiber Placement (AFP), uses a short pulse of heat and pressure at the time of UD tape application to fuse the CFRP layers together as the subsequent layers are applied as shown in Figure 2. If the proper processing conditions are selected, this process results directly in a dense composite without further processing and the fibers are fully extended to provide the maximum stiffness and strength. This method was chosen for this program, and the AFP system used at the Composites Prototyping Center (CPC) is shown in Figure 4.

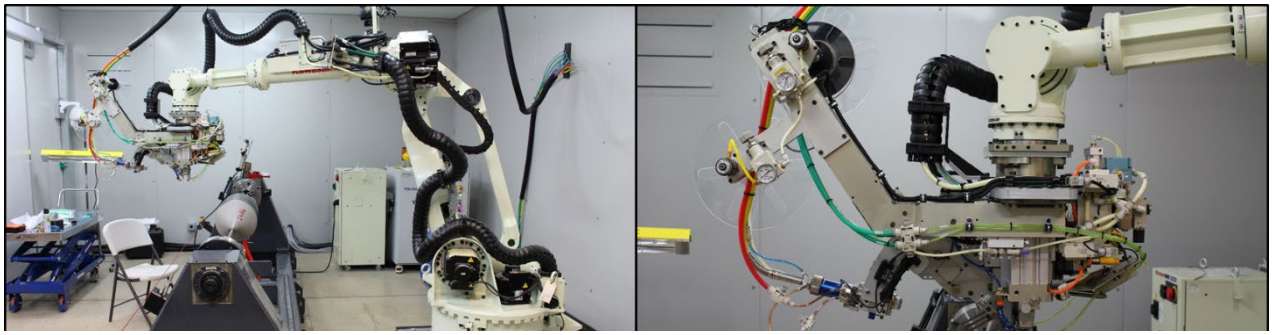

Figure 4. The Automated Fiber Placement (AFP) robot that was operated at CPC, a) the entire robotic system, and b) a close-up of the thermoplastic tape application head.

The selection of AFP puts several requirements on the materials that are processed. First and foremost, the material must be capable of being heated rapidly so that it can be consolidated within the time scale of the process.
Therefore, machines of this type are usually set up to use a thin ribbon of thermoplastic composite unidirectional (UD) tape, as thinness is required for fast heating. Another requirement is that the tape itself must be mostly free of voids and the majority of the fiber tows must be wetted out with the polymer. This is because the heating/compression cycle during AFP is fast and the resin cannot move over long distances during the time that the composite temperature is higher than the polymer melting point.

## 4.4 Polymer Matrix Development

There are many processes to make UD tape, most of which are based on pultrusion. In pultrusion, the carbon fiber tows are spread into a thin ribbon, and subsequently exposed to a molten polymer at relatively low shear rates. The shear is required to force the polymer into the fiber bundles and get nearly void-free materials. To fully impregnate the carbon fiber bundles to make UD tape, the viscosity of the polymer must be low, and it must wet the fiber very well. While wetting is mostly controlled by the sizing on the carbon fiber, the viscosity of thermoplastics is usually controlled by tuning the polymer molecular weight. In this case, because a low viscosity is desired, a low molecular weight is preferred. Polymer impregnation is made even more difficult in that carbon fibers are very small in diameter (7 microns), and are available in relatively large numbers within each tow (12k filaments is about the minimum number of filaments per tow). This is a primary reason that thermosets are currently widely adopted for CFRP applications, as oligomers are low molecular weight materials that retain their low viscosity until they are polymerized.

The toughness of a thermoplastic polymer is also directly related to its molecular weight. However, in this case a high molecular weight is desired to get a high toughness matrix. This is contrary to the requirements for impregnation as explained above. Balancing the need for impregnation and toughness, the Team therefore needed to design a polyamide-based matrix polymer with a composition that provided a proper compromise that would both satisfy the end use and enable the production of high quality tape that will be useful in the AFP.

Finally, the polymer must be able to survive the tape making process with a minimum of degradation so as not to compromise the properties of the UD tape. This entails having a matrix with sufficient thermal, hydrolytic, and oxidative stability. The proprietary polyamide blend developed by DuPont accomplishes these objectives.

## 4.5 Continuous Fiber Reinforced Polymer UD Tape Production

As mentioned previously, there are many processes to make UD tape from polymers and continuous carbon fiber, ranging from those based on polymer powders to melt-based processes. The choice of which process to use for tape fabrication depends on a number of aspects:

1) As mentioned above, the AFP process does not provide much time for polymer redistribution during the process. This means that the tape supplied to the process must be nearly void free and the fibers must be very well aligned.

2) The CPV application puts a premium on a very high volume-fraction of carbon fiber in the composite to maximize the modulus and strength, thereby reducing the weight of composite that is required for each vessel. Each process to make tape has different capabilities in each of these categories.
3) The economics of tape fabrication vary widely amongst the choices of processes that are available. Lower costs of manufacture are preferred, and are associated with processes that directly use molten polymer, as opposed to polymer powders which may require grinding and solvent recycle, or polymer films that require formation of sheet structures.

Regardless of the tape formation process, the tape used during CPV production using AFP must be narrow to enable the tape to be laid down smoothly over surfaces with complex curvatures. However, the process of directly making very narrow tapes is expensive because the throughput in kilograms per hour is directly proportional to the width of the web produced. To overcome this limitation, it was decided to make wide tape webs and slit them to the desired width in a subsequent off-line process.

Weighing the various criteria, the Team selected the Van Wees process for UD tape development (Van Wees UD and Crossply Technology BV, in Tilburg, Netherlands) and all of the tapes discussed in this report were fabricated there under a NDA. Van Wees uses a proprietary tape fabrication process to create very wide rolls of continuous thermoplastic/carbon-fiber UD tape. According to Van Wees, "For impregnation of thermoplastic resins, Van Wees has developed a process in which the resin film is made by melting the polymer in an extruder and metering the film thickness on the impregnation roller. The spread fibers are impregnated up to a certain level on the impregnation roller and post impregnation takes place before final consolidation and being cooled. Speed of impregnation is in the 3–15 meter/minute range[1]." For additional information, the reader should contact Van Wees directly.

After tape fabrication, the web must be slit into usable width tapes. Slitting was done at Van Wees, where tapes down to 12mm wide were produced, and at Pacon Corporation, in Putnam, CT, where tapes of ¼ inch width were produced.

## 4.6 UD Tape Characterization

Tape characterization is a very important part of this work, as the mechanical properties of the resulting vessel will be highly dependent on the properties of the starting materials. In this case, the finished CPV must take full advantage of the carbon fiber and result in high strength, high modulus, and high strain to failure materials in order to successfully compete with the incumbent thermoset systems.

The thermoplastic tape produced at Van Wees was characterized for microstructure and strength by the team at the University of Dayton Research Institute (UDRI), led by Jared Stonecash. The UDRI team did a full range of analyses, including but not limited to physical properties and microstructural characterization. A complete description of the characterization work performed at UDRI is found in Appendix 1. In addition to the work described in the Appendix, complementary tests were conducted at DuPont.

## 4.7 AFP-Produced Ring and Cylinder Production

Once the tape had been characterized and the best tapes selected, the next step was to optimize the subsequent step of the process, namely AFP. This part of the work was led by Lenny Poveromo at the Composites Prototyping Center. There were initially AFP-based two sample-generation paths taken, initially making flat panels, and then settling on a geometry based on rings. The flat-panel work was predicated on the assumption that measuring the engineering properties of materials is usually easier in planar geometries. However, the sample preparation process was difficult to optimize. Samples were made with the tape oriented unidirectionally, however these materials were too highly curved when released from the table on which they were built. It was possible to eliminate this CTE-mismatch effect by going from a unidirectional structure to a quasi-isotropic structure based on a 0/90 architecture. This technique was later abandoned as the 0/90 structure does not represent the hoop-wound strength bearing plies in the targeted CPV. The Team therefore decided to make and test rings because they resemble the final structure much more closely. In this work, rings for testing were fabricated in two ways: first by making them directly, and second by making a long cylinder from which the test rings were cut.

Both processes for making rings start with covering an aluminum mandrel with an even base layer of tape on which the rest of the structure was built. The first layer of tape over the entire aluminum mandrel is made by slowly advancing the tape deposition head along the length of the mandrel as the mandrel rotates, with a very small overlap between the tape layers. Applied this way, the thermoplastic tapes within the first layer are adhered to one another only the edges. There is no adhesion between the UD tape and the aluminum. During the laydown of the first layer the laser is not used with closed-loop temperature control, but rather in manual mode where the power is directly set. This is a consequence that the emissivity of the aluminum substrate is very different from carbon, and a working control scheme would be quite complex.

As shown in Figure 2, once the first tape layer is applied to the cylindrical mandrel, the lathe rotates the mandrel as a laser heats the tape to fuse it to previously-deposited tape layers. Using this method, rings are fabricated on top of the tape-coated mandrel in a step where the mandrel rotates and the tape deposition head is not moved. This results in narrow rings as the tape wraps on itself as shown in Figure 5. These rings were then sent to UDRI for machining and testing. During the fabrication process, where the UD tape is being applied to previously deposited layers, closed loop laser control is used. The power output is based on a temperature measurement from an optical pyrometer. The temperature of this setpoint is referred to in later sections as the process temperature.

In addition to fabricating rings, the Team also fabricated cylinders with the AFP. When making a cylinder, the AFP head lays down material as it rasters over the desired length of the mandrel, just as in the mandrel coating process until the desired thickness is reached. During this process, odd-numbered layers were laid-down from left to right, and even-numbered layers were laid down from right to left. This lead to a very stiff structure that did not tear along the axis of the tape because alternate layers have the opposing pitch. While there is no adhesion between the tape and the aluminum mandrel as in the mandrel-coating step, the layers of tape are strongly bonded to one another due to the melting and resolidification of the overlapping thermoplastic tapes. The reader should note that the detailed microstructure of a cylinder is different than a ring, as the rastering motion of the AFP head creates a tape layer with a helical pitch. As such the carbon fiber is slightly off-axis from a pure circumferential

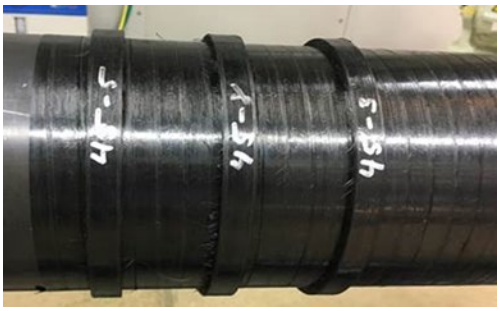

Figure 5. Example of directly-fabricated rings as made with the AFP.

wrap. The helical structure is not present in a directly-fabricated ring. As previously stated, alternate layers during the wrapping of a cylinder have opposite pitch. This suggests that, if the tape is rough and is not processed under optimal conditions, there will be areas where the tape of an outer layer will bridge high spots in a previous layer, and not provide sufficient densification. This is not the case for directly formed rings, but it is the exact microstructure of the hoop-wound section of a composite pressure vessel. Cylinders fabricated using the above-described process were sent to the UDRI team for machining and characterization.

Composite fabrication on the AFP is relatively straightforward in concept. There are several process variables that are known to affect the strength and stiffness of the finished materials. These variables include:

1) Process temperature
2) Compaction roll pressure
3) Process speed
4) Tape tension

There are additional variables that can be used to optimize the process, but these were considered out of the program scope for this phase of the program.

The rings were characterized at UDRI using ASTM D2290-16 using 5.75 in and 12-inch inside diameter rings. The split-ring test fixture is shown mounted in the load frame as Figure 6. Data from this test were used to optimize process conditions for subsequent Type III CPV vessel production. A complete description of the testing methods is included in Appendix 1.

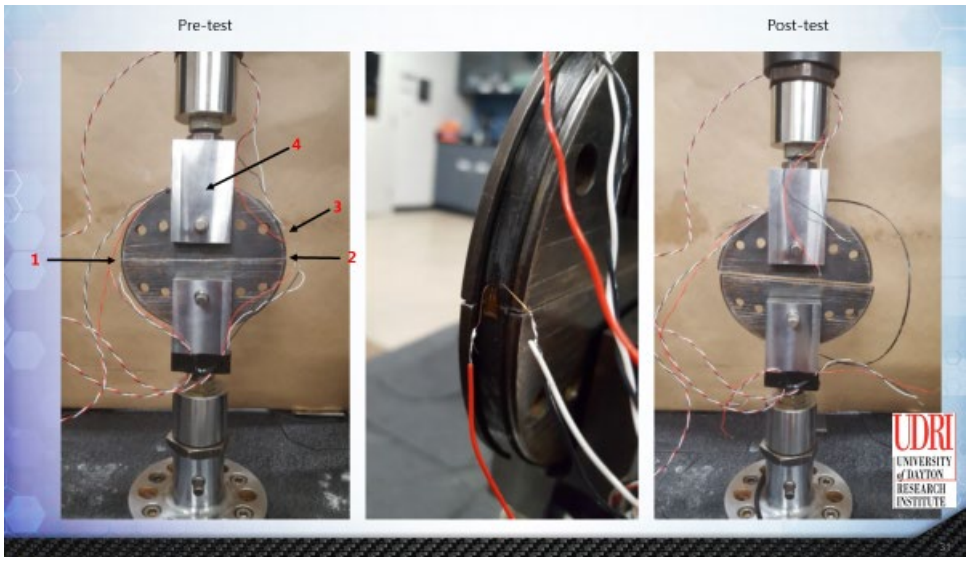


Figure 6. Picture of the split-ring tester showing a) the test ring mounted in the fixture along with the placement of strain gauges, b) a close-up of an applied strain gauge, and c) the sample after failure.

## 4.8 Design and fabrication of a Type III fiber placed composite pressure vessel

Once the processing conditions are optimized using the ASTM D2290-16 test as defined above, the recommended conditions were used for the AFP lay down and consolidation process for the UD tape on an aluminum Type III vessel liner. Prior to making the actual vessel, the composite layer must be designed to withstand the pressure-related stresses that will be present during use.

The first stage was to design and fabricate the vessel liner. This task was done by Steelhead Composites, a commercial CPV manufacturer. Steelhead uses a spinforming process, starting with seamless 6061-O aluminum tubing, to create a pressure vessel liner shown in Figure 7.The liner, after fabrication by spinforming method, is heat treated to 6061-T6 conditions to provide adequate strength and metallurgical enhancements to the aluminum alloy. Finally, the liner is machined for ports and seal interfaces before getting overwrapped with composite. The spinforming process is exemplified with a YouTube video with at the following link: https://www.youtube.com/watch?v=MmksNRyYcpM

The next step of CPV fabrication is the wrapping of the vessel with carbon fiber UD tape using AFP. The vessels fabricated and tested over the course of this work are referred to as lightly wrapped vessels. This refers to the fact that these vessels are not designed to withstand the full pressure of compressed natural gas (CNG) or hydrogen ($H_2$). Rather, these test vessels with relatively simple architectures are designed to withstand moderately low burst pressures (~3,000 psi) with the collected data used to model and validate the material behavior. Based on this data a vessel would be designed that could withstand the full pressure of the intended application.

Figure 7. Assortment of spinformed liners for Type III vessels manufactured by Steelhead Composites.

At this point in the program, an attempt was first made to use AFP to wrap a vessel with traditional cylindrical liner with isotensoid domes. The path pattern was developed by Automated Dynamics (ADC) and the fiber placed wrapping was performed by CPC as shown in Figure 8. The layup consisted of hoop/±45°/hoop plies as detailed below.

1) The first hoop ply,
    a. starting at the midpoint of the vessel and rastering to the left until it reaches the shoulder, the pitch of the raster being just less than the tape width to create a complete area-filling layer on the vessel liner exterior
    b. reversing the raster while maintaining the pitch until it reaches the right shoulder
    c. reversing the raster while maintaining the pitch until it reaches the vessel midpoint
    d. stopping the ply, resulting in two layers of tape completely covering the cylindrical portion of the vessel liner
2) The helical ply
    a. Starting at the midpoint of the vessel a repeated star pattern based on filament winding technology is to create a complete area-filling layer on the vessel liner exterior. This results in two layers of tape completely covering the cylindrical portion of the vessel liner, and significantly thicker region in the tapered section. There is not a good description of this pattern, and the reader is directed to any number of web pages for examples, https://www.youtube.com/watch?v=1A3vaJaNDLY for example.
3) The second hoop ply
    a. This process is identical to the first hoop ply above.

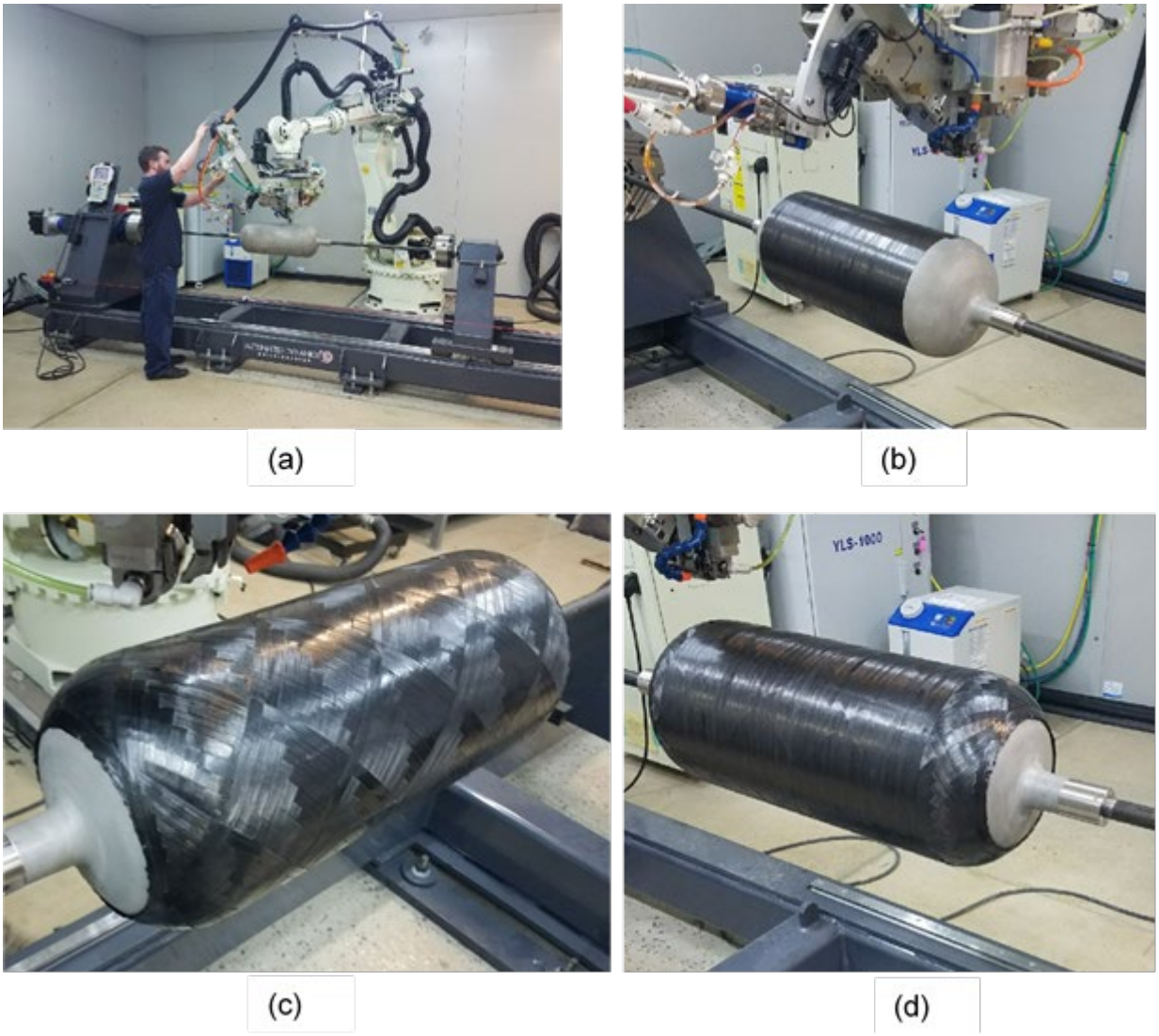


Figure 8. Different stages of overwrapping a traditional cylindrical vessel with domes using AFP (a) machine set-up (b) first hoop layer (c) ±45o layers (d) completed wrap with a final hoop layer.

During this trial fabrication, it was realized that the breadth of the existing AFP head prevented it from coming in close proximity to the ports on either end of the traditional vessel shape with isotensoid domes. Consequently, the wrap patterns cannot be designed to include low angle (</±20º) helical plies that are essential to get the composite coverage near the polar ends. The latter is essential to the design of composite pressure vessels and in providing adequate structural support against blowout loads at high pressures. The first trial AFP layup was extremely successful in demonstrating the AFP process using the polyamide based thermoplastic tapes on a traditional vessel. However, the final vessel was deemed inadequate for pressure testing because of the lack of composite support in the majority of the domed section.

The project team explored options to modify the experiment to enable the low angle helical

plies for vessels with traditional isotensoid domes. Two ideas were identified. The first option was to modify the AFP head to enable it to get closer to the vessel outlet. The second path was to modify the shape of the vessel to allow it to be used with the current AFP head.

All else being equal, the far more attractive option would be to redesign the AFP head. This would enable the use of conventionally shaped vessel liners, and would result in vessels with optimized volume-to-weight ratios that would be attractive to the gas storage industry. A more optimal design would include an AFP head with a compression roller that was narrower and protruded farther from the support structure to allow closer approach to the bung, with an elastomeric roller replacing the current steel design so the various complex curvatures of the cylindrical, transition, and dome regions. Preliminary engineering work by ADC suggested that this option would cost roughly $125,000.

The second option, redesigning the vessel liner, is very inexpensive in comparison. It requires that Steelhead Composite redesign the spin forming process to create the desired shape. This new design, shown in Figure 9, could then be wrapped with composite much closer to the bung and force the vessel failure to occur in the cylindrical section of the vessel, a requirement for materials characterization. The largest drawback of this option is that the resulting vessel will have a reduced volume-to-weight ratio, and will therefore be highly unattractive to industries that are primarily interested in keeping the weight of storage vessels to a minimum. Since that describes the vast majority of the industry that would consider a carbon fiber solution to this problem, the vessel redesign would not be competitive in the long term.

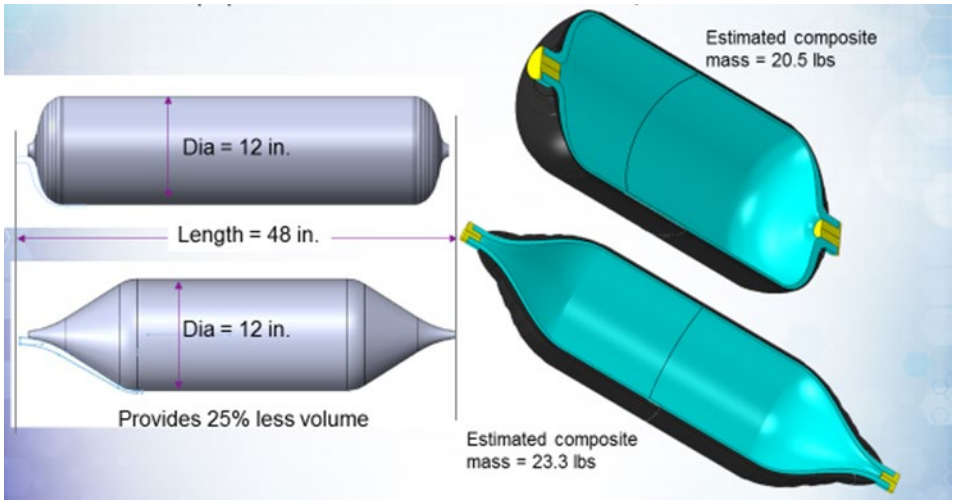

Figure 9. Comparison between conventional vessel design and modified design required to enable current AFP operability.

The best compromise solution was found in altering the shape of the liner that will allow the AFP machine head to get in close proximity to the polar ends as simulated in Figure 10.

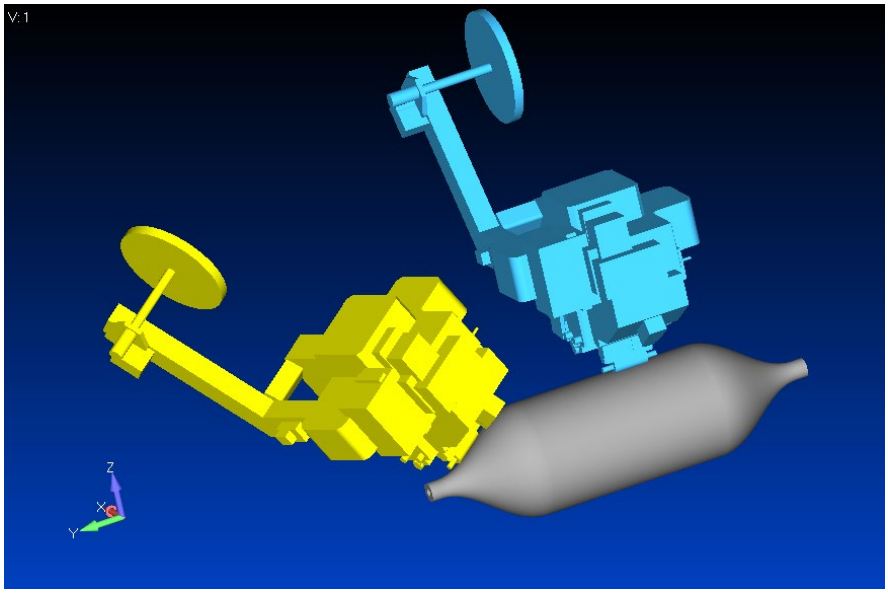


Figure 10. Schematic showing the possibility of using existing AFP head at CPC to provide coverage at the polar ends of a vessel with conical domes.

The Team's decision was that, since the primary output of this part of the program was material characterization, the less expensive approach would suffice. Should the characterization results warrant the production of a redesigned AFP head, the Team would reconsider the decision.

Once the design was complete, Steelhead Composites designed and fabricated the new liners with conical domes using spinforming process. The result is shown in Figure 11. The heat-treated liners were sent to CPC for overwrapping using the AFP process.

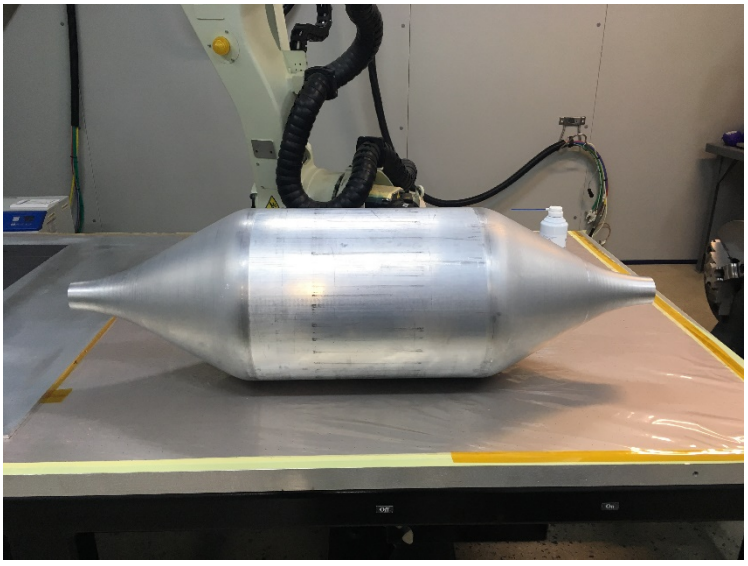

Figure 11. New design for a liner with conical domes designed and fabricated by Steelhead

Composites that enable AFP coverage at the polar ends.

Finite element analysis was performed to ensure that the composite overwrap is designed adequately to handle the burst pressure. The finite element model consisted of an axisymmetric half-section of the vessel with symmetric boundary conditions imposed at half-cylinder (Figure 12). Steelhead used a proprietary pre-processor to model the composite plies taking into account the varying angles of the composite laminate on the vessel (see Figure 13 (a)). The analysis was performed using ABAQUS, a commercial finite element software.4 The composite layup used material properties for the thermoplastic tapes determined from mechanical testing (Section 3.5). A burst pressure of 3,200 psi was initially predicted for the vessel when the longitudinal strain in the composite hoop plies approached 1.5% (Figure 13 (b)). The failure is also predicted to occur in the cylindrical section of the liner where longitudinal strain is of the highest magnitude.

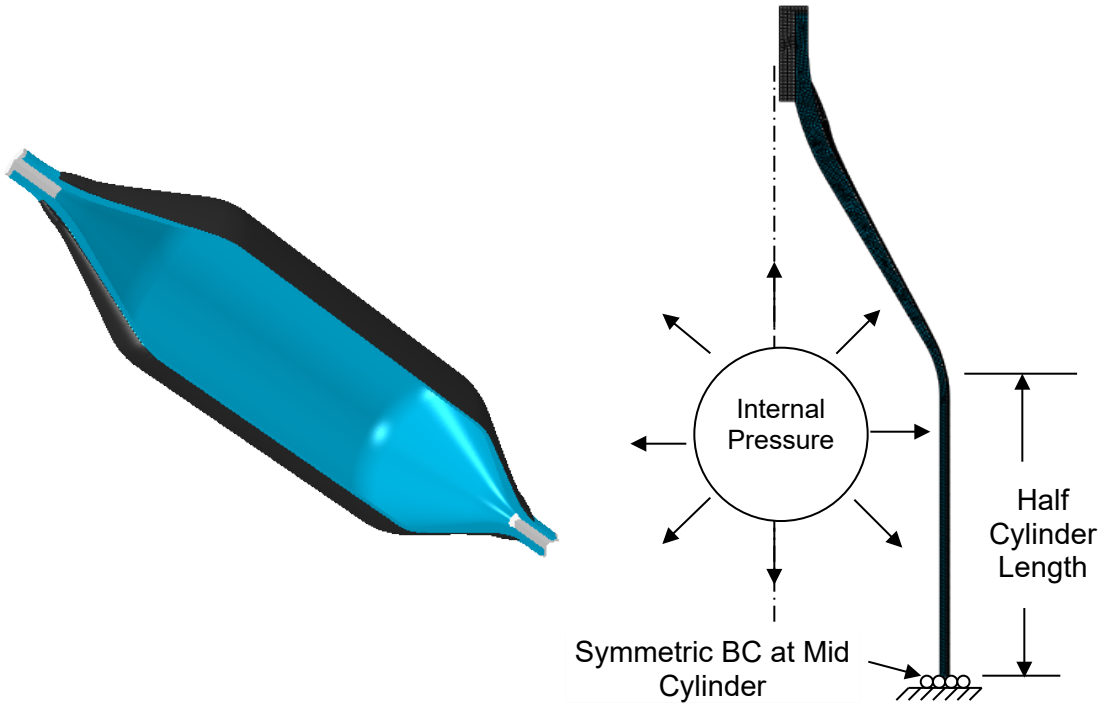


Figure 12. Finite element model and mesh for the Type III composite pressure vessel using a liner with conical domes.

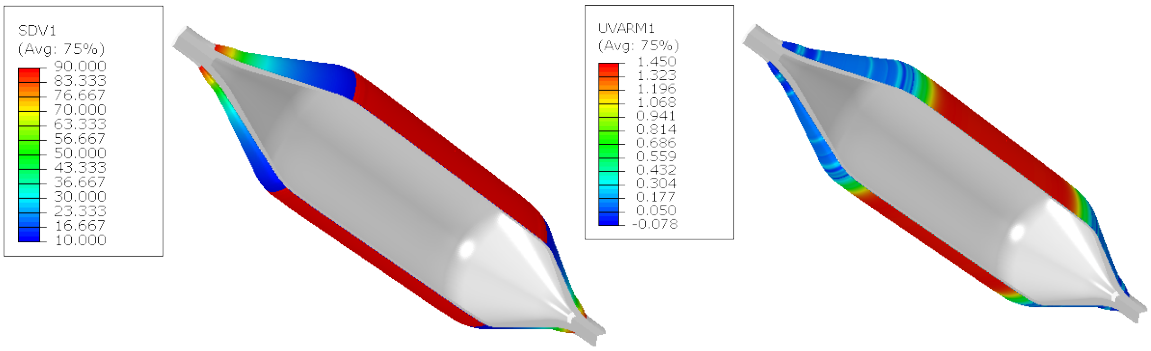


(a) (b)

Figure 13. Contour plots of (a) local laminate angle of the composite plies and (b) maximum longitudinal fiber strain (%)

Prior to the AFP wrapping of this liner with alternate shape using conical domes, the AFP machine had to be programmed for the Computer Numerical Control (CNC) motion of the head that allows for coverage of the liner using fiber-reinforced thermoplastic tapes. The programming of trajectories of the continuous reinforcement on the vessel surface is of vital importance because it allows the evaluation and determination of the trajectories which provide the best mechanical properties within the designer's specified geometrical and physical limits.[5,6] Although commercial programs exist for CNC control of filament winding heads used in traditional manufacturing of composite pressure vessels, codes or algorithms for similar methodologies for fiber placement machines need to be custom designed. This is especially demanded for the non-traditional shape of the liner design adopted for the program. Significant effort was spent by the Team at Steelhead Composites on writing the codes that generated the CNC program for the AFP head. Schematics of the wrap path are shown as Figure 14. This path design was then validated by personnel at Automated Dynamics (ADC), and then downloaded to the AFP robot at CPC.

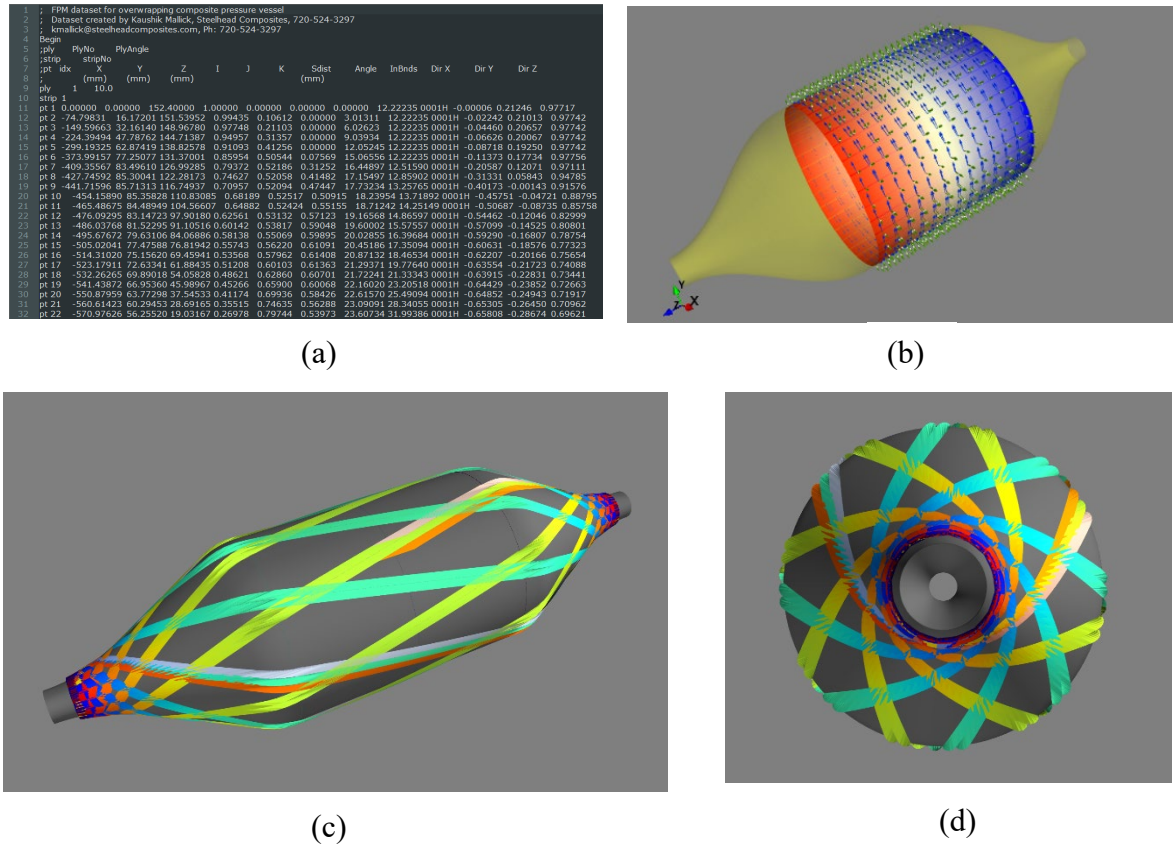


(a) (b)

(c) (d)

Figure 14. CNC control of the AFP head for composite overwrap required a build-from-scratch computer code that generates the (a) path controlling the machine G-code (b) hoop patterns (c) helical path that ensures full coverage without gaps and overlaps; (d) end view displaying a star pattern that is repeated for full coverage.

In the last step of the vessel fabrication process, the aluminum vessel liner was mounted on the AFP system, the UD tape was loaded, and the robot was activated to wrap the vessel. An example of the wrapped vessel at various stages of the process is shown in Figure 15.

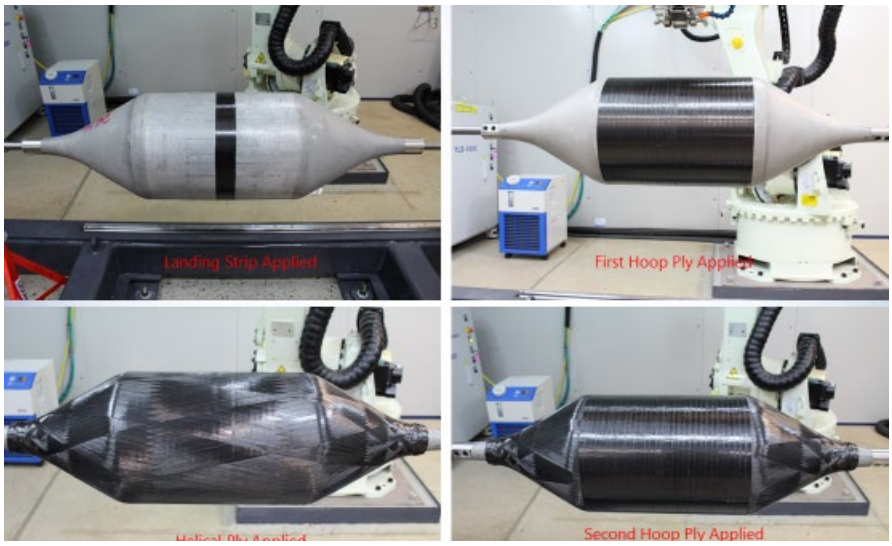


Figure 15. Stages of vessel wrapping for the lightly wrapped composite pressure vessel.

## 4.9 Pressure testing of the fiber placed composite pressure vessel

The testing of the vessel was performed at Steelhead Composites, in Golden, Colorado. Steelhead manufactures thermoset-based composite pressure vessels and as such is well equipped for the testing of the vessels and interpretation of the results.

Prior to testing, strain gauges are wrapped around the circumference of the cylindrical section. This instrumentation is for the purpose of monitoring the expansion of the vessel during testing. The vessel is then hydraulically pressurized with water as the test fluid until the vessel leaks or ruptures.

The testing is done in two phases. In the first the vessel is pressurized to a level substantially less than the designed burst strength. This portion of the test is to verify that the strain gauges are operating in addition to obtaining a plot of strain vs pressure. The resulting plots of the pressure vs hoop strain measured during the initial cycle repeated for 4 times. The plot also compares the test data with FEA predictions.

The second phase of the test is designed to measure the burst strength of the vessel. The water filled vessel is lowered into a test bunker and connected to the water source. A heavy steel cover is used to cover the pit, and observers are moved to a safe distance. The internal pressure is increased, and the pressure value is recorded from the electronic transducer as well as a mechanical pressure gauge.

The failure pressure is combined with the pressure/strain data from the first test, and combined with FEA modeling the failure strain of the composite layer is simulated.

## 4.10 Techno-economic Analysis of Thermoplastic CPV GCS Vessels

In parallel with the experimental work described above, a technoeconomic analysis was performed in order to estimate the cost of manufacture of thermoplastic CPVs for CNG-rated service. In this analysis, the cost of raw materials, labor, and capital productivity, were estimated using a DuPont-proprietary economic model.

# 5. RESULTS AND DISCUSSION

## 5.1 Carbon Fiber

The carbon fibers selected for this program were from two manufacturers: Zoltek and Mitsubishi Rayon (MR). Zoltek PX35 was initially selected for its relatively low cost and availability in 50k tows. Unfortunately, during the initial trial at the tape manufacturer, Van Wees UD and Crossply Technology, the Team had difficulty unwinding the spools due to inconsistent tension within the spools, considerable fiber shedding, and poor spreading the tows prior to tape fabrication. An example of some of the problems unwinding this material are shown in Figure 16. After a considerable time of trying to tune the tow pay-out/spreading processes without a positive result, the Team decided to switch carbon fiber to MR Grafil 34-700. This 12k-tow material unwound from the initial packages with a minimum of shedding, and spread very easily.

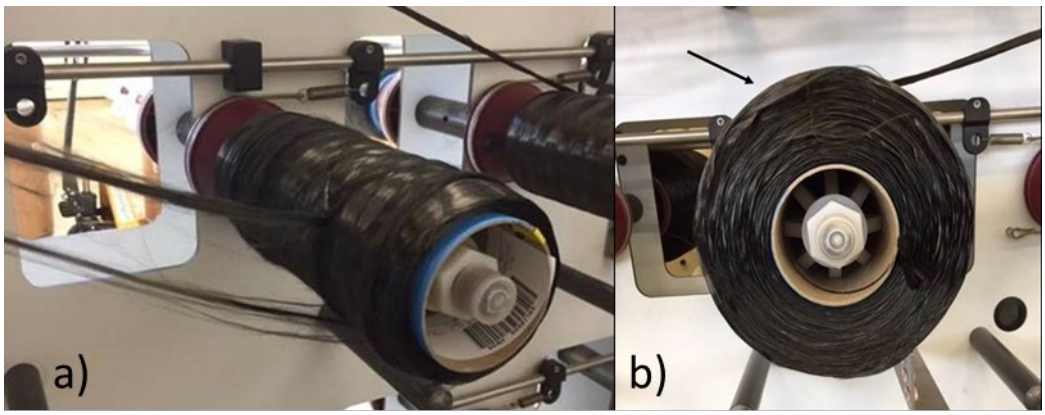


Figure 16. Zoltek carbon fiber spools showing a) tow breaks and b) fiber falling from spool end.

The sizing for both the Zoltek and Grafil continuous tow was selected to be a low melting thermoplastic polyurethane (TPU). The sizing protects the fiber during handling and makes the tows less fuzzy. The TPU is present at a low level so it can dissolve away during impregnation and not inhibit wetting. The electrochemically oxidized CF fiber surface present on the underlying fiber has many functional groups to chemically react with the PA melt via the polymer end groups, resulting in covalent bonding at the interface.

## 5.2 Polymer Characterization

As stated previously, development of suitable mechanical properties in the composites layers of CPV's requires that the carbon fiber be used efficiently. This in turn requires that the carbon fiber be completely wet out by the polymer matrix. The process of wetting out requires that the

polymer matrix be of low viscosity and low wetting angle on the fiber. The data shown for this formulation were produced from polymer blends that were processed in 26mm and 30mm Coperion twin-screw extruders and quenched in water baths prior to palletization into ¼ inch lengths. The materials were then dried overnight for at least 12 hours at 90C and sealed in metalized plastic bags to await testing.

The DuPont-proprietary polymer developed for this program is based on Nylon 6,6 that has been extensively formulated for the sole purpose of being used with continuous carbon fiber. Prior to the rheology experiments, DSC was performed at 10 degrees per minute in sealed aluminum pans. The data are shown in Figure 17.

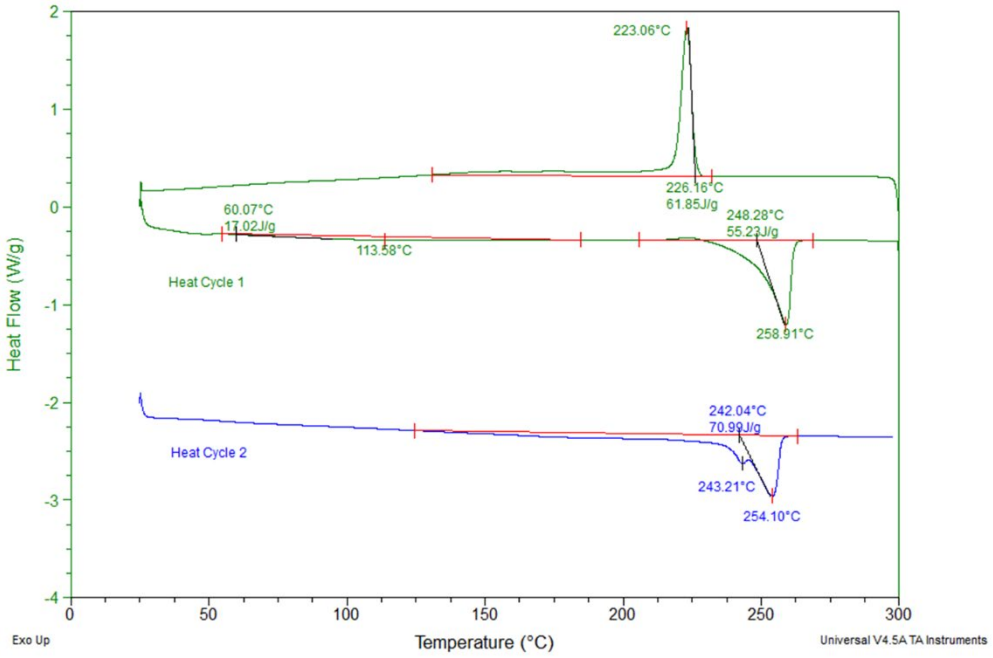


*Figure 17. DSC of polymer formulation.*

The DSC data shows the peak in the melting exotherm to be at 259C, with melting completed by 260C. Crystallization on cooling begins at 226C and peaks at 223C. On the second heating cycle, melting is once again completed by 260C.

Based on the DSC data, the melt flow index of the blend is shown in Figure 18. These measurements were made using the capillary geometry described in ASTM D 1238, with extrudate being collected for 30 seconds with extrapolation to 10 minutes. Relative to unformulated Nylon 6,6, the blend used in this work has a melt flow index roughly ten times higher than Nylon 6,6 at 275C, indicating that it will penetrate carbon fiber bundles at a much higher rate than the unformulated polymer.

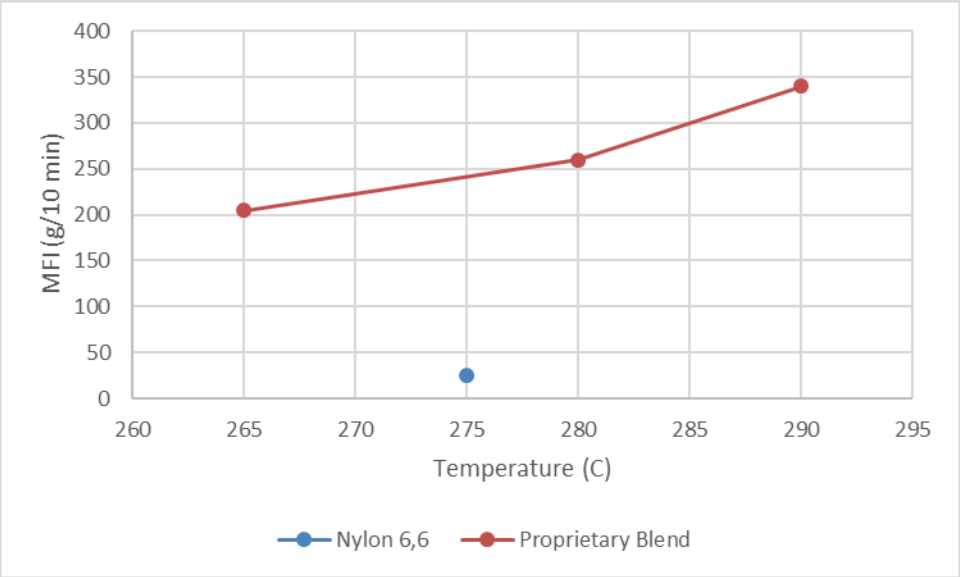


Figure 18. Melt flow index of proprietary blend compared to Nylon 6,6 using ASTM D 1238.

The shear rate dependence is shown in
Figure 19. The data was acquired with a capillary rheometer using the method described in ASTM D 3835-16. This data confirms that the viscosity decreases as the temperature increases, as expected from the melt flow index data. It can also be seen that the material is shear thinning,

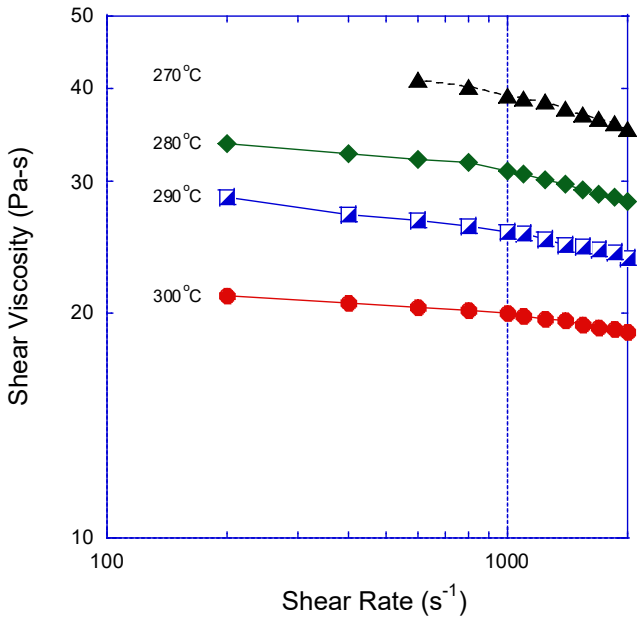


Figure 19. Shear rate dependence of matrix polymer using ASTM D 3835-16.

with the amount of shear thinning decreasing with increasing temperature. Finally, it appears that the material is approaching a Newtonian Plateau at the highest temperature tested. All of these observations are consistent with the Team's expectations based on knowledge of the formulation.

The molecular weight of the polymer was tested using size exclusion chromatography (SEC) at various stages in the process, as shown in Figure 20.

Figure 20. Molecular weight distribution of matrix polymer as compounded (blue), after tape fabrication (black), and after AFP ring fabrication (red). Internal Nylon 6,6 standard shown in green.

## 5.3 Unidirectional Tape Fabrication

As mentioned previously, after evaluating a wide variety of potential partners, the Team selected Van Wees UD and Crossply Technology for the fabrication of UD tape. Van Wees, located in Tilburg, NL, uses a proprietary machine design to make wide webs of continuous UD tape. For impregnation of thermoplastic resins, Van Wees has developed a process in which the resin film is made by melting the polymer in an extruder and metering the film thickness on an impregnation roller. The spread fibers are impregnated up to the desired level on the impregnation roller and post impregnation takes place before final consolidation and being cooled. The speed of impregnation is in the 3–15 meter/minute range[3]. The Team partnered with Van Wees under a non-disclosure agreement, which prevents the disclosure of machine design and further process details in this report. The Reader is directed to contact Van Wees directly for additional details on the process.

In this program, the small tows of the Mitsubishi Rayon 34-700 12k were very easy to spread, and there were no issues with tow breakage or non-uniform tensions. The low fiber count required that more spools were mounted on the supply creel, but this added little complexity and the potential benefit that spools of lower tow count fiber are longer than larger tows, leading to fewer spool changes during processing. The resulting tapes appeared to be well

impregnated up to speeds of 40 kg of tape per hour of production. After web fabrication, the tapes were slit to the widths desired for the remainder of this work.

While at Van Wees, the proprietary process was optimized to reduce the amount of residual porosity. The Team arrived at a set of conditions that resulted in less than 2% void volume, and these conditions were used to produce two master rolls – numbers 11 and 13.

### 5.4 Unidirectional Tape Characterization

The UD tape was characterized by the Team at UDRI, and the results presented in Table 3 show that at the same concentration of carbon fiber, the MR-based materials had higher strength and modulus. Furthermore, when the carbon concentration was increased to 64 weight percent (53 volume percent), the modulus and strength increased, as expected. The MR samples, produced a failure mode which was audibly louder and more energetic in appearance than the Zoltek samples. All specimens tested exhibited the same failure mode at varying intensities. Per ASTM D3039-14 Fig. 4, the failure mode for every specimen was "XVV" Standing for X – Explosive, V – Various Failure Areas, and V – Various Failure Locations. Unfortunately, the average strength of the tape, 190 ksi, was well below the theoretical value of 370 ksi, indicating that the tape is not being optimally fabricated. The broken tapes are shown in Figure 21 and Figure 22, confirming that the energy of break for the MR-based materials is indeed higher.

Table 3. Summarized tape tension results comparing Zoltek and MR carbon fibers. Different sample numbers represent different locations on the roll from which the tapes were harvested.

| Material | Fiber Wt % | Avg. Ultimate Tensile Strength (ksi) | Std. Dev. | Avg. Young's Modulus (Msi) | Std. Dev. | Avg. Tensile Strain at Max Load (%) | Std. Dev. | Failure Mode | # of Specimens tested |
|---|---|---|---|---|---|---|---|---|---|
| Panex 35 + Polyamide (2A) | 59 | 154.43 | 23.99 | 12.71 | 0.01 | 2.68 | 0.2 | XVV | 3 |
| Panex 35 + Polyamide (2B) | 59 | 109.10 | 13.21 | 10.47 | 0.26 | 2.20 | 0.6 | XVV | 3 |
| Panex 35 + Polyamide (2C) | 59 | 154.34 | 5.19 | 12.49 | 0.49 | 2.83 | 0.6 | XVV | 3 |
| MR34-700 + Polyamide (4A) | 59 | 182.05 | 8.92 | 14.90 | 0.51 | 2.48 | 0.2 | XVV | 3 |
| MR34-700 + Polyamide (4B) | 59 | 161.08 | 22.64 | 11.50 | 1.25 | 2.50 | 0.1 | XVV | 3 |
| MR34-700 + Polyamide (4C) | 59 | 174.82 | 10.88 | 13.10 | 0.64 | 2.76 | 0.3 | XVV | 3 |
| MR34-700 + Polyamide (5A) | 64 | 203.00 | 17.60 | 14.58 | 0.29 | 2.51 | 0.3 | XVV | 3 |
| MR34-700 + Polyamide (5B) | 64 | 190.49 | 26.37 | 14.05 | 0.23 | 2.98 | 0.2 | XVV | 3 |
| MR34-700 + Polyamide (5C) | 64 | 180.86 | 8.55 | 14.05 | 2.03 | 2.74 | 0.1 | XVV | 3 |

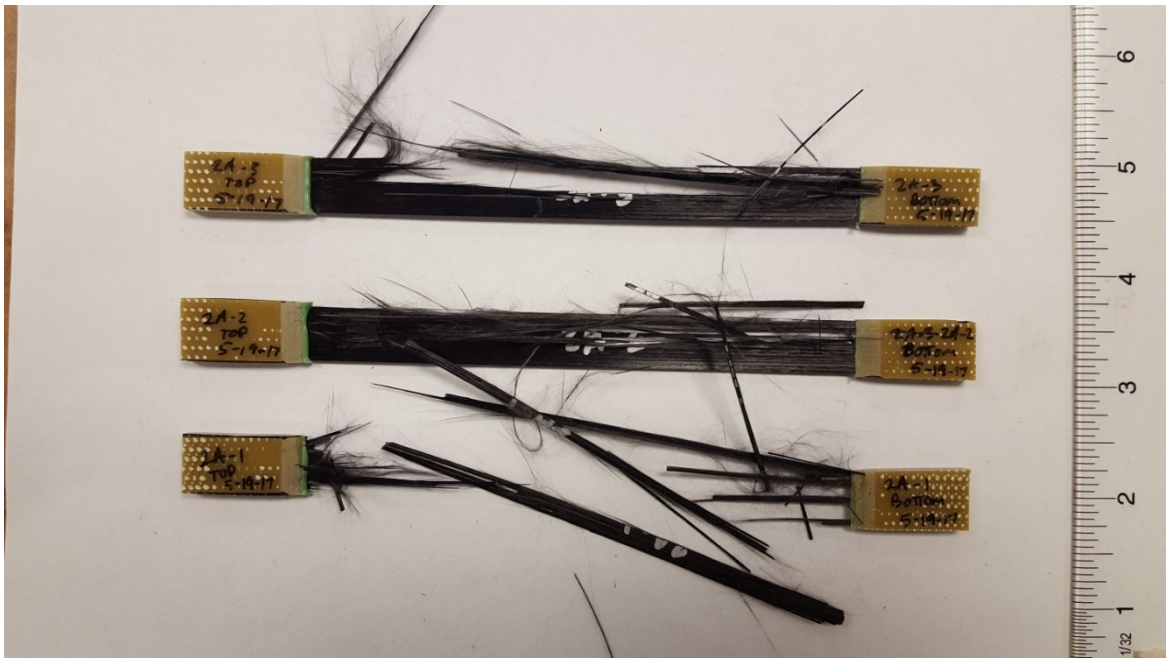

Figure 21. Example tape fracture with Panex 35 carbon fiber with polyamide.

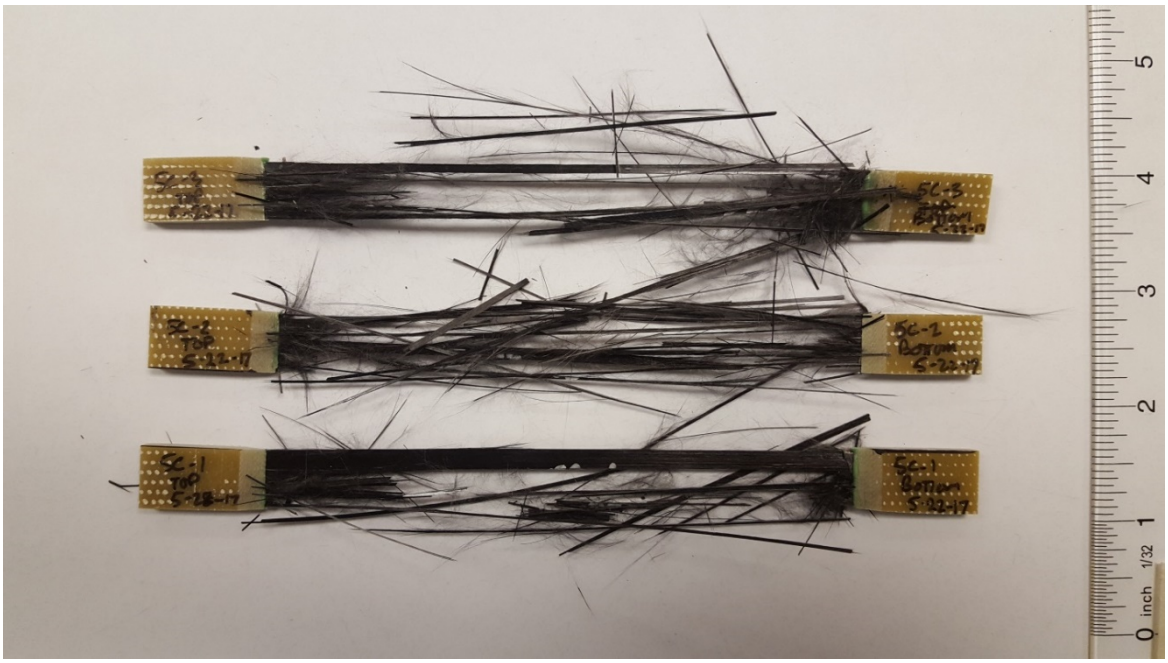

Figure 22. Example tape fracture with MR 34-700 carbon fiber with polyamide.

Microstructural characterizations of the tape were also performed. Figure 23 shows the surface of one of the tape samples, and reveals an area of misalignment on the surface. While the majority of the fiber does appear to be well aligned, areas such as this on the tape surface are not uncommon, and are due to idiosyncrasies of the Van Wees process. It can also be seen that there are inconsistencies in the amount of polymer resin on the tape surface, leading to shiny and matt areas. This effect disappears at higher resin content.

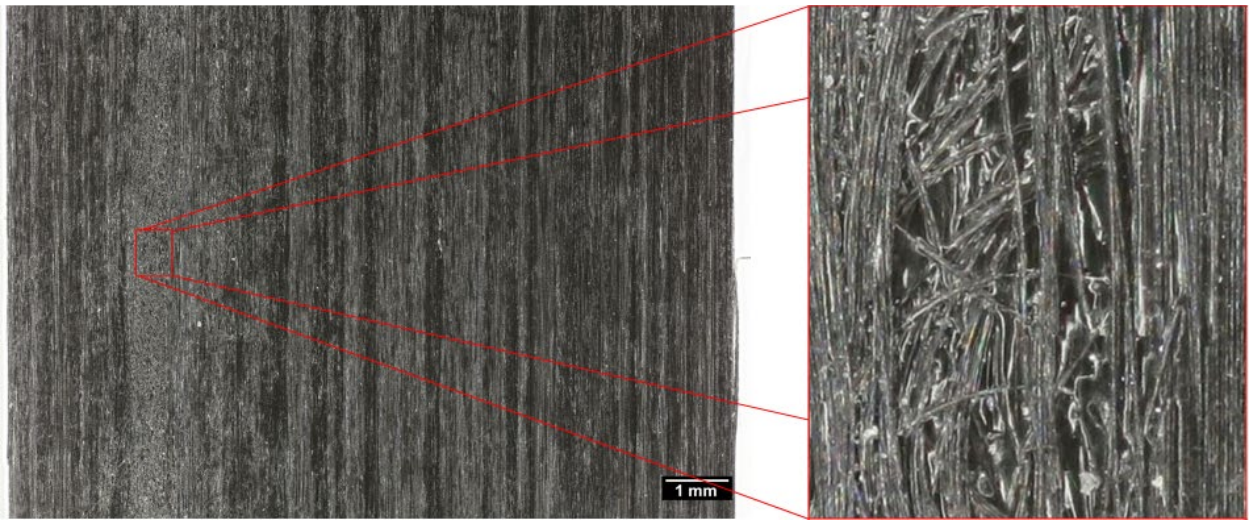


Figure 23. Optical micrograph of tape surface on Roll 13.

Fiber volumes were measured on several tape samples, and the results are shown in Table 4and Table 5 for tape rolls made under different processing conditions. Both show a slightly lower fiber concentration than predicted by the process conditions, and some residual porosity, with Roll 13 having more voids than Roll 11. However, the standard deviations on these values are relatively high, and the data should be viewed with this in mind.

Table 4. Fiber volume and void content for Roll 11B.

| | Laminate Physical Properties Determinations | | | | | | | |
|---|---|---|---|---|---|---|---|---|
| Tested By: | Daniel Korthauer | | | | | | | |
| Specimen Number | Wc (spec. wt.) (x.xxxx g) | Wf (Fiber wt.) (x.xxxx g) | F.C. (Fiber cont.) (x.xx Wt.%) | R.C. (Resin Cont.) (x.xx Wt.%) | Vf (Vol. of Fibers) (x.xxxx cm3) | Vc (Vol. of Comp.) (x.xxxx cm3) | Fiber Volume (x.xx Vol.%) | Void Volume (x.xx Vol.%) |
| 11B-PP4 | 1.0987 | 0.6558 | 59.6887 | 40.31 | 0.3643 | 0.7643 | 47.67 | 1.50 |
| 11B-PP5 | 1.0602 | 0.6617 | 62.4128 | 37.59 | 0.3676 | 0.7312 | 50.28 | 1.91 |
| 11B-PP6 | 1.1352 | 0.6794 | 59.8485 | 40.15 | 0.3774 | 0.7722 | 48.88 | -0.65 |
| | | **Avg. =** | **60.65** | **39.35** | | **Avg. =** | **48.94** | **0.92** |

Table 5. Fiber Volume and Void Content for Roll 13A.

| | Laminate Physical Properties Determinations | | | | | | | |
|---|---|---|---|---|---|---|---|---|
| Tested By: | | | | | | | | |
| Specimen Number | Wc (spec. wt.) (x.xxxx g) | Wf (Fiber wt.) (x.xxxx g) | F.C. (Fiber cont.) (x.xx Wt.%) | R.C. (Resin Cont.) (x.xx Wt.%) | Vf (Vol. of Fibers) (x.xxxx cm3) | Vc (Vol. of Comp.) (x.xxxx cm3) | Fiber Volume (x.xx Vol.%) | Void Volume (x.xx Vol.%) |
| 13A-PP1 | 1.0336 | 0.6404 | 61.9582 | 38.04 | 0.3558 | 0.7084 | 50.22 | 1.09 |
| 13A-PP2 | 1.1359 | 0.6729 | 59.2394 | 40.76 | 0.3738 | 0.7845 | 47.65 | 0.57 |
| 13A-PP3 | 1.1201 | 0.6779 | 60.5214 | 39.48 | 0.3766 | 0.7789 | 48.35 | 1.85 |
| | | **Avg. =** | **60.57** | **39.43** | | **Avg. =** | **48.74** | **1.17** |

As shown in Figure 24 and Figure 25, the room temperature strength of Roll 11 is slightly higher than Roll 13, while the modulus is the same within experimental error. In order to see if this was due to creep of the PA matrix during testing, the test was run as -65F (-54C), with the result shown in Figure 26 and Figure 27. The tensile strength was shown to decrease slightly, while the modulus was mostly unchanged, suggesting that matrix creep was not a likely cause for the lower-than-theoretical mechanical testing results.

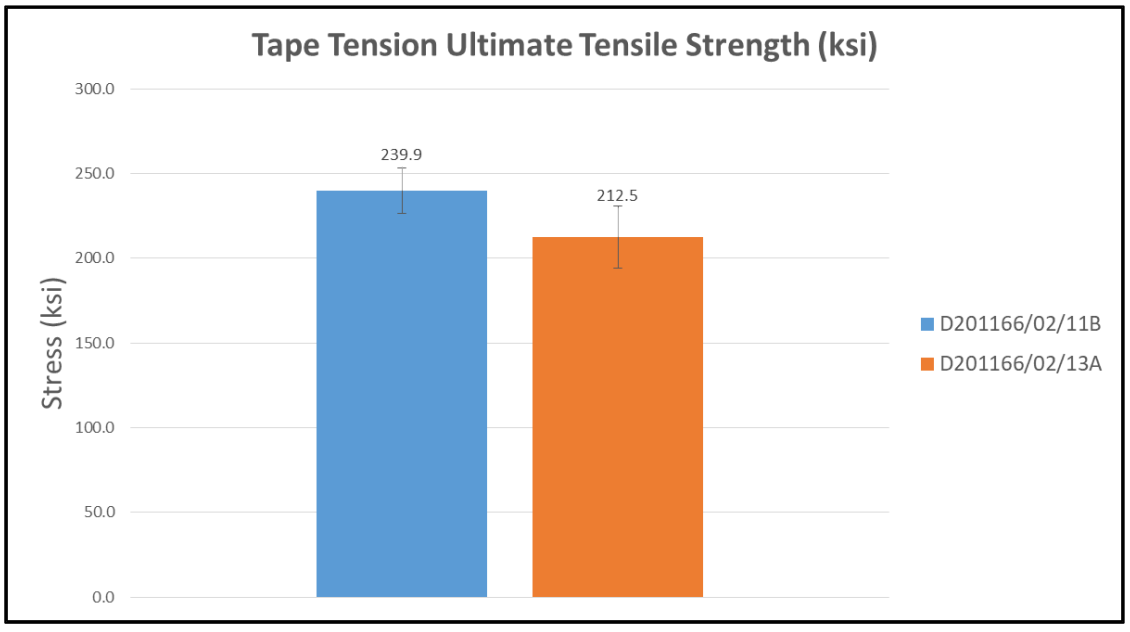


Figure 24. Single layer tape tensile strength results for Rolls 11B and 13A.

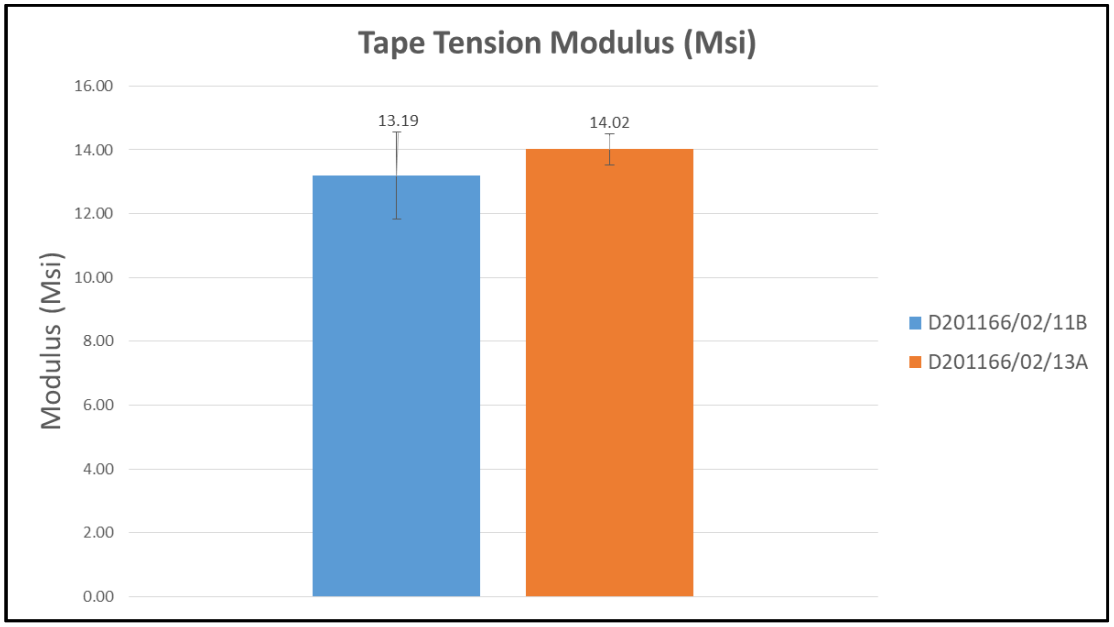


Figure 25. Single layer tape tensile modulus results for Rolls 11B and 13A.

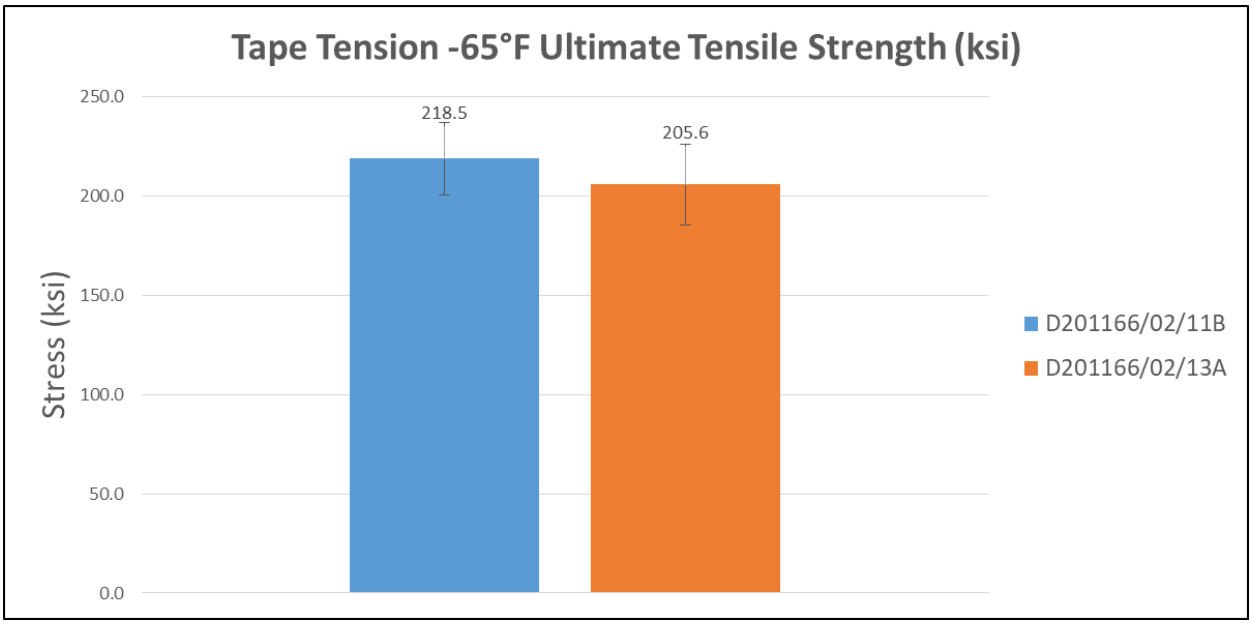


Figure 26. Tensile strength results for Rolls 11B and 13A at -65F.

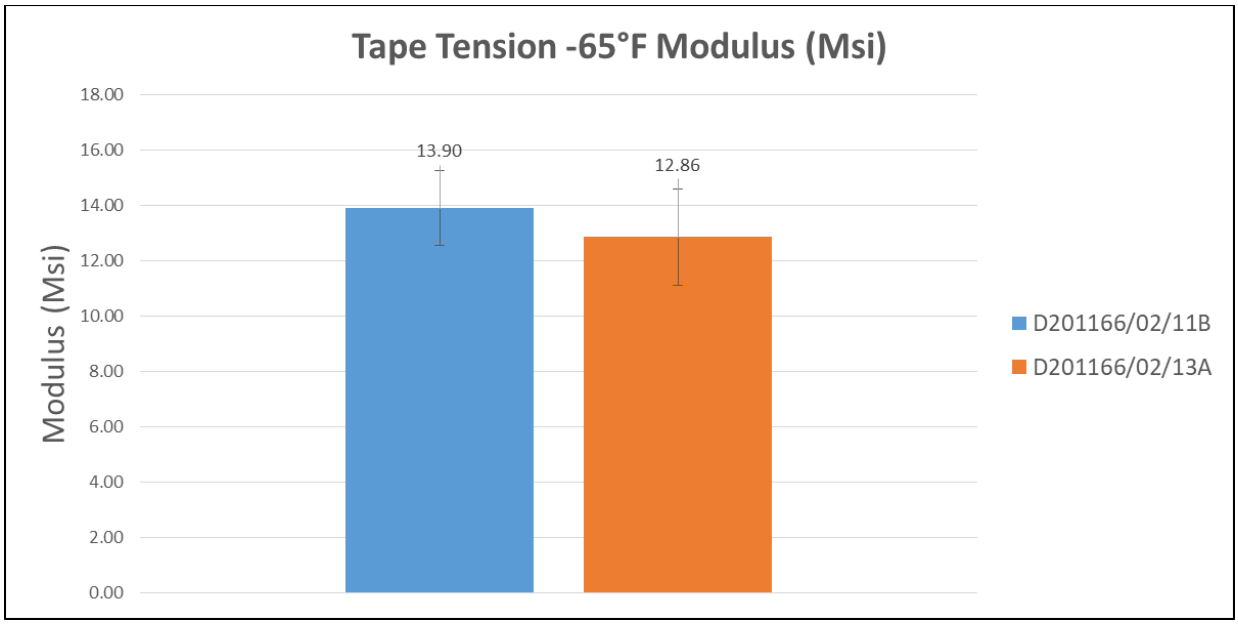


Figure 27. Tensile modulus results for Rolls 11B and 13A at -65F.

Tapes of various lengths were tabbed and tensile tested. The five inch tests were run at UDRI, with the rest being performed at DuPont. The results are shown in Table 6 The yarn grips are shown in Figure 28.

Table 6. Effect of gauge length on tape strength.

| Gauge Length (in) | Failure Stress (ksi) | St. Dev, (ksi) |
|---|---|---|
| 2 | 251 | 10.9 |
| 4 | 235 | 16.8 |
| 5 | 240 | 13.4 |
| 8 | 214 | 16.7 |
| Yarn grips | 232 | 31 |

A Weibull plot of the strength of the tape as a function of gauge length is shown in Figure 29. As expected, the data shows that the strength decreases as the gauge length increases. This means that increasing the length of the sample increases the number of flaws in the sample. If the flaw size distribution is normal, increasing the number of flaws will increase the size of the largest flaw present, decreasing the strength of the materials being tested. However, the data is over too limited a gauge length to determine the actual length functionality in the traditional Weibull sense.


Figure 28. Yarn grips used for tensile testing. Note that there is not a well-defined gauge length.

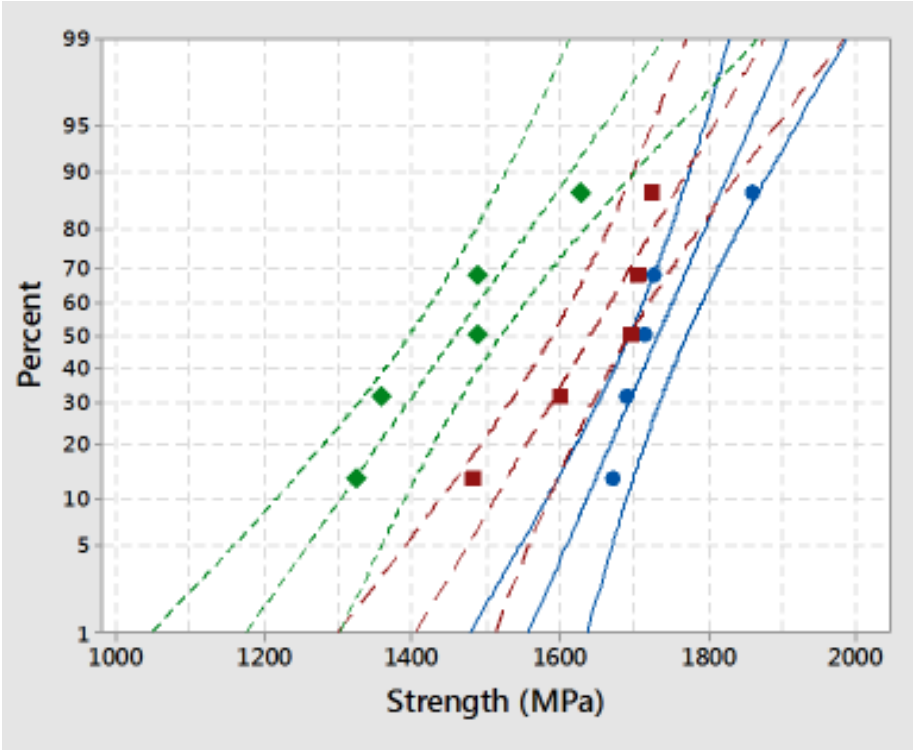


Figure 29. Weibull plot of failure strength as a function of the tape gauge length for materials tested at DuPont, blue – 2 inch, red – 4 inch, and green – 8 inch.

In order to understand the flaws further, the tapes were subsequently tested at two different widths, with the results shown in Figure 30 and Figure 31. All of the tapes tested were from Master Roll 11, with different samples being taken from different portions of the rolls. The first feature of this graph is that the strength of the tapes are reasonably uniform from end to end, validating that the tape manufacturing process is reasonably consistent. It can be seen from the data that the ½ inch and ¼ inch tapes had very similar strengths.

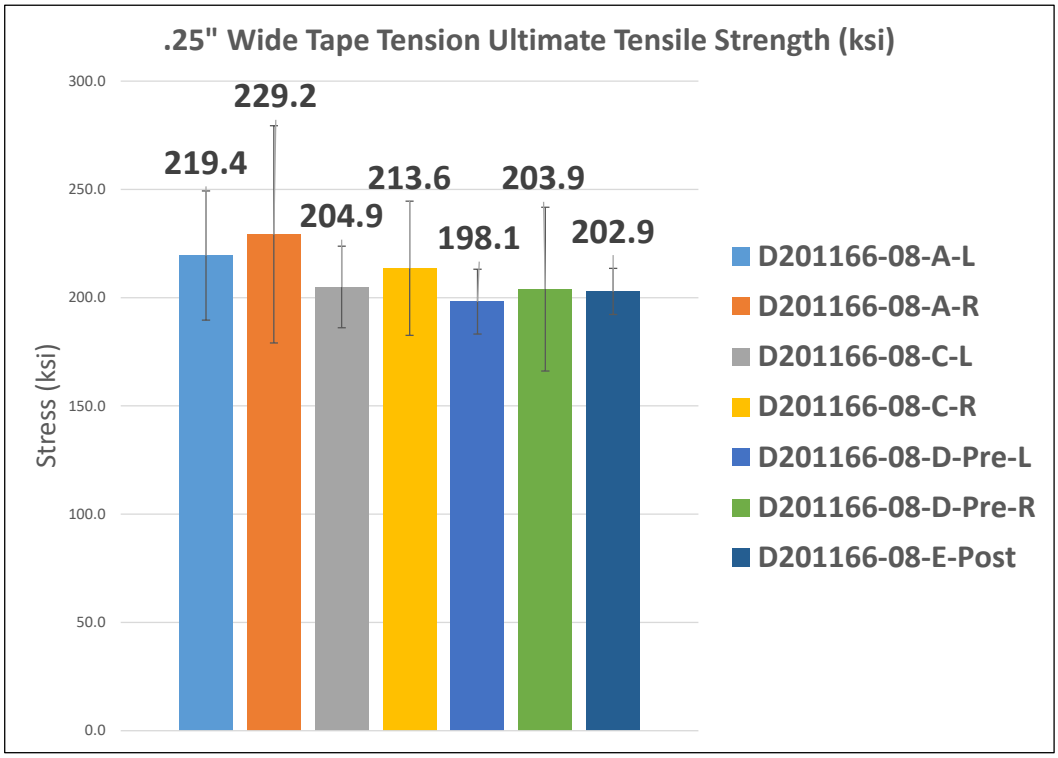


Figure 30. Tensile strength of Roll 11 tapes of quarter inch width. Each bar is data from the same tape taken at various portions along the roll.

When the data is aggregated with respect to the tape width, the result is somewhat clearer. This is illustrated in Figure 32, where the Weibull Plot shows the distributions for the different tape widths coinciding. This result suggests that the strength limiting defect is not associated with the volume of the tape, but rather with the length of the tape. This is a somewhat surprising result and suggests that the strength limiting flaws might be associated with the edges and surfaces of the tape.

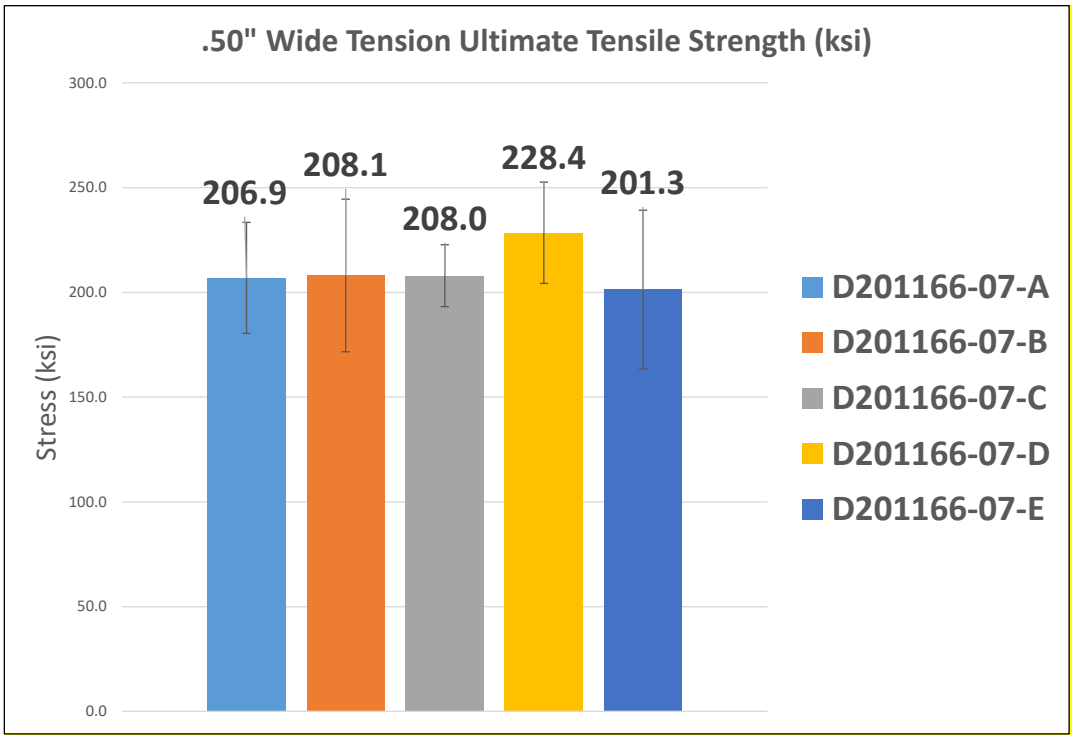


Figure 31. Tensile strength of Roll 11 tapes of half inch width. Each bar is data from the same tape taken at various portions along the roll.

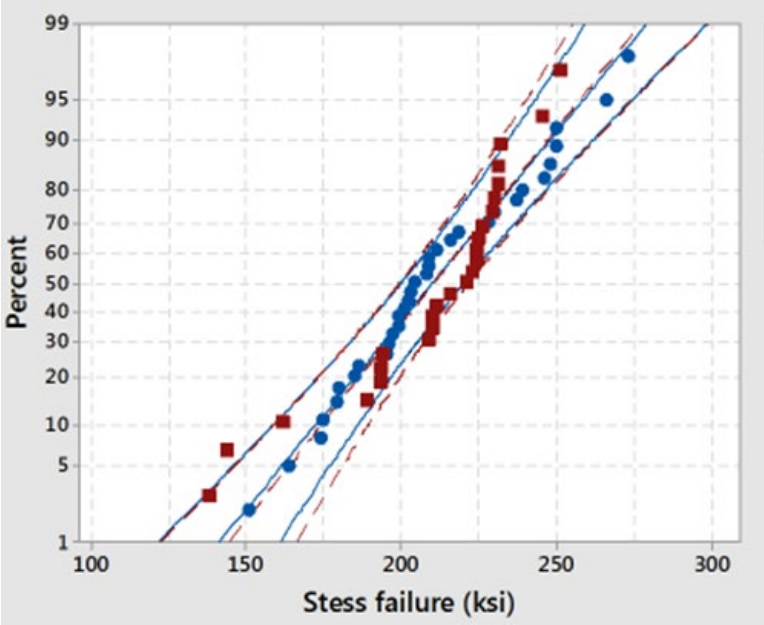


Figure 32. Weibull plot of failure strength as a function of tape width, red - half inch, blue - quarter inch.

Five specimens were tested for short beam shear (SBS) strength according to ASTM D2344-16. The results are shown in Table 7. The average strength was 9,561.4 psi

Table 7. Short beam shear results from AFP ring made at 330C, 12 inches per second, and 200 pounds pressure.

| | Specimen label | Width (in) | Thickness (in) | Extension @ Max. Load (in) | Maximum Load (lbf) | Short Beam Shear Strength (psi) | Failure Mode |
|---|---|---|---|---|---|---|---|
| 1 | 07-11-SBS-1 | 0.248 | 0.1247 | 0.040 | 387.5 | 9,417.4 | Interlaminar Shear/ Inelastic Deformation |
| 2 | 07-11-SBS-2 | 0.253 | 0.1265 | 0.045 | 418.4 | 9,804.8 | Interlaminar Shear/Inelastic Deformation |
| 3 | 07-11-SBS-3 | 0.252 | 0.1269 | 0.037 | 407.6 | 9,540.7 | Interlaminar Shear/Inelastic Deformation |
| 4 | 07-11-SBS-4 | 0.247 | 0.1227 | 0.035 | 394.5 | 9,758.2 | Interlaminar Shear/Inelastic Deformation |
| 5 | 07-11-SBS-5 | 0.243 | 0.1213 | 0.044 | 365.0 | 9,286.0 | Interlaminar Shear/Inelastic Deformation |
| Mean | | 0.249 | 0.1244 | 0.041 | 394.6 | 9,561.4 | |
| Stand. Dev. | | 0.004 | 0.002 | 0.004 | 20.399 | 220.774 | |
| Coeff. of Var. % | | 1.68 | 1.94 | 10.26 | 5.17 | 2.31 | |

The physical properties of the ring used to fabricate the SBS samples are shown in Table 8. It should be noticed that the void volume was very low for this sample.

Table 8. Physical properties for ring used for fabrication of short beam shear samples.

| Specimen Number | Wc (spec. wt.) (x.xxxx g) | Wf (Fiber wt.) (x.xxxx g) | F.C. (Fiber cont.) (x.xx Wt.%) | R.C. (Resin Cont.) (x.xx Wt.%) | Vf (Vol. of Fibers) (x.xxxx cm3) | Vc (Vol. of Comp.) (x.xxxx cm3) | Fiber Volume (x.xx Vol.%) | Void Volume (x.xx Vol.%) |
|---|---|---|---|---|---|---|---|---|
| 201166-07-11-PP-1 | 1.7011 | 1.0202 | 59.9730 | 40.03 | 0.5668 | 1.1651 | 48.64 | 0.09 |
| 201166-07-11-PP-2 | 1.5668 | 0.9258 | 59.0886 | 40.91 | 0.5143 | 1.0732 | 47.93 | -0.32 |
| 201166-07-11-PP-3 | 1.5552 | 0.9222 | 59.2978 | 40.70 | 0.5123 | 1.0674 | 48.00 | -0.02 |
| | | **Avg. =** | **59.45** | **40.55** | | **Avg. =** | **48.19** | **-0.08** |

Photomicrographs were obtained from polished cross-sections of the tape, representative images of which appear in Figure 33. From these images, it can be seen that there is a small amount of residual porosity in the tape. That porosity is located within incompletely impregnated fiber tows. It can also be seen in Figure 34 that, if the tape if broken by hand in bending, the fracture surface has undried fibers protruding. This is due to a relatively small number of unwetted carbon fibers in the tape, consistent with the optical microscopy results.

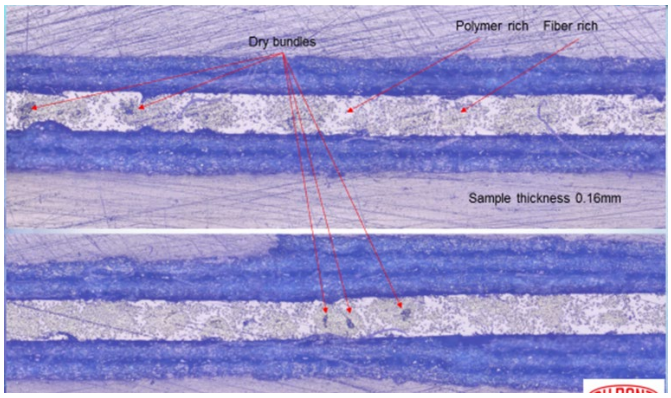


Figure 33. Photomicrographs of polished cross-sections of UD tape. The tape thickness is 0.17mm. The dark blue material is tape used to prevent potting material intrusion into the tape during sample preparation.

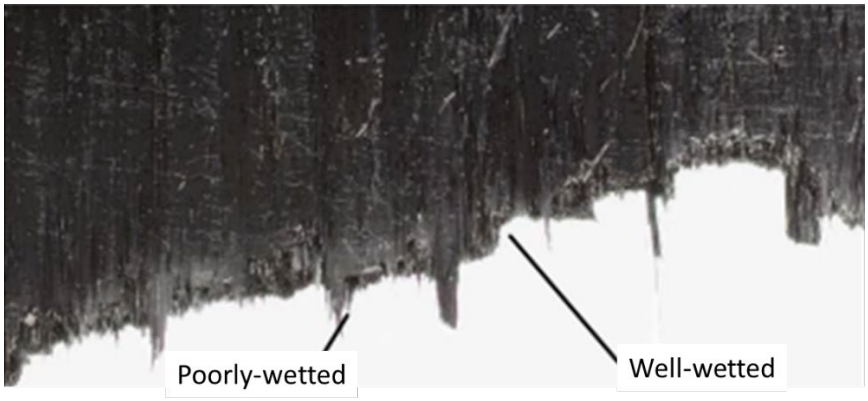


Figure 34. Optical micrograph of tape fracture surface confirming the presence of unwetted fiber bundles.

The next characterization was to press plaques of the tape, where the fiber ran in one direction only. At DuPont, a 1mm by 3" by 10" plaque was molded at 310C and 140 psi, and held at temperature for 2 minutes before being quenched between cold platens. After cutting to a 1 inch width with a diamond-impregnated wet saw and not further preparing the edges, the specimen was tested in bending. This material had a modulus of 18.5 Msi and a strength of 290 ksi, as compared to the theoretical properties of this composite were 15.3 Msi for the modulus and 315 ksi for the strength. The above-theoretical modulus is accounted for by the polymer flash that escaped the mold during processing while the strength was 92% of the theoretical value. This result suggests that the molding conditions further impregnated the tows, and the fiber is not significantly degraded by the tape-making process. The lack of porosity is confirmed in the polished cross-section shown in Figure 35.

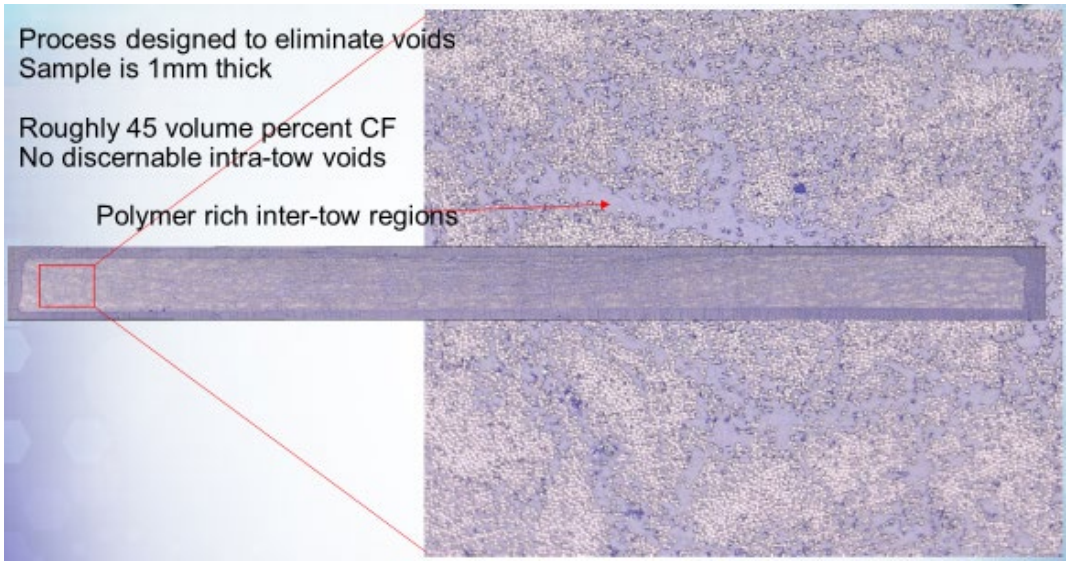

Figure 35. Photomicrograph of a polished cross-section of 1mm thick plaque showing no residual porosity.

A similar study was performed at UDRI, with the processing conditions described in Appendix 1. In contrast with the work described above, this material was tested in tension. In

Table 9, the elastic modulus of 19 Msi suggests that the volume content of carbon fiber content is about 56 volume percent, although the strength is well below the predicted level of 390 ksi.

An image of a representative sample after tensile testing is shown in Figure 36. The state of debris shows that the failure was explosive, resulting in the complete disintegration of the sample. A polished cross-section of a similar sample, shown in Figure 37, suggests a very low level of, if any, residual voids in the sample after pressing. The inter-tape interfaces are not visible, indicating complete consolidation of the sample.

These 3 mini-panels had an average UTS of 291 ksi. These are the best results we have seen to date with one specimen exhibited a tensile strength of 316.8 ksi. While this sample does not include enough specimens to be statistically significant, the results did show an increase in performance over the single ply tension tests and the flat panel laminates originally produced at CPC with Automated Dynamics equipment. This would suggest that producing flat laminates via the ATP process is too difficult and may require specialized tooling in order to develop flat samples with the properties to which this material should be entitled.

As a result of the tape testing, the Team concluded that the as-fabricated tape can be described as follows:

1) The carbon fiber being mostly aligned in the machine longitudinal direction of the tape with minority areas of misalignment on the surfaces
2) The surfaces of the tapes vary in resin content
3) There is a small but measurable level of intra-bundle voids, or “dry bundles”. The void level is shown to be less than 2%.
4) The strength and modulus of the tapes were found to be less than theoretical
5) The strength loss is believed to be associated with the edges of the tapes
6) The voids in the tape as well as the voids between tapes were eliminated by hot pressing
7) Hot pressed plaques attained theoretical levels of modulus, although the strength was still less than expected.

Table 9. Results of tensile testing for pressed UD plaque at UDRI. Each data point is for a separate sample cut from a single plaque.

| Specimen I.D. | Load of First Audible Pinging (lbs) | Stress of First Audible Pinging (ksi) | Stress at Faillure (ksi) | Strain at Failure (%) | Modulus (1.3% to 2.3%) (Msi) | Failure Mode |
|---|---|---|---|---|---|---|
| 20180209-1-T1 | 2900 | 137 | 257.6 | 1.59 | 15.30 | XVV |
| 20180209-1-T2 | 5000 | 234 | 302.9 | 1.94 | 21.10 | XVV |
| 20180209-2-T3 | 5100 | 234 | 316.8 | 1.71 | 20.63 | XVV |
| 20180209-2-T4 | 4567 | 209 | 279.8 | 1.43 | 20.17 | XVV |
| 20180209-3-T5 | 2850 | 133 | 292.3 | 1.81 | 18.12 | XVVw Longitudinal |
| 20180209-3-T6 | 3498 | 160 | 296.3 | 1.43 | 18.77 | XVV |
| **Average** | **3986** | **184** | **291.0** | **1.64** | **19.02** | |
| **Standard Dev.** | **941** | **43** | **18.6** | **0.20** | **1.95** | |
| **Coeff. Of Var** | **24%** | **23%** | **6%** | **12%** | **10%** | |

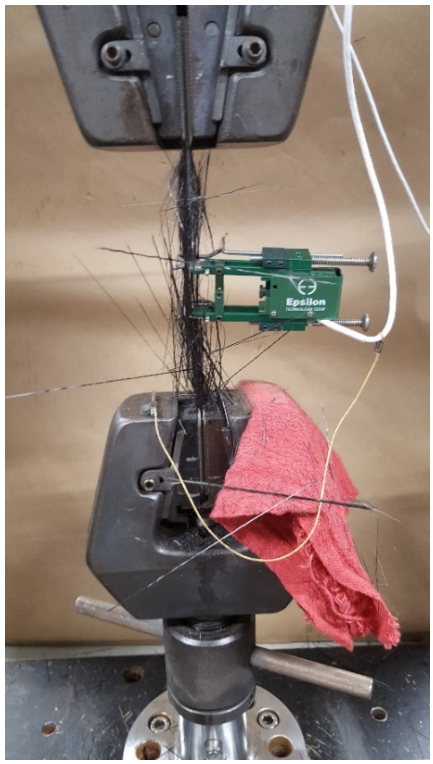


Figure 36. Explosive fracture resulting from tension testing of UDRI compression molded tape laminate.

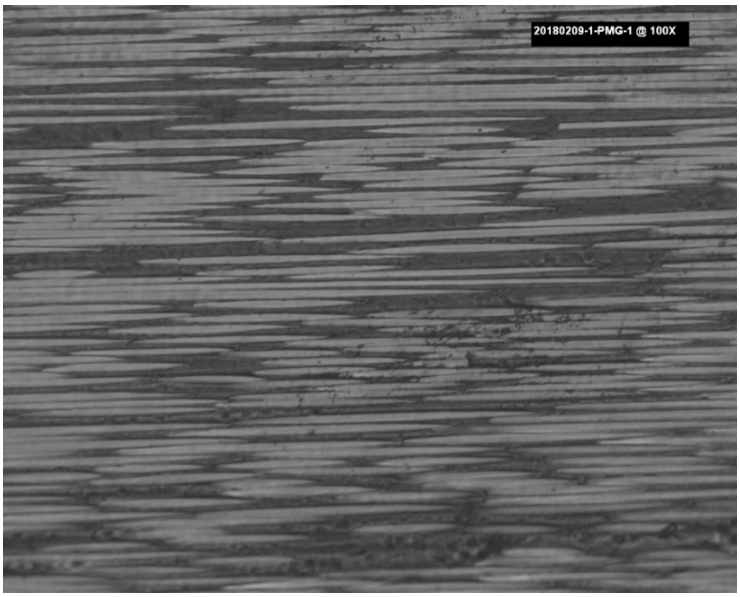

Figure 37. Optical microscopy of polished cross-section of UDRI compression molded laminate.

## 5.5 AFP Condition Optimization

Because it had been demonstrated that complete consolidation of the tape during hot pressing resulted in attaining the theoretical composite modulus, the Team decided that, rather than optimize the tape fabrication process, it was important to understand how the tape properties translated to vessel properties. Therefore, after tape characterization, the conditions for tape laydown using AFP were explored and optimized. The three processing conditions over which the laydown optimization experiment was initially designed were: processing laydown temperature, consolidation pressure, and laydown speed. The rings were made by first laying down a single layer of UD tape that covered the entire mandrel. Over this, multiple rings were built by continuously wrapping the tape over itself with keeping the laydown head stationary, and with the laser continuously fusing each progressive layer. A single layer of tape is 0.17 mm thick, and the robot was programmed to apply 25 layers. A typical ring build is shown in Figure 5. After fabrication, the rings were sent to UDRI for trimming to one quarter inch widths and subsequent characterization As described in Appendix 1.

The experiment was designed with three independent process variables; with the laydown temperature varied from 330 to 390 degrees C, the laydown rate varied from 3 to 12 inches per minute, and the compaction pressure varied from 150 to 200 pounds. The design called for the fabrication of samples at the corners of the cubic process-variable space. The resulting data was imported into Minitab, where it was modeled for effects and statistical significance. The individual design data along with the experimental results are shown in Appendix 1. Some combinations of process variables are not included, as the high temperature sometimes resulted in failure of the AFP process when the tape stuck to the compaction roller.
Before starting AFP optimization, the best tape had to be chosen from the tape optimization effort performed at Van Wees. For this, the team used a variety of processing conditions to identify the material to be used in the remainder of the study. The processing conditions are

listed in Appendix 1, Table 21. Table 10 through Table 12 show the detailed data on the effect of varying the AFP processing temperature (300°C to 390°C), the compaction force (150 lbs. to 200 lbs.), and the lay down speed (3 in./second to 12 in./second), on tapes made under three different fabrication conditions at Van Wees. The strength results show that Tape Roll 11 generated rings with the highest strength.

Table 10. ASTM D2290 tension results (RT dry)

| Ring I.D. | Roll I.D. | Matrix | Compaction (lbs) | Processing Temperature (°C) | Lay Down Speed (in./s) | Specific Gravity | Ultimate Tensile Strength (ksi) |
|---|---|---|---|---|---|---|---|
| 201166-03-5 | 9B | VZL36D | 150 | 300 | 3 | 1.4083 | 163.1 |
| 201166-03-12 | 9C | VZL36D | 150 | 300 | 3 | 1.4265 | 167.5 |
| 201166-03-2 | 9B | VZL36D | 150 | 300 | 12 | 1.4096 | 145.9 |
| 201166-03-14 | 9C | VZL36D | 150 | 330 | 3 | 1.4398 | 171.5 |
| 201166-03-8 | 9B | VZL36D | 150 | 330 | 12 | 1.4174 | 171.3 |
| 201166-03-13 | 9C | VZL36D | 150 | 330 | 12 | 1.4320 | 170 |
| 201166-03-10 | 9C | VZL36D | 200 | 300 | 3 | 1.4276 | 168.8 |
| 201166-03-3 | 9B | VZL36D | 200 | 300 | 12 | 1.4416 | 145.5 |
| 201166-03-11 | 9C | VZL36D | 200 | 330 | 3 | 1.4025 | 168.5 |
| 201166-03-4 | 9A | VZL36D | 200 | 330 | 12 | 1.4233 | 166.9 |
| 201166-03-15 | 9D | VZL36D | 200 | 330 | 12 | 1.4333 | 167.6 |
| 201166-03-1 | 9A | VZL36D | 200 | 360 | 7.5 | 1.4402 | 172.5 |

Table 11. ASTM D2290 tension results (RT dry)

| Ring I.D. | Roll I.D. | Matrix | Compaction (lbs) | Processing Temperature (°C) | Lay Down Speed (in./s) | Specific Gravity | Ultimate Tensile Strength (ksi) |
|---|---|---|---|---|---|---|---|
| 201166-04-5 | 10A | VZL36D modified | 150 | 300 | 3 | 1.4255 | 168.1 |
| 201166-04-12 | 10A | VZL36D modified | 150 | 300 | 3 | 1.4272 | 164.6 |
| 201166-04-2 | 10A | VZL36D modified | 150 | 300 | 12 | 1.4214 | 174.8 |
| 201166-04-11 | 10A | VZL36D modified | 150 | 330 | 3 | 1.4319 | 158.5 |
| 201166-04-14 | 10A | VZL36D modified | 150 | 330 | 3 | 1.4332 | 169.9 |
| 201166-04-8 | 10A | VZL36D modified | 150 | 330 | 12 | 1.4408 | 177.5 |
| 201166-04-13 | 10A | VZL36D modified | 150 | 330 | 12 | 1.4335 | 162.5 |
| 201166-04-10 | 10A | VZL36D modified | 200 | 300 | 3 | 1.4289 | 175.9 |
| 201166-04-3 | 10A | VZL36D modified | 200 | 300 | 12 | 1.4356 | 183 |
| 201166-04-4 | 10A | VZL36D modified | 200 | 330 | 12 | 1.4334 | 179.9 |
| 201166-04-15 | 10A | VZL36D modified | 200 | 330 | 12 | 1.4407 | 188.9 |

Table 12. ASTM D2290 tension results (RT dry).

| Ring I.D. | Roll I.D. | Matrix | Compaction (lbs) | Processing Temperature (°C) | Lay Down Speed (in./s) | Specific Gravity | Ultimate Tensile Strength (ksi) |
|---|---|---|---|---|---|---|---|
| 201166-05-5 | 11A | VZL36D modified | 150 | 390 | 3 | 1.4509 | 190.1 |
| 201166-05-12 | 11A | VZL36D modified | 150 | 390 | 3 | 1.4630 | 197.4 |
| 201166-05-2 | 11A | VZL36D modified | 150 | 390 | 12 | 1.4678 | 191.6 |
| 201166-05-8 | 11A | VZL36D modified | 150 | 390 | 12 | 1.4624 | 200.8 |
| 201166-05-7 | 11A | VZL36D modified | 200 | 330 | 3 | 1.4523 | 173.6 |
| 201166-05-11 | 11A | VZL36D modified | 200 | 330 | 3 | 1.4578 | 191.6 |
| 201166-05-4 | 11A | VZL36D modified | 200 | 330 | 12 | 1.4314 | 182.3 |
| 201166-05-15 | 11A | VZL36D modified | 200 | 330 | 12 | 1.4598 | 196.4 |
| 201166-05-6 | 11A | VZL36D modified | 200 | 360 | 7.5 | 1.4561 | 181.3 |
| 201166-05-9 | 11A | VZL36D modified | 200 | 360 | 7.5 | 1.4608 | 190.9 |
| 201166-05-10 | 11A | VZL36D modified | 200 | 390 | 3 | 1.4673 | 207.2 |
| 201166-05-14 | 11A | VZL36D modified | 200 | 390 | 3 | 1.4640 | 199 |
| 201166-05-3 | 11A | VZL36D modified | 200 | 390 | 12 | 1.4602 | 193 |
| 201166-05-13 | 11A | VZL36D modified | 200 | 390 | 12 | 1.4700 | 206.3 |

The resulting data is summarized in Figure38, Figure 39, and Figure 40, and shows the relationships between these process variables and the measured properties. In all cases, graphs with white backgrounds indicate statistically significant dependencies, where graphs with gray backgrounds indicate a lack of statistical significance.

Figure 38 shows that the ring thickness after the laydown of 25 tape layers was affected by all of the independent process variables with statistical significance. The temperature is shown to have the largest single effect because the reduction in polymer viscosity allowed the tape to spread more under the compaction roller. Similarly, because reducing the application speed allowed for enhanced heat soak, a reduced laydown rate also produced thinner rings. Finally, because a higher compaction pressure results in enhanced spreading, increased pressure results in thinner rings. There were no significant interactions between the process variables.

It should be noted that the maximum thickness measured for any process variable combination was 3.4 mm. Assuming that no compaction took place, a 25 layer ring should be 3.7mm thick. This suggests that under the mildest processing conditions, there was a measureable level of compaction, and the layers were almost entirely fused. Under more energetic laydown conditions, the ring thickness was reduced to 2.7mm, or a 27% reduction over a ring consisting of underformed tape. In these samples, the ring was significantly broader at the outer surface than at the inner surface, showing that the amount of tape spreading increased as the ring-building process progressed.

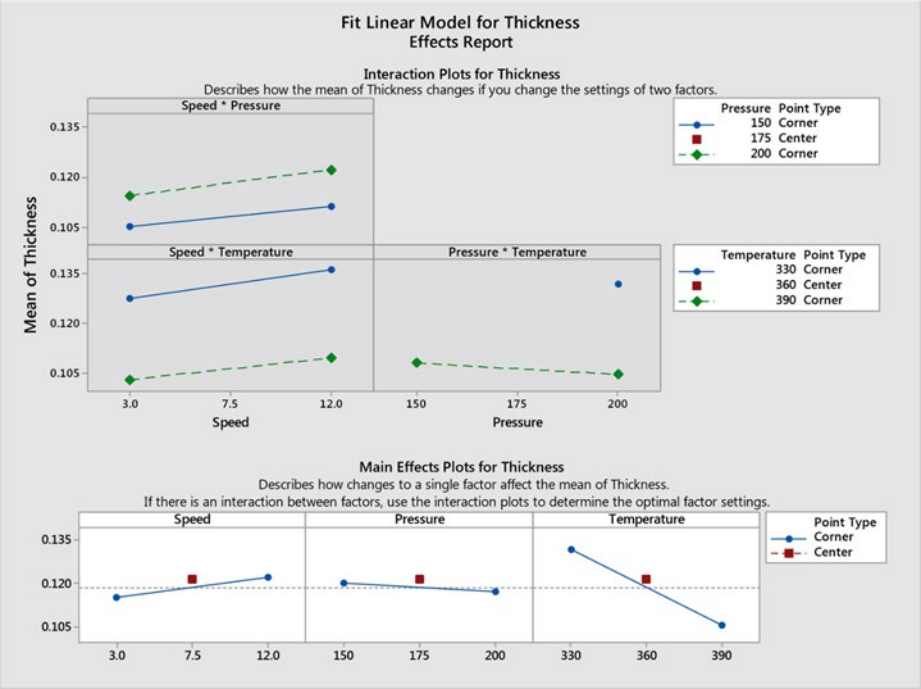


Figure 38. Results of designed experiment - dependence of ring thickness in inches on process variables.

The ring density, measured using the Archimedes method, is shown as a function of the process variables in Figure 39. In contrast to the ring thickness, density is shown to be only a function of the process temperature. It is clearly shown that the ring density increases with laydown temperature, indicating that the inter-tape and intra-tow voids are being eliminated during the process at high temperatures. This corroborates the thickness data shown above. Once again, there are no statistically significant interactions between the process variables.

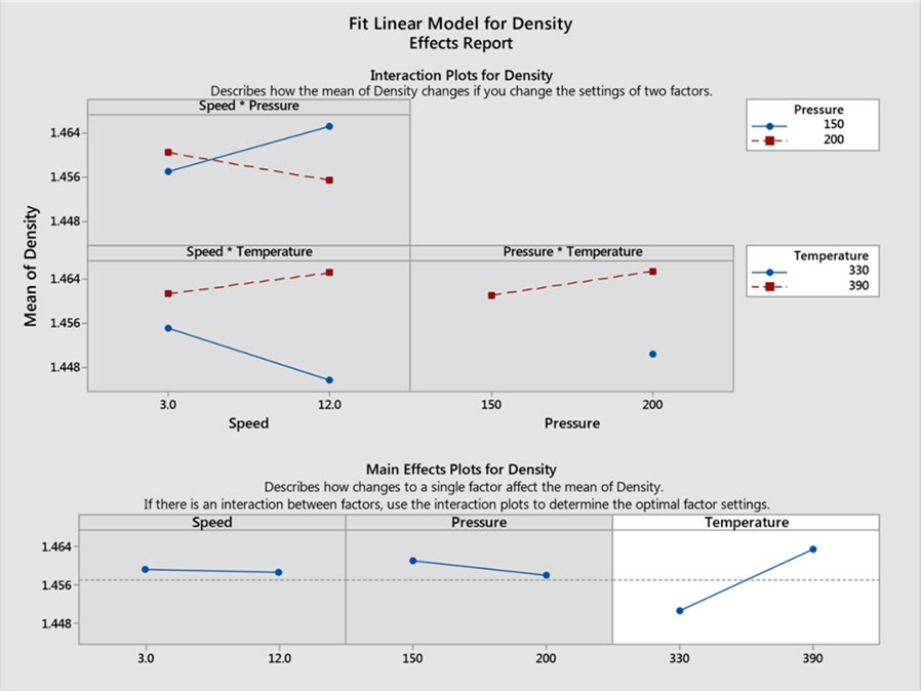


Figure 39. Results of designed experiment - dependence of ring density in g/cc on process variables.

The strength of the rings was measured using ASTM D2290-16 and results are shown in Figure 40. In this test, the ring is placed around a split disc mounted on a test frame, and each half is pulled such that the ring breaks predominantly in tension, As described in Appendix 1. The results of this test show that temperature is the only variable of statistical significance, with increased temperature improving the strength markedly.

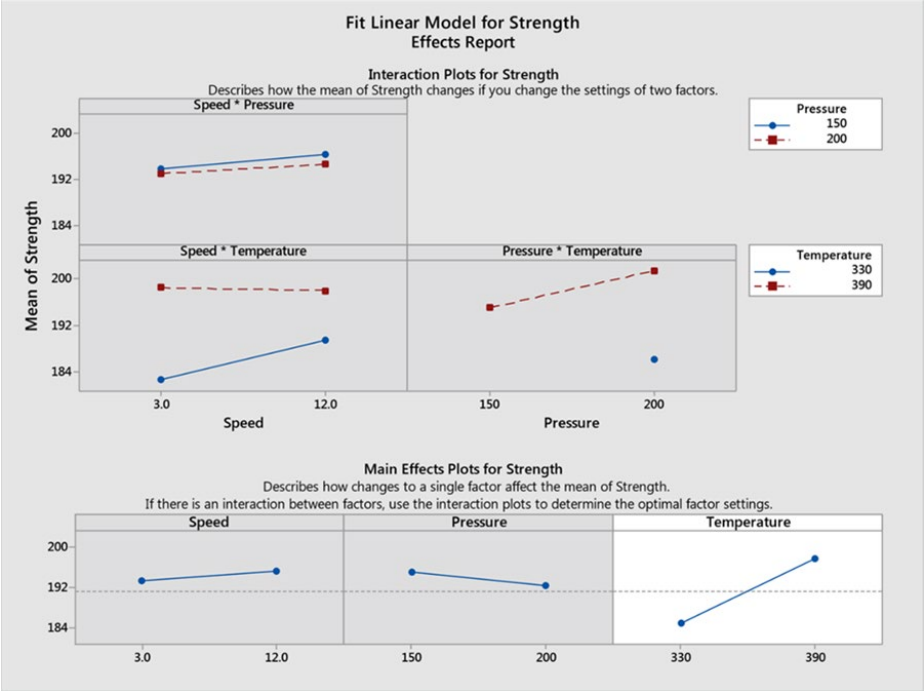


Figure 40. Results of designed experiment - dependence of ring strength in ksi on process variables.

The strength results corroborate the density results in that the strength and density reflect how well the defects in the composite are eliminated. In this case the most obvious defects are the inter-tape and intra-tow voids. Elimination of intra-tow voids, or dry-fiber, has been shown to increase strength as decreasing voids allows more of the fiber to be involved in resisting the load that is applied. Dry, or un-wetted fibers, are unable to cooperatively bear the test-load, resulting in premature composite failure.

Table 13 tabulates the fiber volume and void content for the 5.75” diameter rings. While they all have a low void content, ring 201166-5-1 has a significantly higher fiber volume content and would be expected to have improved mechanical properties as a result.

Table 13. Summary of physical properties for 5.75” diameter ring specimens.

| Specimen Number | Wc (spec. wt.) (x.xxxx g) | Wf (Fiber wt.) (x.xxxx g) | F.C. (Fiber cont.) (x.xx Wt.%) | R.C. (Resin Cont.) (x.xx Wt.%) | Vf (Vol. of Fibers) (x.xxxx cm3) | Vc (Vol. of Comp.) (x.xxxx cm3) | Fiber Volume (x.xx Vol.%) | Void Volume (x.xx Vol.%) |
|---|---|---|---|---|---|---|---|---|
| 201166-3-7-PP-1 | 1.5792 | 0.8740 | 55.34 | 44.66 | 0.4856 | 1.1113 | 43.69 | 0.65 |
| 201166-3-7-PP-2 | 1.5320 | 0.9242 | 60.33 | 39.67 | 0.5134 | 1.0789 | 47.59 | 2.99 |
| 201166-3-7-PP-3 | 1.6021 | 0.8766 | 54.72 | 45.28 | 0.4870 | 1.1290 | 43.13 | 0.50 |
| | | **Avg. =** | **56.80** | **43.20** | | **Avg. =** | **44.81** | **1.38** |
| 201166-4-7-PP-1 | 1.7303 | 0.9927 | 57.37 | 42.63 | 0.5515 | 1.2117 | 45.51 | 1.09 |
| 201166-4-7-PP-2 | 1.6777 | 0.9348 | 55.72 | 44.28 | 0.5193 | 1.1749 | 44.20 | 0.33 |
| 201166-4-7-PP-3 | 1.6667 | 0.9385 | 56.31 | 43.69 | 0.5214 | 1.1655 | 44.73 | 0.46 |
| | | **Avg. =** | **56.47** | **43.53** | | **Avg. =** | **44.82** | **0.63** |
| | | | | | | | | |
| 201166-5-1-PP-2 | 1.4095 | 0.8836 | 62.69 | 37.31 | 0.4909 | 0.9654 | 50.85 | 1.37 |
| 201166-5-1-PP-3 | 1.4104 | 0.8654 | 61.36 | 38.64 | 0.4808 | 0.9660 | 49.77 | 0.74 |
| 201166-5-1-PP-4 | 1.0512 | 0.6646 | 63.22 | 36.78 | 0.3692 | 0.7180 | 51.42 | 1.35 |
| 201166-5-1-PP-5 | 1.0832 | 0.7039 | 64.98 | 35.02 | 0.3911 | 0.7424 | 52.67 | 2.51 |
| 201166-5-1-PP-6 | 1.0571 | 0.6652 | 62.93 | 37.07 | 0.3696 | 0.7196 | 51.36 | 0.87 |
| | | **Avg. =** | **65.65** | **34.35** | | **Avg. =** | **53.27** | **1.37** |

As a result of this optimization work, it was concluded that high temperatures were most beneficial, with high compaction pressure and low speed helping somewhat. Unfortunately, while the Team would have liked to design a CPV process at 390C, the process temperature had to be limited to 360C to limit degradation of the polyimide during AFP processing.

The strengths measured in this portion of the work, up to 210 ksi, were too low to enable the production of pressure vessels that could compete with a process based on filament-wound towpreg, understanding that the theoretical strength for this composite should be closer to 370 ksi and towpreg-based CPV vessels routinely attain 300 ksi strengths. Microstructural characterization suggested that the fiber tows were almost completely wet out at the most aggressive processing conditions, so the Team reduced the thickness of the fabricated 5.75 inch diameter rings to 1mm, as the reduced bending during testing should result in a purer tensile loading at the point where the D-rings in the test fixture are closest. Directly-fabricated rings were therefore made with 10 layers of tape to account for compaction during processing. In parallel, the Team studied rings that were cut from 1mm thick cylinders of 5.75 and 12 inch inside diameters. The 12-inch geometry was chosen for two reasons. First, the larger diameter because it results in purer tensile field than the smaller cylinder, and second, this is the ID of the composite layer on the vessel that was to be built. Cylinders were made by rastering the AFP head down the length of the cylindrical mandrel, with a pitch that matches the tape width (12mm). For this test, the cylinder was made of 5 layers, with the laydown direction alternating to enhance the strength of the cylinder. The combination of these three geometries allows the direct comparison of true hoop geometries to slightly off-axis geometries at 5.75” ID, and the slightly off-axis geometries at two diameters.

For this part of the study, the tape was sourced from the same mother roll as the previously discussed 5.75 in ID rings, the process temperature was set to 360C, the compression weight was set at 200 pounds, and the laydown speed was 6 inches per second.

Based on the tensile data that is shown in Table 14 it can be seen that there was no statistically significant difference between the strength of the rings in the previous part of the study, with a thickness of roughly 3 mm, and the 1 mm thick rings made under the same processing conditions in this part of the study, 207 ksi. In addition, Table 14 shows that there is not significant difference between the previous rings and ring cut from cylinders made under the same conditions, 192 ksi. Finally, Table 14 shows that cylinders made under the same conditions but with a 12" ID were significantly stronger, with the mean strength of 236 ksi. This suggests that the stress state in the larger rings has less of a bending component, and that this is beneficial for the material being tested.

Table 14. Strength of rings as a function of diameter and initial form.

| Temperature (C) | Compression Load (lbs) | Laydown Rate (in/sec) | Initial shape | Diameter (in) | Thickness (mm) | Avg. Strength (ksi) |
|---|---|---|---|---|---|---|
| 360 | 200 | 6 | Ring | 5.75 | 3 | 210 |
| 360 | 200 | 6 | Ring | 5.75 | 1 | 207 |
| 360 | 200 | 6 | Cyl. | 5.75 | 1 | 192 |
| 360 | 200 | 6 | Cyl. | 12 | 1 | 236 |

Several conclusions can be drawn from this data. First, the thickness of the rings that were fabricated directly had no effect on the strength. Second, rings fabricated directly and those cut from filament-wound cylinders have the same strength, within experimental error. Finally, the large ID rings are statistically stronger than the smaller rings, most likely due to the bending moment that is induced in the ring as it deforms from circular to oval over the course of the test.

Based on input from ADC and others, the Team evaluated the effect of AFP tape tension on ring mechanical properties. It was suggested that wrapping the tape on the mandrel at higher tension would result in better-aligned fiber, thus increasing the modulus of the composite layer. Tape tension is defined here as the amount of force on the tape that is required to turn the payout reel in the deposition head. The work reported prior to this was taken with the tape tension set to 1.3 pounds. In this part of the work, the tension was varied from 1.3 to 4 pounds.

Two cylinders were fabricated for this study with the AFP system set to the best-known conditions (speed - 12 inches per second, temperature - 360C, compaction load - 200 lbs), each 7 layers of tape, 12 inches in diameter and 1mm thick, and each cut into 5 individual rings for ASTM D2290-16 testing. The cylinders were made side-by-side on an aluminum mandrel that had been treated with FreKote mold release.

The results are shown in Table 15. Based on these results, it does not appear that increasing the tape tension had a measurable effect on hoop strength.

Table 15. Effect of tape tension on hoop strength of 12 inch diameter rings.

| Sample | Tension (lbs) | Hoop Strength (ksi) | Average Hoop Strength (ksi) | Standard Deviation (ksi) |
|---|---|---|---|---|
| 1F-1 | 1.3 | 218 | 205 | 25 |
| 1F-2 | 1.3 | 225 | | |
| 1F-3 | 1.3 | 214 | | |
| 1F-4 | 1.3 | 161 | | |
| 1F-5 | 1.3 | 207 | | |
| 2F-1 | 4.0 | 185 | 202 | 18 |
| 2F-2 | 4.0 | 196 | | |
| 2F-3 | 4.0 | 229 | | |
| 2F-4 | 4.0 | 210 | | |
| 2F-5 | 4.0 | 189 | | |

Infrared thermography was performed during the direct fabrication of the 1mm thick, 5.75 inch ID rings shown in Table 14 and is shown as Figure 41. During this thermograph, the cylindrical substrate was rotating such that the hottest area where the tape was applied on the top of the rotated away from the camera, returning to the visible side only after it has cooled on the backside of the mandrel. The area shown represents the temperatures of the substrate just before a new layer is applied. The temperatures displayed in the upper left portion of the Figure are readings taken within the small box located just below the laser plume (bright white feature at the center of the thermograph) and indicate that just prior to tape application the substrate temperature is less than 37C, well below the softening point of the polymer matrix.

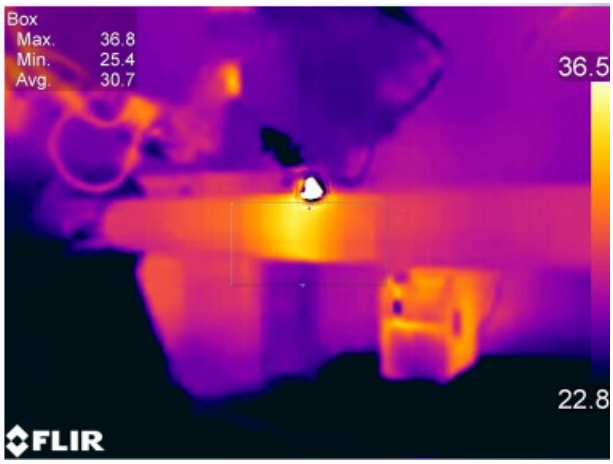


Figure 41. IR Thermograph taken during the direct fabrication of the 1mm thick rings.

Optical micrographs of a polished cross-section, taken with the polished surface perpendicular to the fiber axis, of an as-fabricated ring are shown in Figure 42. These images suggest that the rings are mostly void-free. Therefore the AFP conditions under which the process is running are such that the polymer is wicking into the intra-tow voids and mostly filling the inter-tape regions. In addition, it is easily seen that there are polymer-rich zones between the original

tapes, ensuring excellent adhesion between the tape layers after deposition.

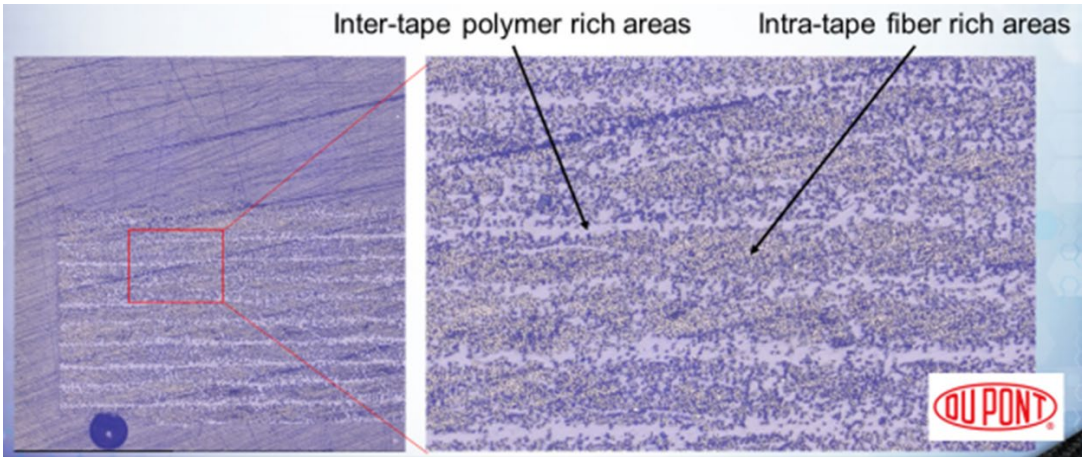


Figure 42. Optical micrographs of polished cross sections of as-fabricated 5.75 inch ID rings, showing no residual voids after AFP process. The ring is 1mm thick.

Optical micrographs of a polished cross-section, taken with the polished surface parallel to the fiber axis, of an as-fabricated ring are shown in Figure 43. While this sample was cut from a cylinder, the presence of fiber ends in these images suggest that not all of the fibers are aligned in the hoop direction. These defects are most likely due to carbon fiber debris created during the tape fabrication process. While these defects account for a minority of the carbon fiber present, this does represent material that does not contribute to the strength of the ring, and may in fact be a strength limiting defect.

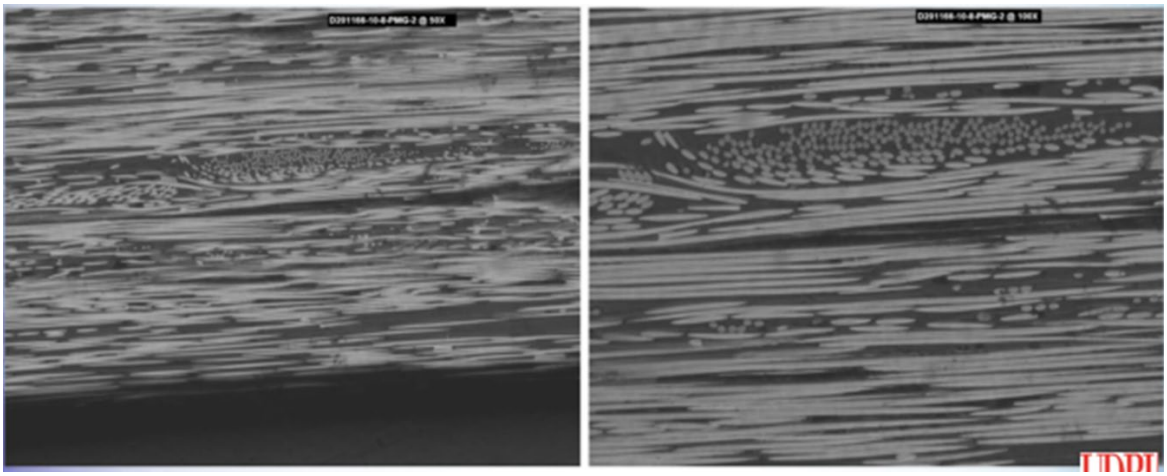

Figure 43. Optical micrographs of polished cross sections of as-fabricated 12 inch ID rings, showing no residual voids after AFP process. The ring is 1mm thick.

## 4.8 AFP Vessel Fabrication – Fluted Envelope

The vessel fabrication started with the design process. Steelhead Composites designed the vessel by successive simulations of how proposed vessel shapes would interact with the existing AFP head. The final proposed shape is shown in Figure 9. The vessel was fabricated from 6061 aluminum by Steelhead using the spinforming process. The as-fabricated vessel dome is shown

in Figure 44. After fabrication, the vessel liner was heat treated and provided to CPC for composite over-wrapping. The composite overwrap was done using the similar layers to those described for the conventional vessel, although the detailed design of the overwrap was different to account for the different vessel shape. The tape used, while of the same composition, was ¼ inch wide in order to reduce or eliminate venetian-blinding. Two tapes were applied simultaneously, with the tension of each being independently controlled by the AFP head. The overwrap process is depicted in Figure 45, showing the hoop, helical, and hoop plies. Two vessels were made this way, and the AFP process ran without upset through each ply, although the process was stopped between plies to replenish the tape sources.

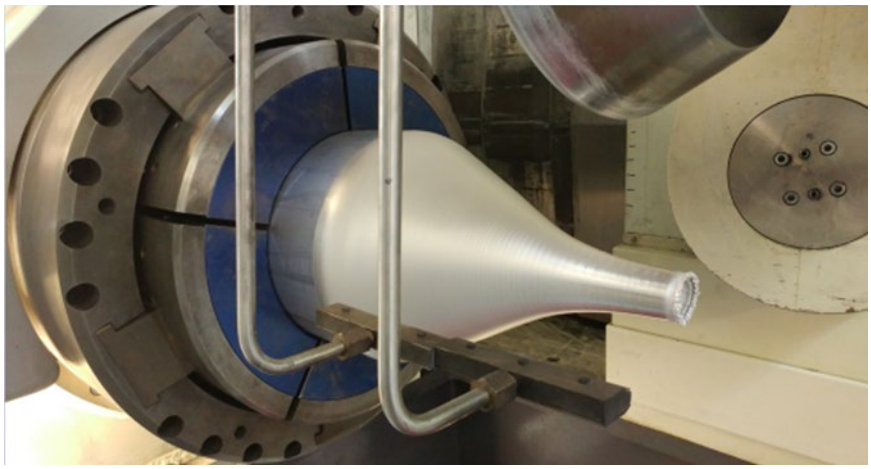

Figure 44. As-fabricated dome on fluted vessel.

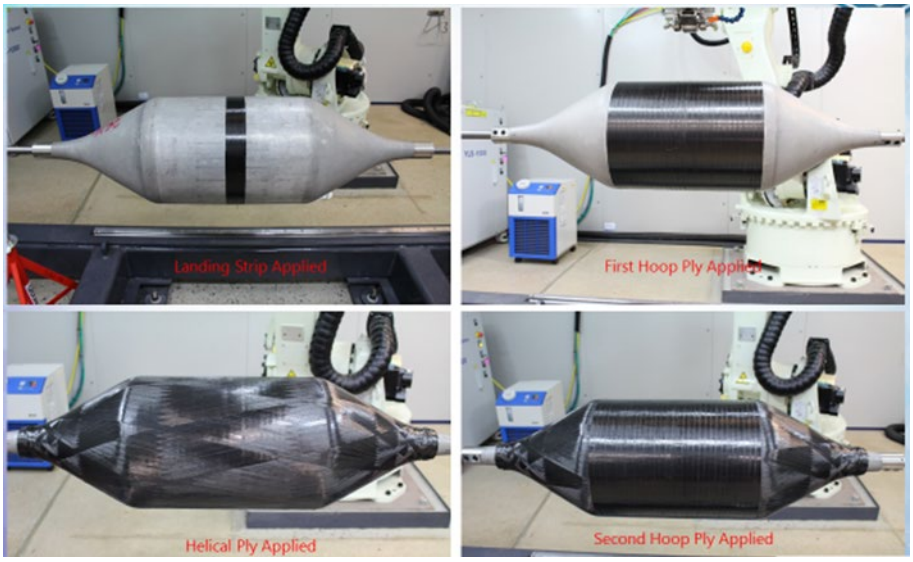


Figure 45. Stages of fluted vessel wrapping including, in order of the process, application of the landing ply, the first hoop ply, the helical ply, and the second hoop ply.

A close-up of the wrapped cylinder appears as Figure 46. It is evident that the venetian-blinding has been eliminated with the exception of the near-bung area where the tape thickness was exaggerated as every helical tow winds around the vessel at the bung. The surface is relatively

smooth, with the UD tape being space filling as designed.

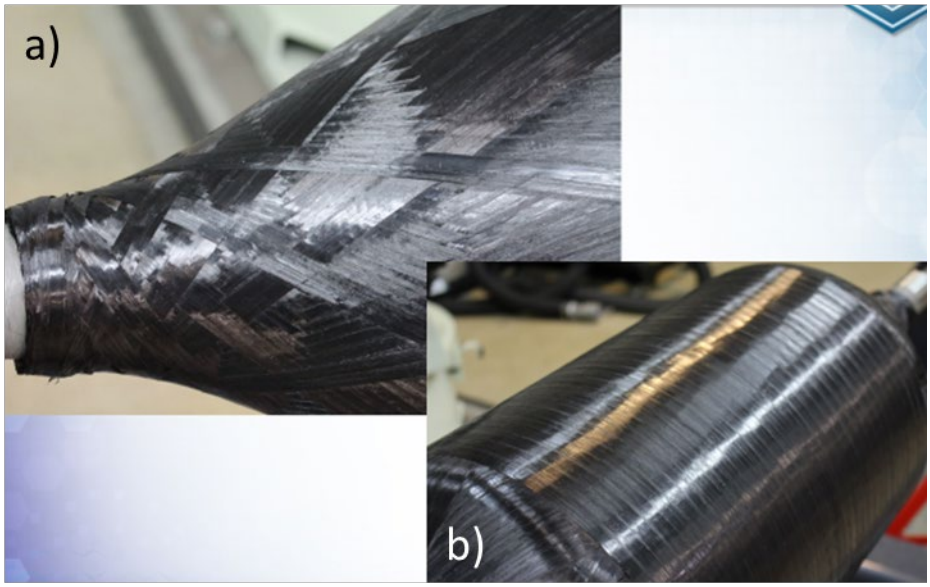


Figure 46. Close up of wrapped vessel, including the helical and hoop plies.

The finished vessel shown in 45 was subsequently sent to Steelhead composites for testing.

## 5.6 CPV Vessel Testing

As stated previously, the testing is done in two phases. In the first the vessel is pressurized to a level substantially less than the designed burst strength. This portion of the test is to verify that the strain gauges are operating in addition to obtaining a plot of strain vs pressure. Figure 47

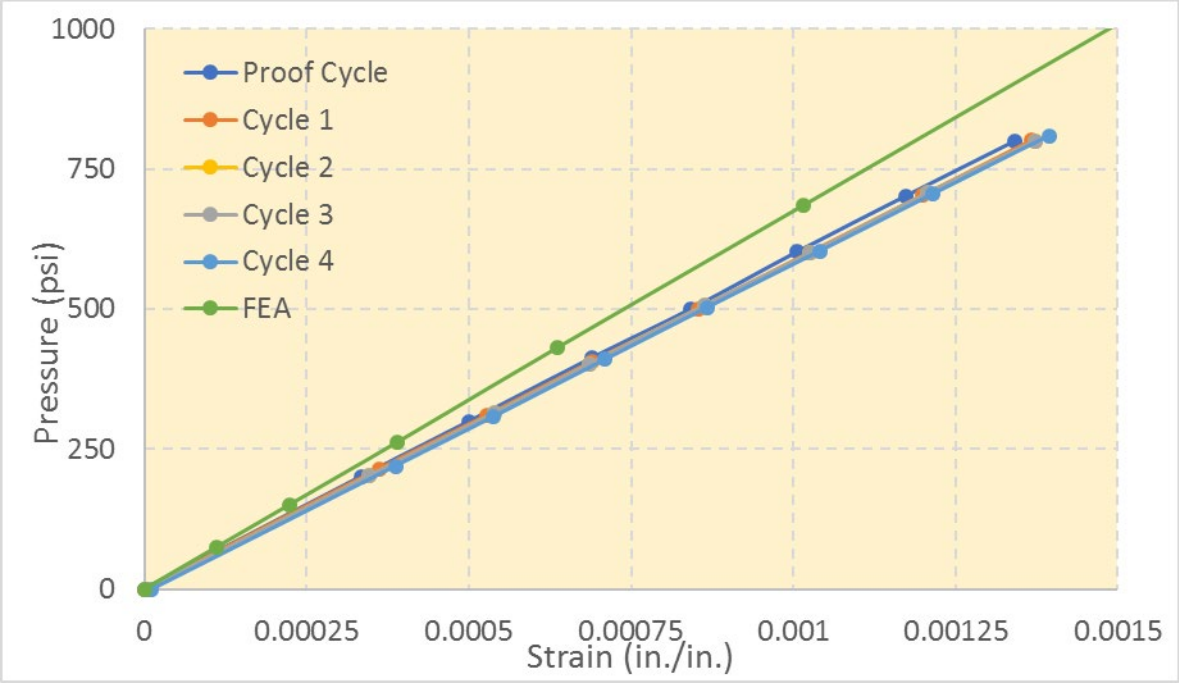

Figure 47. Pressure vs hoop strain measured during the initial pressurization cycles, compared with FEA prediction.

shows the pressure vs hoop strain measured during the initial cycle repeated for 4 times. The plot also compares the test data with FEA predictions. The FEA model was based on a composite layer containing 50 volume percent carbon fiber, the modulus of which was 33.4 Msi. The plot shows that the FEA results under predicts the strain values for a given pressure, which indicates that the as-fabricated composite reinforcement is less stiff than what was used in the FEA model.

An interesting detail of the pressure/strain behavior is that the fitted line extrapolates through the origin. This indicates that the composite begins to expand as soon as pressure is applied to the vessel interior, since the strain gauge is mounted on the exterior surface of the vessel. This is different from the usual behavior of thermoset composite based pressure vessels, where there is generally a minimum pressure that must be exceeded for the strain in the composite to become non-zero. The thermoset observations are due to the thermoset being cured at elevated temperatures, where the aluminum vessel has slightly expanded. On cooldown from cure, the aluminum liner shrinks away from the composite layer, leaving a gap between the materials. On pressurization, the liner must expand prior to contacting the composite layer, resulting in the delay before strain is registered on the strain gauge. The behavior shown here indicates that the composite layer is in contact with the aluminum liner, as expected.

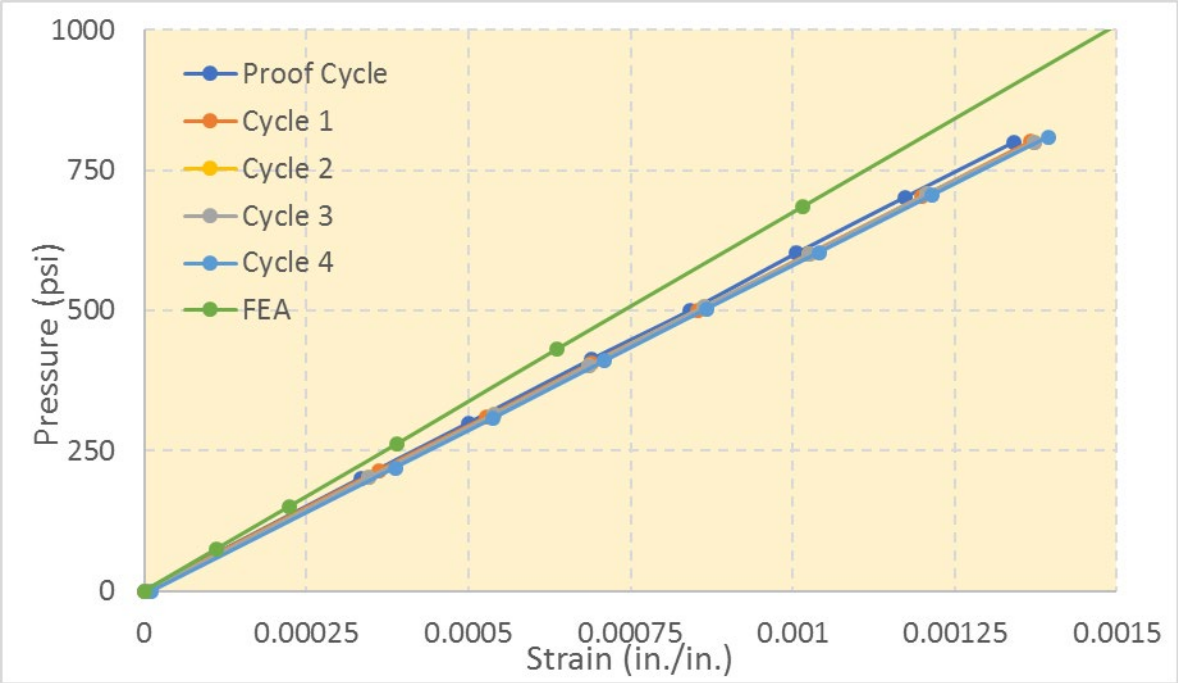


Figure 47. Pressure vs hoop strain measured during the initial pressurization cycles, compared with FEA prediction.

The second phase of the test is designed to measure the burst strength of the vessel. The water filled vessel is lowered into a test bunker and connected to the water source. A heavy steel cover is used to cover the pit, and observers are moved to a safe distance. The internal pressure is increased, and the pressure value is recorded from the electronic transducer as well as a

mechanical pressure gauge.

During the burst test of a fiber reinforced thermoplastic composite vessel, failure is usually defined by a sudden loss of pressure. The thermoplastic vessel failed differently, however, because it did not lose all the pressure on the first event. Rather, there was an audible pop accompanied by a drop in the internal pressure, but the failure was not catastrophic. Because the internal pressure did not drop to zero, pressurization was resumed until a final rupture took place, again coincident with an audible sound of rupture as is typical of a burst failure of a composite pressure vessel. The final burst pressure was noted as the peak pressure at this catastrophic failure.

During the burst test, the vessel structure undergoes significant nonlinear deformation as indicated in the FEA prediction of the pressure vs strain curve shown in Figure 48. This is because the aluminum liner yields plastically while restrained by the composite overwrap. The final rupture is typically initiated in the composite plies which has strain to failure significantly lower than aluminum. Figure 48 shows the test data point at rupture indicating that the longitudinal strain in the composite hoop layer is 1.2% at the rupture pressure. This is in agreement with the lower strain to failure for the fiber reinforced thermoplastic composite material observed in coupon testing.

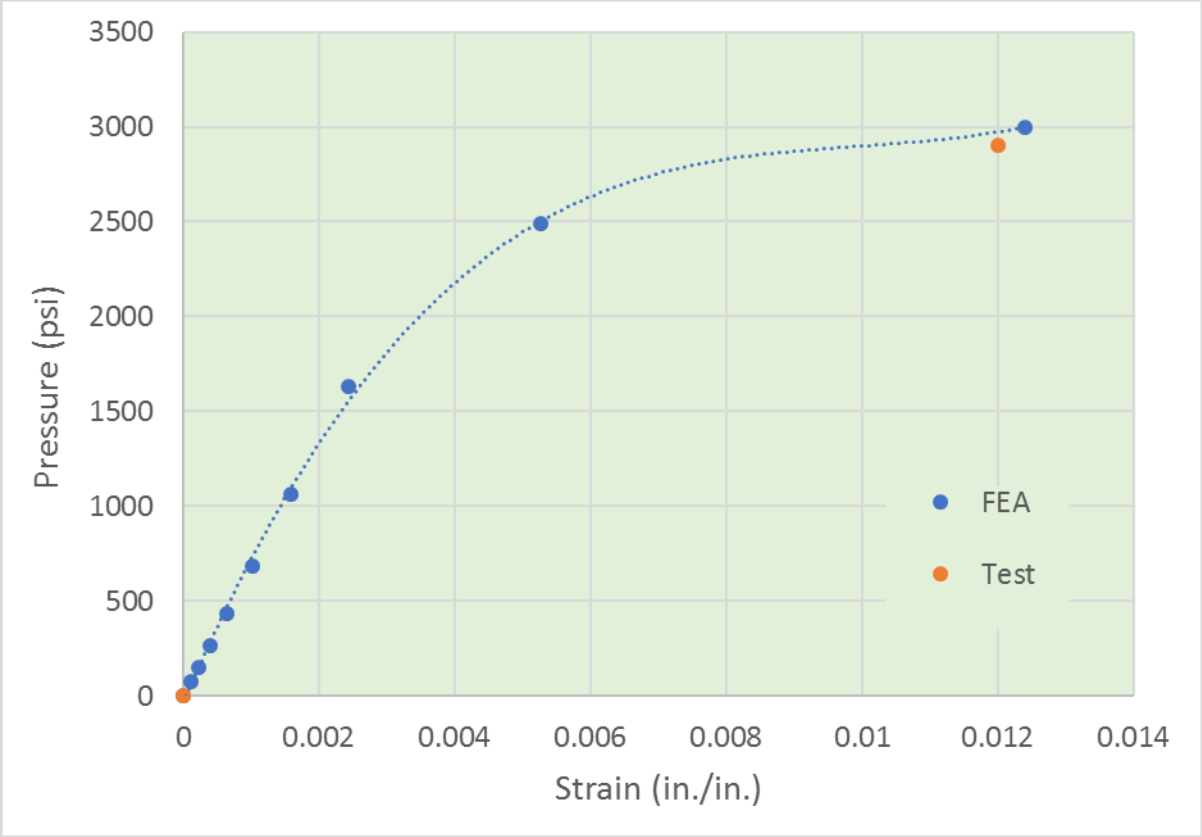


Figure 48. FEA prediction of pressure vs hoop strain, compared with test data at rupture pressure.

One significant observation made during the burst test was the mode of failure in the composite plies. The clean mode of rupture in the cylindrical section with an axially running crack is expected and meets design predictions (Section 3.7). However, the condition of the composite plies post rupture displayed precise rupture zone as shown in Figure 49a, indicating a ductile failure mode. This needs to be contrasted with the brooming effect typically observed in vessels fabricated with fiber reinforced thermoset composites Figure 49b. The unique failure mode of the AFP vessel is a testimony to the toughness and benign failure characteristics of the fiber reinforced thermoplastic composites.

Putting aside the possibility of graceful failure, the pressure testing clearly revealed two problems; a lower than required stiffness, and a lower than required failure strain. Many carbon-fiber CPV materials have a strain to failure up to 1.8%. The higher failure strain allows these composites to be used to much higher pressures than the materials tested in this program. To make matters worse, the stiffness of the tested materials is roughly 10% less than what was expected, allowing the failure strains to be reached at lower pressures than was desired.

The combination of low modulus and low failure strain relative to thermoset systems will require that more carbon fiber be used to stiffen the structure than is currently used for thermosets. Since carbon fiber is the most expensive component of the system, adding fiber makes vessels produced with these materials non-competitive. If, however, the materials and

processes can be optimized to improve the strength and failure strain translation from the fiber to the vessel, this conclusion will need to be revisited.

(a) (b)

Figure 49. Picture of the composite pressure vessel fabricated with (a) fiber reinforced thermoplastic composites, post rupture compared with the same for a vessel fabricated with (b) fiber reinforced thermoset composites

The Team tested the effect of tape tension on the performance of lightly-wrapped pressure vessels by putting a hoop layer (2 plies at ±89º) on aluminum vessel liners that were 6 inches in diameter and 20.5 inches long, the cylindrical section being 14.2 inches long. In this configuration, the dome is strong enough to not require composite reinforcement and was therefore not wrapped with tape. The vessels were wrapped with tape tensions set at 1.3 and 4 pounds, referred to as “low” and “high” tensions respectively. Both vessels failed cleanly in the hoop section. A picture of the low-tension vessel after testing is shown in Figure 50.

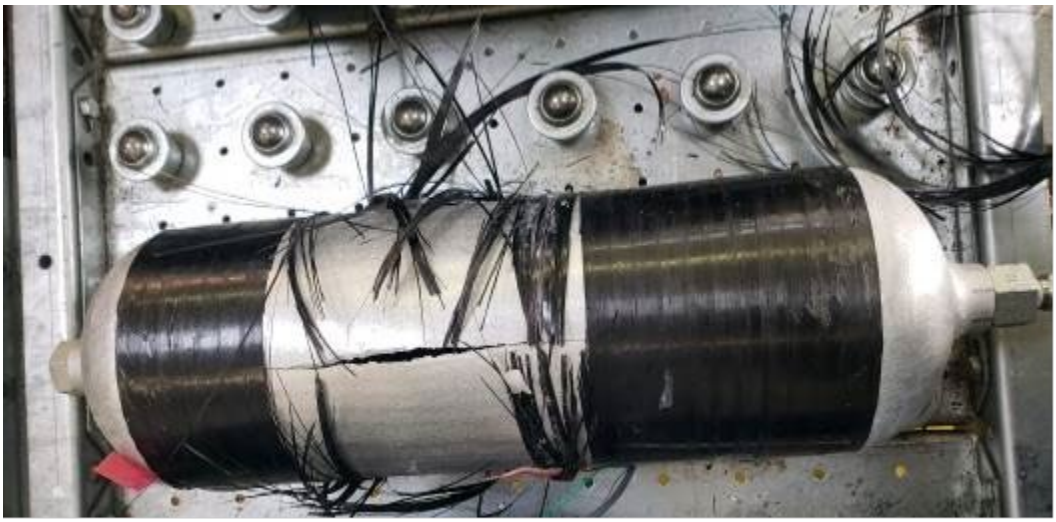

Figure 50. Picture of low tension vessel after pressure testing.

In the low tension-case, the data in Figure 51 show an initial elastic region up to a pressure of 2000 psi whereupon the aluminum liner yields. This is the point at which the majority of the stress is transferred to the composite layer. The vessel subsequently failed at 3073 psi with a composite strain of 1.2%. This failure strain was identical to that measured in the larger cylinder, the data from which is shown in Figure 48. In the high-tension case, the combined stiffness of the liner and composite is clearly higher than the low-tension system, making it appear that the composite is working with the liner from the start of the pressurization cycle. However, it appears that the entire system failed at 1963 psi. The reason for this is failure currently unknown, and more testing will be required to understand the statistical significance and failure mechanisms embodied here.

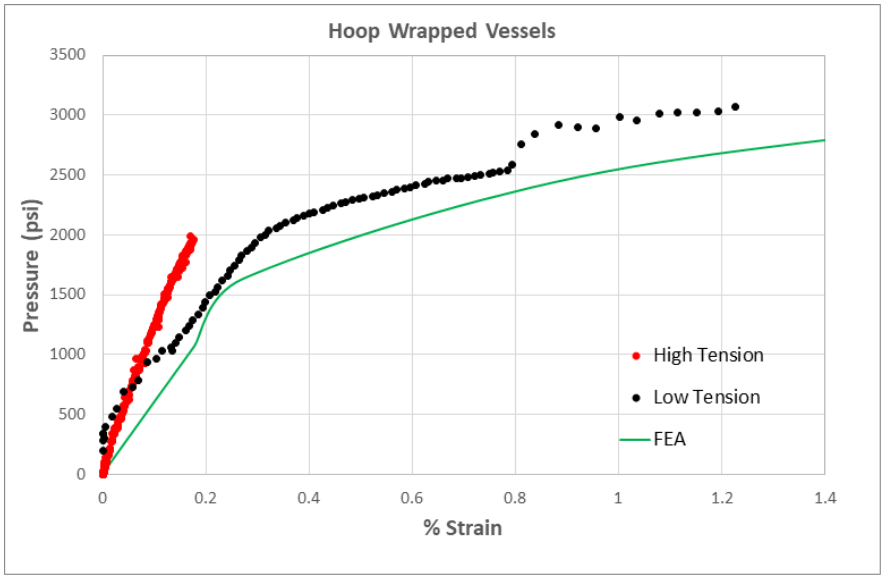


Figure 51. Pressure vs. strain behavior for low tension (black) and high tension (red) test vessels.

The carbon fiber used in a CPV is the highest cost component of the system. Therefore, considering the process that was developed over the course of this work, the Team at Steelhead Composites developed a laydown pattern that could reduce the weight of a CPV vessel. This weight reduction is based on AFP processing not requiring continuous filaments during the helical ply.

The helical ply is composed of many crossed tapes, as is illustrated in Figure 14c. Every time the tape reversed laydown direction, it must be wrapped around the dome. This leads to an amount of material on the dome in far excess of the amount required to contain the pressure in the vessel. This is referred to as parasitic weight. In addition, as can be seen in the figure, when each layer of tape crosses the one below it must either decrease or increase in height as it goes over the tape edge. While seemingly insignificant, the “bridging” effect results in either a polymer rich area or a pore, either of which is a weak area in the structure.

The AFP process is fundamentally different. While the process relied on in this work was based on winding a continuous tape throughout the helical ply, AFP has the ability to start and stop

tapes layers during the process. There are several potential advantages to this:

1) Zero degree plies can be used to reinforce the domes. This eliminates all cross-overs in the cylindrical section of the vessel, saving weight. These are depicted in Figure 52.
2) Should a true helix be required, it can be designed such that the sense of rotation is constant, leading to space-filling layers without any cross-overs.
3) Elimination of crossovers removes areas where the tape crosses between high and low areas, i.e. bridging. Reducing bridging will reduce flaw populations and result in a stronger vessel.
4) Specialize winding patterns can be developed for the domes to enhance structural integrity while reducing weight. These include circumferential wafers as shown in Figure 53.

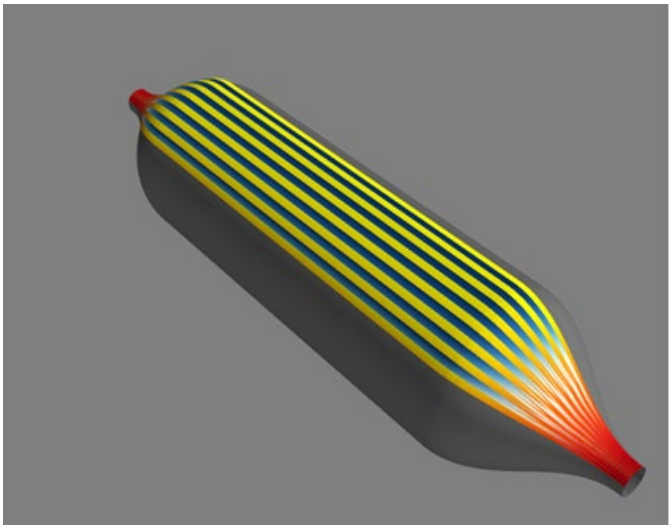

Figure 52. Depiction of zero degree plies that could be made with AFP.

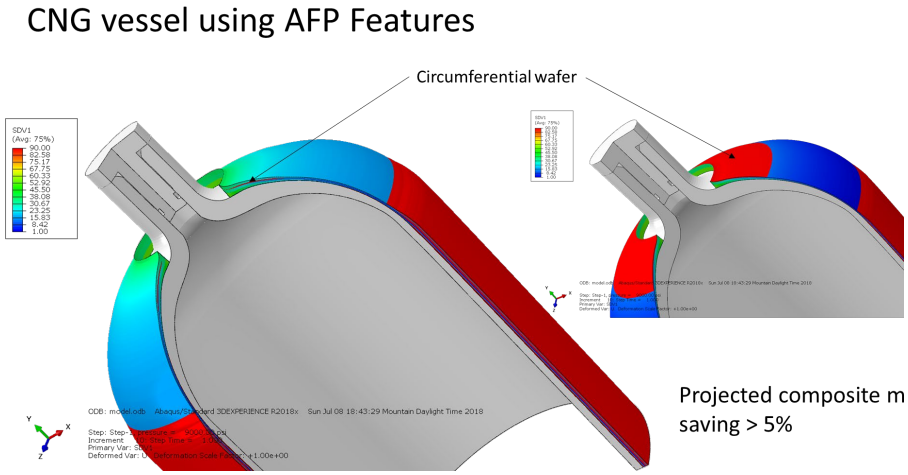


Figure 53. Location of circumferential wafers to reinforce the dome while saving weight.

Using these strategies, it is projected that the weight of carbon fiber could be reduced by over 5%, reducing the raw materials cost of the CPV.

## 4.10 Technoeconomic Analysis

A technoeconomic analysis of the cost of manufacturing (COM) of a composite pressure vessel was performed by Stephen Tieri (DuPont). This analysis was designed to compare the COM for thermoset and thermoplastic CPVs in both the Type III and Type IV configurations, for a total of 4 possible base cases. The analysis is built out of a number of assumptions that must be explicitly laid out at the start. This particular treatment uses a baseline CNG-capable (350 bar) composite vessel that is 80 liters in volume, and assumes an annual production rate of 30,000 units.

A schematic of the process flows for thermoplastic and thermoset Type III systems appears as Figure 54. While these two processes share many common steps, the diagram clearly shows that the automated fiber placement system takes the place of three thermoset-related processes; filament winding, B-stage curing, and final curing.

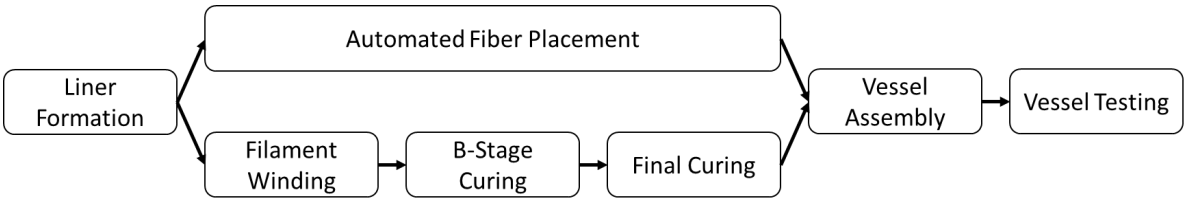


Figure 54. Process flow for thermoset and thermoplastic Type III CPV systems.

There are 6 cases shown in the following Tables. The first two cases, in columns labeled Type III, are based on modeling of Type III thermoset vessels on aluminum liners. The thermoplastic case in the column labeled AFP is based on the assumption that the carbon fiber is used at the equivalent efficiency as the thermoset-based case, and therefore the same amount is required on the vessel. Based on the work in this done as part of this program, this level of performance has not been achieved for the thermoplastic systems, but it is the Team's opinion that there is nothing fundamental that prevents this. The next two cases pertain to Type IV vessels, and the same caveats apply as need to be considered in the Type III cases. The last two cases, labeled "Light Vessels" are included for aspirational purposes only. The assumption here is that through careful modeling and simulation, 15% of the composite weight can be removed while still maintaining the safety of the vessel due to the inherent toughness of the thermoplastic matrix. It should be noted here that the required properties of the composites have not been demonstrated, nor have the details designs that would enable this to come to fruition, nor have the regulatory agencies been engaged for the potential acceptance of this advanced design. However, some modeling work by the Steelhead Team has suggested that this may be possible due to more efficient vessel design enabled by AFP.

A summary of the cost structure appears as Table 16. When looking at the fixed and variable costs, it is important to understand that this is an estimate, likely good to within 20%. This indicates that the total Costs of Manufacture for thermoset and thermoplastic CPV CNG vessels are the same to the level of significance of this work. A summary of the fixed costs is included as Table 17, while the variable cost estimate appears as Table 18. Some portions the fixed and

variable costs were omitted from these tables as they were deemed insignificant.

Table 16. Summary of costs for various vessel type. Capital and investment costs: thousands of dollars. Fixed, variable and total costs: dollars per vessel.

| | | Type III | | Type IV | | Light Vessels | |
|---|---|---|---|---|---|---|---|
| | | Filament Wound | AFP | Filament Wound | AFP | AFP Type III | AFP Type IV |
| Capital equipment | $M | 3,600 | 4,900 | 3,400 | 5,700 | 4,900 | 5,700 |
| Project level investment | $M | 9,000 | 12,200 | 8,400 | 14,300 | 12,200 | 14,300 |
| Fixed Cost | $/unit | 200 | 174 | 190 | 177 | 174 | 177 |
| Variable Cost | $/unit | 730 | 758 | 615 | 650 | 606 | 578 |
| **Total Cost** | $/unit | **930** | **932** | **805** | **827** | **780** | **755** |

Table 17. Fixed cost breakdown. Costs are listed in thousands of dollars per year.

| | Type III | | Type IV | | Light Vessels | |
|---|---|---|---|---|---|---|
| | Filament Wound | AFP | Filament Wound | AFP | AFP Type III | AFP Type IV |
| Operations | 3,538 | 2,677 | 3,390 | 2,559 | 2,677 | 2,559 |
| Maintenance | 349 | 473 | 326 | 555 | 473 | 555 |
| Plant Overhead | 1,366 | 1,366 | 1,308 | 1,035 | 1,366 | 1,035 |
| Depreciation | 600 | 814 | 560 | 954 | 814 | 954 |
| Taxes and Insurance | 135 | 183 | 126 | 215 | 183 | 215 |
| **Total Fixed Cost** | **5,988** | **5,213** | **5,710** | **5,318** | **5,213** | **5,318** |

It should be noted that for this analysis, the fabrication of the aluminum vessel liner for Type III vessels is included as part of this analysis, along with the cost of the spinforming equipment. In contrast, it is assumed that the plastic liner for Type IV vessels is purchased, as there are many companies that are capable of supplying these and similar shapes. Converting the annual costs shown to the distributed amount per vessel requires dividing these number by the 30,000 annual units produced.

Table 18. Variable cost breakdown for materials, including waste due to the process. Cost is listed as dollars/vessel.

| | Type III | | Type IV | | Light Vessels | |
|---|---|---|---|---|---|---|
| | Filament Wound | AFP | Filament Wound | AFP | AFP Type III | AFP Type IV |
| **Materials** | | | | | | |
| Thermoset matrix | 72 | | 91 | | | |
| carbon fiber | 384 | | 482 | | | |
| UD CF tape | | 483 | | 606 | 331 | 535 |

| | | | | | | |
|---|---|---|---|---|---|---|
| Aluminum cylinder | 273 | 273 | | | 273 | |
| Boss | | | 25 | 25 | | 25 |
| Polymer liner | | | 15 | 15 | | 15 |
| Test fluids | 0.05 | 0.05 | 0.05 | 0.05 | 0.05 | 0.05 |
| **Utilities** | | | | | | |
| Electricity | 0.90 | 2.10 | 1.70 | 3.60 | 2.10 | 3.60 |
| **Total Variable Cost** | **730** | **758** | **615** | **650** | **606** | **578** |

The cost of capital, as summarized in Table 16 shows that the investment cost for these two processes is very similar for these structures. The costs shown assume that the installation will be made in an "established site", i.e. one that has all of the required structural and utility elements intact. Some of this difference is due to the cost of the individual operating units, as accounted for under "capital equipment". The remainder is due to items such as engineering, management, and site preparation costs, and it also includes a 35% contingency due to the preliminary nature of the estimate. The number of operating units required for each process is shown in

Table 19. These results were calculated based on the laydown rates and vessel masses shown in Table 20.

The components of the fixed cost are outlined in Table 17 with the exception of items that were deemed insignificant. Of note in this table is that raw materials that are wasted in the process, i.e. materials that are not eventually included in the finished vessel, are included. Waste levels were estimated using conventional estimates, but it should be noted that due to the inherent differences in the processes, the carbon fiber and thermoset matrix waste levels were assumed to be higher than the thermoplastic tape waste due to the nature of the process. This assumption compensated for some part of the higher cost of the UD tape that is required for the thermoplastic system.

Table 19. Required Unit operations. Where more than one unit required, 24/7 operation is assumed. Liners for Type IV vessels are purchased from external source.

| | Type III | | Type IV | | Light Vessels | |
|---|---|---|---|---|---|---|
| | Filament Wound | AFP | Filament Wound | AFP | AFP Type III | AFP Type IV |
| Spinforming | 1 | 1 | | | 1 | |
| Al/Plastic liner anneal | 1 | 1 | 1 | 1 | 1 | 1 |
| Filament Winding | 2 | | 3 | | | |
| B-Stage Cure | 1 | | 1 | | | |
| Full Cure | 1 | | 1 | | | |
| AFP | | 2 | | 3 | 2 | 3 |
| Hydro Test | 1 | 1 | 1 | 1 | 1 | 1 |
| Gaseous Leak test | | | 1 | 1 | | 1 |

Table 20. Underlying assumptions for Cost of Manufacture estimate.

| | | Type III | | Type IV | | Light Vessels | |
|---|---|---|---|---|---|---|---|
| | | Filament Wound | AFP | Filament Wound | AFP | AFP Type III | AFP Type IV |
| Annual Production | Units/yr | 30,000 | 30,000 | 30,000 | 30,000 | 30,000 | 30,000 |
| Vessel volume | Liter | 80 | 80 | 80 | 80 | 80 | 80 |
| Vessel mass | kg/unit | 41.0 | 40.8 | 29.0 | 28.8 | 34.7 | 24.5 |
| Liner mass | kg/unit | 21.3 | 21.3 | 3.2 | 3.2 | 21.3 | 3.2 |
| Carbon fiber weight in composite | % | 68 | 68 | 68 | 68 | 68 | 68 |
| Boss mass | kg/unit | | | 1.1 | 1.1 | | 1.1 |
| Carbon fiber mass | kg/unit | 13.3 | 13.3 | 16.7 | 16.7 | 9.1 | 13.7 |
| Polymer mass | kg/unit | 6.2 | 6.2 | 7.8 | 7.8 | 4.3 | 6.5 |
| Shoulder foam mass | kg/unit | 0.2 | | 0.2 | | | |
| Polymer cost | $/kg | 8.7 | | 8.7 | | | |
| Carbon fiber cost | $/kg | 28.66 | | 28.66 | | | |
| Al Blank cost | $/kg | 11.51 | 11.51 | | | 11.51 | |
| UD tape cost | $/kg | | 24.50 | | 24.50 | 24.50 | 24.50 |
| Boss cost | $/unit | | | 24.54 | 24.54 | | 24.54 |
| Plastic Liner cost | $/unit | | | 15 | 15 | | 15 |
| Laydown rate | m/sec | | 2 | | 2 | 2 | 2 |
| Electricity cost | $/kWh | 0.069 | 0.069 | 0.069 | 0.069 | 0.069 | 0.069 |

Finally, it must be noted that while the variable components of the costs of manufacture of thermoplastic and thermoset systems are very similar, this does not include the manufacturer's return on investment (ROI). In the example here, the investment required is not vastly different between the two manufacturing methods, and therefore for an equivalent price point the ROI will be similar. However, for a hydrogen-capable vessel, the investment for the filament wound system is not increased, while the AFP-based system will require a project-level capital expenditure of roughly $23 million to cover 6 AFP units. This difference is primarily due to the manufacturing capacity of a three-spindle filament winding unit when compared to a single spindle AFP unit, and number of AFP units that would need to be installed to meet the manufacturing cycle time for hydrogen vessels. Depending on the manufacturer's economic models and their expected returns, the return on these capital costs could add a significant

amount to the thermoplastic hydrogen vessel cases when compared to the thermosets, and suggests that either the selling price of thermoset vessels will be lower than thermoplastic ones at the same level of ROI, or that the profitability of a thermoset-based company will be higher than one based on thermoplastics at the same asking price. Estimates for selling price will not be made in this document as the underlying business model assumptions for individual potential manufacturers will differ.

### 4.11 Market Assessment

An extensive market survey was performed, taking advantage of published multiclient studies as well as interviews with OEM and Tier 1 partners. The results can be summarized as:

- CPV is an existing & growing market, majority are all steel or aluminum constructions but converting to various composite designs for weight savings.
- CPVs are primarily thermoset resin based but can be manufactured with thermoplastic composites as well. Both glass and carbon fiber are used for reinforcement. Carbon fiber is growing in preference due to its higher performance and lower weight.
- The main manufacturing process is filament winding. Wet winding is when dry fibers are passed through a thermoset resin application portion before being laid on a mandrel. Dry winding is when a pre-preg is laid down on the mandrel.
- 5.4% CAGR market growth is expected over the next 5 years due to the conversion to alternative fuels for the transportation market and the low cost of natural gas.
- Total addressable materials market is $1.9B and 155 ktons by 2023. (TS & TP CPVs)
- Key to entering this market as a material supplier is collaboration with existing tank manufacturers with a strong value proposition and market pull.

The high pressure CPV market can be segmented into the following areas – CNG transport vehicles, CNG powered vehicles, hydrogen fuel cell vehicles, and a final category that contains everything from aerospace and industrial applications, to self-contained breathing apparatus. In addition to segmenting this market by application, there are significant differences by region, but some trends hold worldwide. For instance, in CNG-capable vessels, the strongest growth will emerge in busses, light trucks, and utility vehicles, while passenger cars are unlikely to become a strong market. This is in contrast to the hydrogen market, where the growth is forecast to be in passenger cars as fuel cells begin to gain better traction especially in Japan.

## 6. BENEFITS ASSESSMENT

While this program was able to demonstrate the critical steps in the process for fabrication of CPV using thermoplastic-based carbon fiber UD tapes, the Team was unable to validate the value proposition on which the program was based. In addition, while the cost of capital to produce thermoplastic Type III and Type IV vessels is similar for CNG, without improvements in either the cost of capital or the laydown rates, these structures are not likely to compete with thermoset systems from a COM perspective when considering hydrogen service.

## 7. COMMERCIALIZATION

Based on the current market assessments and COM estimations, there are no plans to commercialize mass produced CPV for CGS at this time.

# 8. ACCOMPLISHMENTS

Over the course of this work, the Team demonstrated the critical steps required to fabricate composite pressure vessels for compressed gas storage.

1) Polyamide-based polymer formulations with sufficient toughness were designed and formulated, and were shown to fully impregnate low-count carbon fiber tows through the course of unidirectional tape and CPV vessel fabrication.
2) Unidirectional polyamide/carbon fiber tape was fabricated using a commercial scale process, producing up to 35 kg per hour of 170 micron thick well-aligned material with less than 2% voids and a minimum of fiber damage.
3) Automated fiber placement conditions were demonstrated and optimized using designed experiments.
4) Vessel wrap patterns were designed and transferred to the automated fiber placement robot.
5) Vessel liners were fabricated and wrapped with polyamide-based carbon fiber unidirectional tape using an automated fiber placement robot.
6) Lightly wrapped CPV vessels were burst tested and composite layer properties were modeled.

In addition to these successful demonstrations,

7) Vessels wrap patterns were designed for the automated fiber placement process that uses carbon fiber more efficiently than filament winding, enabling up to a 5% decrease in weight of composite required for compressed gas storage.
8) A technoeconomic model was created that indicates the cost of manufacture of the thermoplastic and thermoset systems to be almost equivalent, although the cost of capital is significantly higher for the thermoplastic case for hydrogen-capable service.

Optimization of each step of vessel fabrication was not within the scope of this project. The results obtained point towards a significant opportunity to leverage this work to validate the performance and cost benefits of thermoplastics in energy storage applications.

# 9. CONCLUSIONS

This project provides key insights regarding challenges that will be faced for implementation of thermoplastic Type III compressed gas storage vessels.

1) The target market for these structures is no longer CNG, but is changing to hydrogen CGS.
2) The cost of manufacture (COM) for hydrogen-capable thermoplastic systems will be higher than similar thermoset systems once the return on investment is included.
3) The strength and failure strain developed in the thermoplastic composite rings was below that currently shown in thermoset systems. If not improved, this requires more carbon

fiber to be used for thermoplastics, increasing the cost of both carbon fiber and capital.
4) The toughness and recyclability were not characterized.
5) The market for compressed natural gas vessels is in the early stages of development for mass adoption. There is a great deal of uncertainty regarding future growth projections.

# 10. RECOMMENDATIONS

For further improvements and optimization to be made, work should focus in the following areas

1) A modified AFP head should be fabricated to enable wrapping of isotensoid vessel domes
2) Tape fabrication and laydown conditions should be globally optimized with vessel properties so that thermoplastic composite properties can be shown to match those of thermoset systems
3) Less expensive automated fiber placement robots and faster laydown rates should be explored to reduce capital costs
4) Demonstration of higher toughness and recyclability expected from thermoplastic systems remains to be demonstrated

As the market and technology evolves, economic and/or regulatory actions may drive the reduction of the cost of capital for AFP, or dramatically reduce the cost of carbon fiber. Either of these scenarios would provide a basis for pursuing further optimization in order to prove the value of thermoplastics in composite pressure vessels for compressed gas storage.

# 11. REFERENCES


1. https://www.vanwees.nl/
2. Handbook of Composites, Second Edition, S.T. Peters, 1998, Springer US, DOI 10.1007/978-1-4615-6389-1
3. https://www.vanwees.nl/2015/03/van-wees-program-of-machines-and-equipment-for-the-composites-industry/
4. ABAQUS 2018 Users Manual.
5. "Filament Winding: A Unified Approach", Sotiris Koussios, TU Delft Repositories, 2004.
6. "Analytical and Numerical Modelling of the Filament Winding Process", Hugo Faria, PhD Thesis, Universidade do Porto 2013
7. ISO/TR 13086-1:2011, Gas cylinders - Guidance for design of composite cylinders — Part 1: Stress rupture of fibres and burst ratios related to test pressure, https://www.iso.org/obp/ui/#iso:std:iso:tr:13086:-1:ed-1:v1:en

# APPENDICES

## Appendix 1. Testing and Evaluation

University of Dayton Research Institute

Impregnated Tape Tension Testing

Several samples of impregnated thermoplastic tape were shipped from DuPont to UDRI to evaluate. These tape specimens were visually inspected, measured for dimensions, and then tested for tensile properties, using ASTM D3039 as a guide. Tape specimens were also sectioned and tested for fiber and void content according to ASTM D3171, Procedure B (acid digestion).

**ASTM D3039 Tension Testing**

All specimens were tested as single, unidirectional tape ply.

1) **Sample Preparation**
   a) Specimen Extraction Method – Nine sets of three specimens each were prepared from rolls of thermoplastic tape. Specimens were measured and then cut to a length of 7 inches using a paper shear to ensure sharp, accurate cuts. The width and thickness of the specimens were measured as received.
   b) Tab Fabrication: 1 inch long tabs were cut from G11 Fiberglass sheet, beveled at 7°, and cut wider than the group of specimens to be adhered to. These tabs were .063" thick.
   c) Surface Preparation – The specimens were masked with polyethylene tape one inch from each end and wiped with acetone to remove any grease or dirt on the bonding site. The fiberglass tabs were grit-blasted to ensure a rough bonding surface and then wiped with Acetone.
   d) Tab Bonding – The tabs were then bonded to the ends of the specimens using 3M™ ScotchWeld™ Epoxy Adhesive 1838 B/A – Green, and held in place using a combination of 1 and 2 inch binder clips, shown in Figure 55.Glass beads were mixed into the adhesive to control bond line thickness (.0049" diameter). Specimens were then placed in an oven at 190°F (88°C) for 1 hour to fully cure the epoxy.
   e) Sample Separation – Each specimen was then trimmed on a band saw to free it from the bonded group of samples as well as trim the tabs to match the width of the specimen.

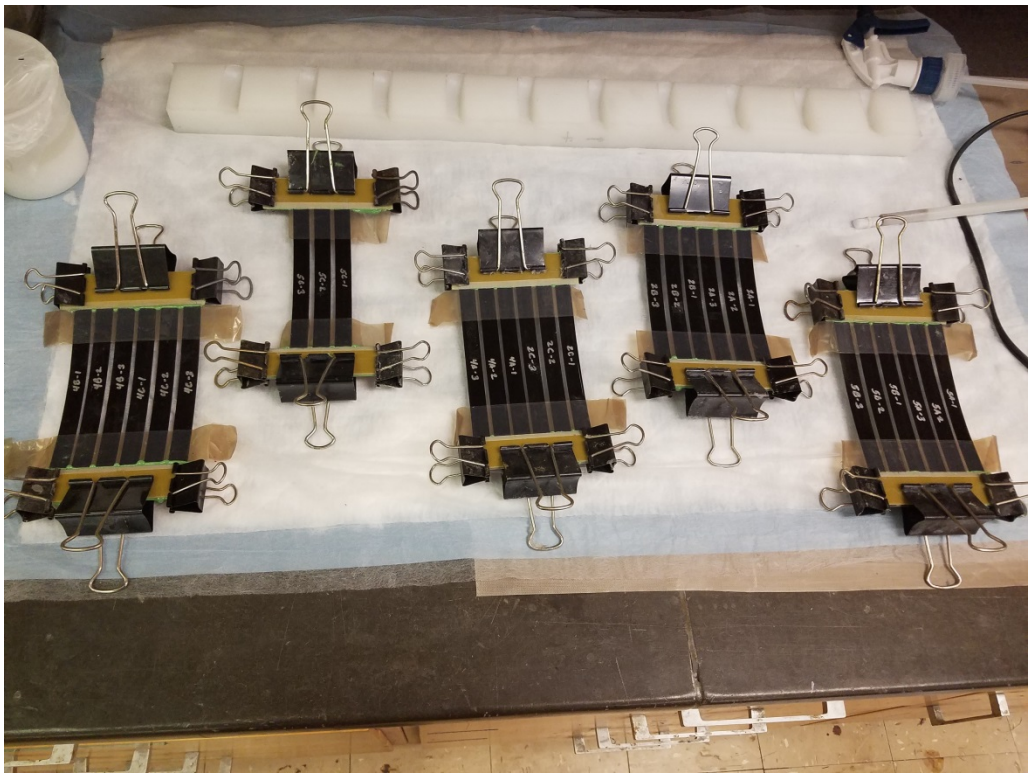

Figure 55. Tape tensile testing samples with bonded tabs.

**2) Testing Procedure**

a) Prior to testing, all specimens were dried for 16 hours at 90°C in order to remove any moisture absorbed by the nylon. Specimens were removed from conditioning no more than 30 minutes prior to testing.

b) Each specimen was loaded into the test frame by utilizing a straight fiberglass strip to center the sample in the grips and pre-loaded to approximately 15 lbs. to provide a straight and taut surface to mount the extensometer, as shown in Figure 56

c) Specimens were subsequently tested at room temperature and relative humidity according to ASTM D3039-14 at a crosshead speed of .05”/minute on a calibrated Instron test frame. An extensometer with a 1 inch gage length and 0.2 inches of travel was utilized.

d) After a drop of 40% in load, compared to the maximum load achieved, the test was considered complete and specimens were evaluated for “failure mode” which is a 3 character code as described in ASTM D3039-14.

e) Specimens were then unloaded from the testing frame and photographed.

Figure 56. Mounted tensile specimen with extensometer.

As part of this evaluation, the physical properties, including carbon fiber content and void volume, were measured with 1.0 gram samples. This specimen size is in good concert with ASTM D3171, which states "6.2 *Coupon Size*—Ability to estimate void content is also determined by coupon size and limitations of measuring apparatus. For example, with just limitations of the analytical balance (accurate to 0.2 mg), a coupon of 0.2 g with a void volume of 1.0 % would have an uncertainty of 10 % (reported void volume in the range of 0.9 to 1.1 %) on the void volume calculation as a result of possible balance error. A 1-g sample would have an uncertainty of 2 % in the void volume calculation (reported void volume in the range of 0.98 to 1.02 %) because of possible balance error for the same 1.0 % void volume".

**Compression Molding of Unidirectional Tape Thermoplastic Prepreg**

Due to the lower than expected tension results on the single ply tape specimens, UDRI investigated compression molding several layers of 2" wide tape into a unidirectional laminate and then subsequently testing it for tension properties. The hypothesis was that compression molding would drive the fiber content higher and give a true measure of what the nylon/carbon thermoplastic tapes were capable of in terms of mechanical performance. The compression molded laminates had a stacking sequence of [0°]8 and were fabricated to be 2" wide and 12" long. An image of the tape is shown in Figure 57.

The processing conditions for laminate fabrication are as follows:

1) Pre-heat press to 608°F
2) Total thickness of aluminum shims is .040" thick.
3) Place 8 strips of 2" wide x 12" long thermoplastic tape (8 plies thick) and soldered together at each corner inside the aluminum shim mold.
4) Once press is at temperature, open the press and load the preform and shims into the tool all at once. Close press. Apply 360 psi of pressure. Once the thermocouple on tool reaches 608°F, let dwell for 3 minutes. Initiate cooling to 212°F. Keep tool under pressure. Once tool reaches 200°F, remove from press. De-mold part.

The resulting laminate is shown in Figure 58

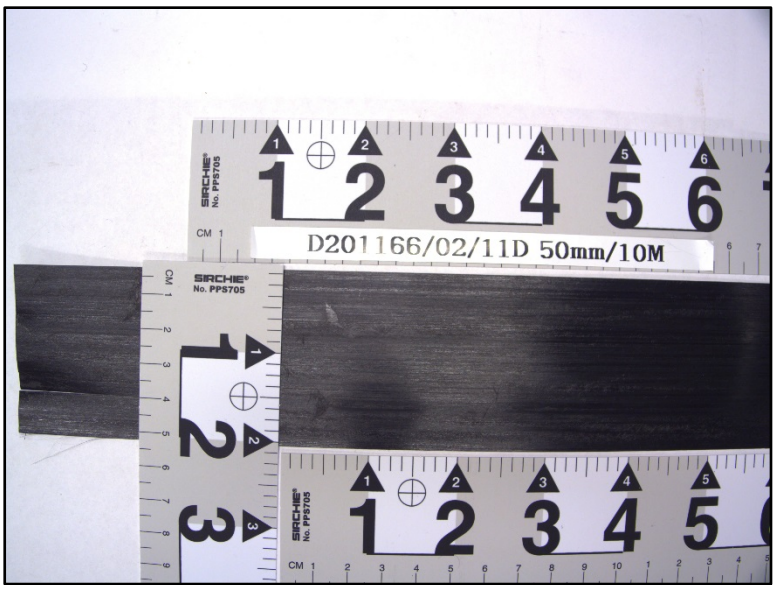

Figure 57. Two inch wide tape used in compression molding.


Figure 58. Compression molded thermoplastic laminate test panels.

Specimens were then sectioned on a diamond wet saw, tabbed, dried, measured for dimensions, and tested at room temperature dry conditions. Two specimens per panel were tested for tension properties according to ASTM D3039.

## Subcomponent Testing

Cylindrical sections were received at UDRI from CPC for test and evaluation. The overarching fabrication and test matrix is detailed in Table 21.

### ASTM D2290 Hoop Tension Testing on Ring Sections

Hoop Tension Testing was performed on tank sections that were 5.75" in diameter early on, and later were tested with 12" diameter sections. Specimens were dried at 90°C for 16 hours and then instrumented with four (4) axial strain gages. See Figure 59 for location of strain gages. All specimens were tested at room temperature dry conditions at a test speed of .1"/minute on an Instron test frame. Figure 60 shows a ring after testing.

- 4 bonded gages were placed on rings to monitor strain throughout the test. Gages 1 and 2 were placed 180° apart on the split in the fixture, Gage 3 was placed 12° outside of the split in the fixture, and Gage 4 was placed at the top of the ring (90° from split in fixture). Gages 1 and 2 were placed to monitor for even loading, Gage 3 was placed to compare strain from unsupported section of the ring to a section supported by the fixture, and Gage 4 was placed to monitor if friction along the fixture changed strain along the specimen.
- Gages 1 and 2, located on the split of the fixture, showed a non-linear behavior. Gages 3 and 4, located on ring section supported by the fixture, showed linear behavior.

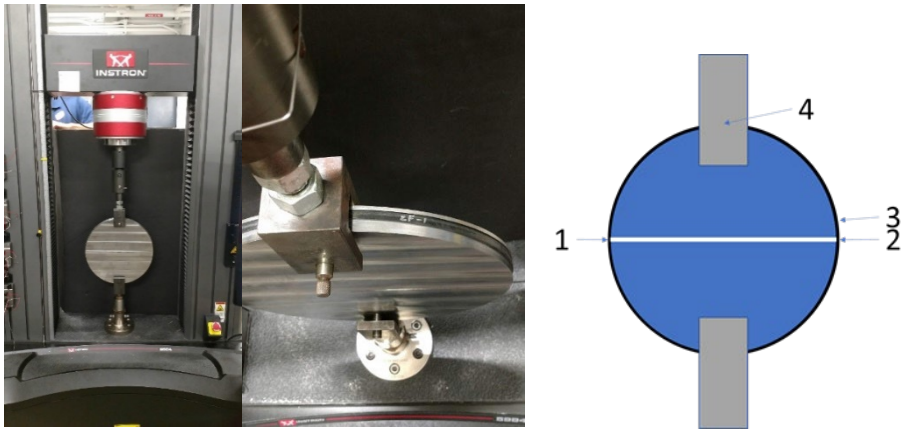


Figure 59. Test setup for ASTM D2290 Split Ring Tension test, including locations of strain gauges.

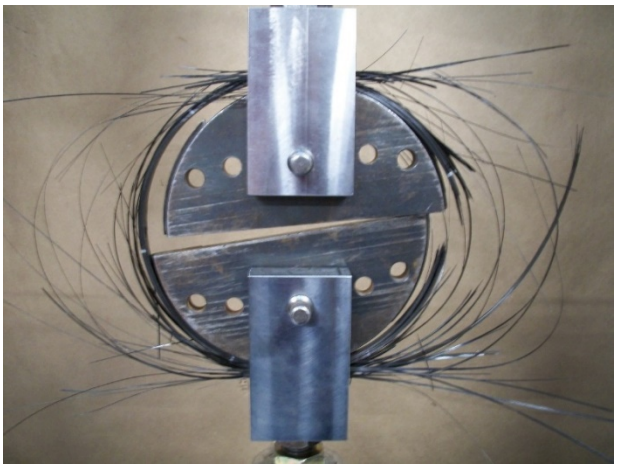

Figure 60. ASTM D2290 Split Ring Tension, with 5.75 inch ring after testing.

Table 21. Ring process condition matrix.

| Ring I.D. #'s | Roll I.D. # | Fiber | Matrix | Compaction Force (lbs.) | Processing Temperature (°C) | Lay-Down Speed (in./second) | Test Purpose |
|---|---|---|---|---|---|---|---|
| 201166-03-5 | 9B | GRAFIL34-700WD 12K 0,3%R | VZL36D | 150 | 300 | 3 | Split Ring Tension & Density |
| 201166-03-12 | 9C | GRAFIL34-700WD 12K 0,3%R | VZL36D | 150 | 300 | 3 | Split Ring Tension & Density |
| | | | | | | | |
| 201166-03-2 | 9B | GRAFIL34-700WD 12K 0,3%R | VZL36D | 150 | 300 | 12 | Split Ring Tension & Density |
| | | | | | | | |
| 201166-03-14 | 9C | GRAFIL34-700WD 12K 0,3%R | VZL36D | 150 | 330 | 3 | Split Ring Tension & Density |
| | | | | | | | |
| 201166-03-8 | 9B | GRAFIL34-700WD 12K 0,3%R | VZL36D | 150 | 330 | 12 | Split Ring Tension & Density |
| 201166-03-13 | 9C | GRAFIL34-700WD 12K 0,3%R | VZL36D | 150 | 330 | 12 | Split Ring Tension & Density |
| | | | | | | | |
| 201166-03-10 | 9C | GRAFIL34-700WD 12K 0,3%R | VZL36D | 200 | 300 | 3 | Split Ring Tension & Density |
| | | | | | | | |
| 201166-03-7 | 9A | GRAFIL34-700WD 12K 0,3%R | VZL36D | 200 | 330 | 3 | Microscopy & Physical Properties |
| 201166-03-11 | 9C | GRAFIL34-700WD 12K 0,3%R | VZL36D | 200 | 330 | 3 | Split Ring Tension & Density |
| | | | | | | | |
| 201166-03-3 | 9B | GRAFIL34-700WD 12K 0,3%R | VZL36D | 200 | 300 | 12 | Split Ring Tension & Density |
| | | | | | | | |
| 201166-03-4 | 9A | GRAFIL34-700WD 12K 0,3%R | VZL36D | 200 | 330 | 12 | Split Ring Tension & Density |
| 201166-03-15 | 9D | GRAFIL34-700WD 12K 0,3%R | VZL36D | 200 | 330 | 12 | Split Ring Tension & Density |
| | | | | | | | |
| 201166-03-1 | 9A | GRAFIL34-700WD 12K 0,3%R | VZL36D | 200 | 360 | 7.5 | Split Ring Tension & Density |
| | | | | | | | |
| 201166-04-5 | 10A | GRAFIL34-700WD 12K 0,3%R | VZL36D modified | 150 | 300 | 3 | Split Ring Tension & Density |
| 201166-04-12 | 10A | GRAFIL34-700WD 12K 0,3%R | VZL36D modified | 150 | 300 | 3 | Split Ring Tension & Density |
| | | | | | | | |
| 201166-04-2 | 10A | GRAFIL34-700WD 12K 0,3%R | VZL36D modified | 150 | 300 | 12 | Split Ring Tension & Density |
| | | | | | | | |
| 201166-04-11 | 10A | GRAFIL34-700WD 12K 0,3%R | VZL36D modified | 150 | 330 | 3 | Split Ring Tension & Density |
| 201166-04-14 | 10A | GRAFIL34-700WD 12K 0,3%R | VZL36D modified | 150 | 330 | 3 | Split Ring Tension & Density |
| | | | | | | | |
| 201166-04-8 | 10A | GRAFIL34-700WD 12K 0,3%R | VZL36D modified | 150 | 330 | 12 | Split Ring Tension & Density |
| 201166-04-13 | 10A | GRAFIL34-700WD 12K 0,3%R | VZL36D modified | 150 | 330 | 12 | Split Ring Tension & Density |
| | | | | | | | |
| 201166-04-10 | 10A | GRAFIL34-700WD 12K 0,3%R | VZL36D modified | 200 | 300 | 3 | Split Ring Tension & Density |
| | | | | | | | |
| 201166-04-3 | 10A | GRAFIL34-700WD 12K 0,3%R | VZL36D modified | 200 | 300 | 12 | Split Ring Tension & Density |
| | | | | | | | |
| 201166-04-7 | 10A | GRAFIL34-700WD 12K 0,3%R | VZL36D modified | 200 | 330 | 3 | Microscopy & Physical Properties |
| | | | | | | | |
| 201166-04-4 | 10A | GRAFIL34-700WD 12K 0,3%R | VZL36D modified | 200 | 330 | 12 | Split Ring Tension & Density |
| 201166-04-15 | 10A | GRAFIL34-700WD 12K 0,3%R | VZL36D modified | 200 | 330 | 12 | Split Ring Tension & Density |
| | | | | | | | |
| 201166-05-5 | 11A | GRAFIL34-700WD 12K 0,3%R | VZL36D modified | 150 | 390 | 3 | Split Ring Tension & Density |
| 201166-05-12 | 11A | GRAFIL34-700WD 12K 0,3%R | VZL36D modified | 150 | 390 | 3 | Split Ring Tension & Density |
| | | | | | | | |
| 201166-05-2 | 11A | GRAFIL34-700WD 12K 0,3%R | VZL36D modified | 150 | 390 | 12 | Split Ring Tension & Density |
| 201166-05-8 | 11A | GRAFIL34-700WD 12K 0,3%R | VZL36D modified | 150 | 390 | 12 | Split Ring Tension & Density |
| | | | | | | | |
| 201166-05-7 | 11A | GRAFIL34-700WD 12K 0,3%R | VZL36D modified | 200 | 330 | 3 | Split Ring Tension & Density |
| 201166-05-11 | 11A | GRAFIL34-700WD 12K 0,3%R | VZL36D modified | 200 | 330 | 3 | Split Ring Tension & Density |
| | | | | | | | |
| 201166-05-4 | 11A | GRAFIL34-700WD 12K 0,3%R | VZL36D modified | 200 | 330 | 12 | Split Ring Tension & Density |
| 201166-05-15 | 11A | GRAFIL34-700WD 12K 0,3%R | VZL36D modified | 200 | 330 | 12 | Split Ring Tension & Density |
| | | | | | | | |
| 201166-05-1 | 11A | GRAFIL34-700WD 12K 0,3%R | VZL36D modified | 200 | 360 | 7.5 | Microscopy & Physical Properties |
| 201166-05-6 | 11A | GRAFIL34-700WD 12K 0,3%R | VZL36D modified | 200 | 360 | 7.5 | Split Ring Tension & Density |
| 201166-05-9 | 11A | GRAFIL34-700WD 12K 0,3%R | VZL36D modified | 200 | 360 | 7.5 | Split Ring Tension & Density |
| | | | | | | | |
| 201166-05-10 | 11A | GRAFIL34-700WD 12K 0,3%R | VZL36D modified | 200 | 390 | 3 | Split Ring Tension & Density |
| 201166-05-14 | 11A | GRAFIL34-700WD 12K 0,3%R | VZL36D modified | 200 | 390 | 3 | Split Ring Tension & Density |
| | | | | | | | |
| 201166-05-3 | 11A | GRAFIL34-700WD 12K 0,3%R | VZL36D modified | 200 | 390 | 12 | Split Ring Tension & Density |
| 201166-05-13 | 11A | GRAFIL34-700WD 12K 0,3%R | VZL36D modified | 200 | 390 | 12 | Split Ring Tension & Density |

**12” Diameter Split Disk Tension Testing**

Ring test specimens were scaled up to be more representative of the actual CGS storage tank diameter. Thin-walled, 12” diameter specimens were wound on aluminum liner and shipped to UDRI.

Some of these sections arrived at UDRI as cylinders with no mandrel. Others arrived at UDRI still on the aluminum liner. In the latter case, the composite tank portion was removed from the aluminum liner and then subsequently machined into test coupons. Great care was taken to ensure that the composite was machined with water and a speed conducive to not damaging the fiber edges. The 12” diameter required machining a special test fixture as well, but the split ring nature of the test remained exactly the same.

When the tape tension was increased during fabrication, removing the composite from the liner proved very difficult. Liquid nitrogen was pumped into the hollow cavity in the liner in an attempt to get the composite portion to slide off. This was unsuccessful, and the UDRI machine shop had to cut each ring specimen, along with cutting through the aluminum liner, one at time, as shown in Figure 61.

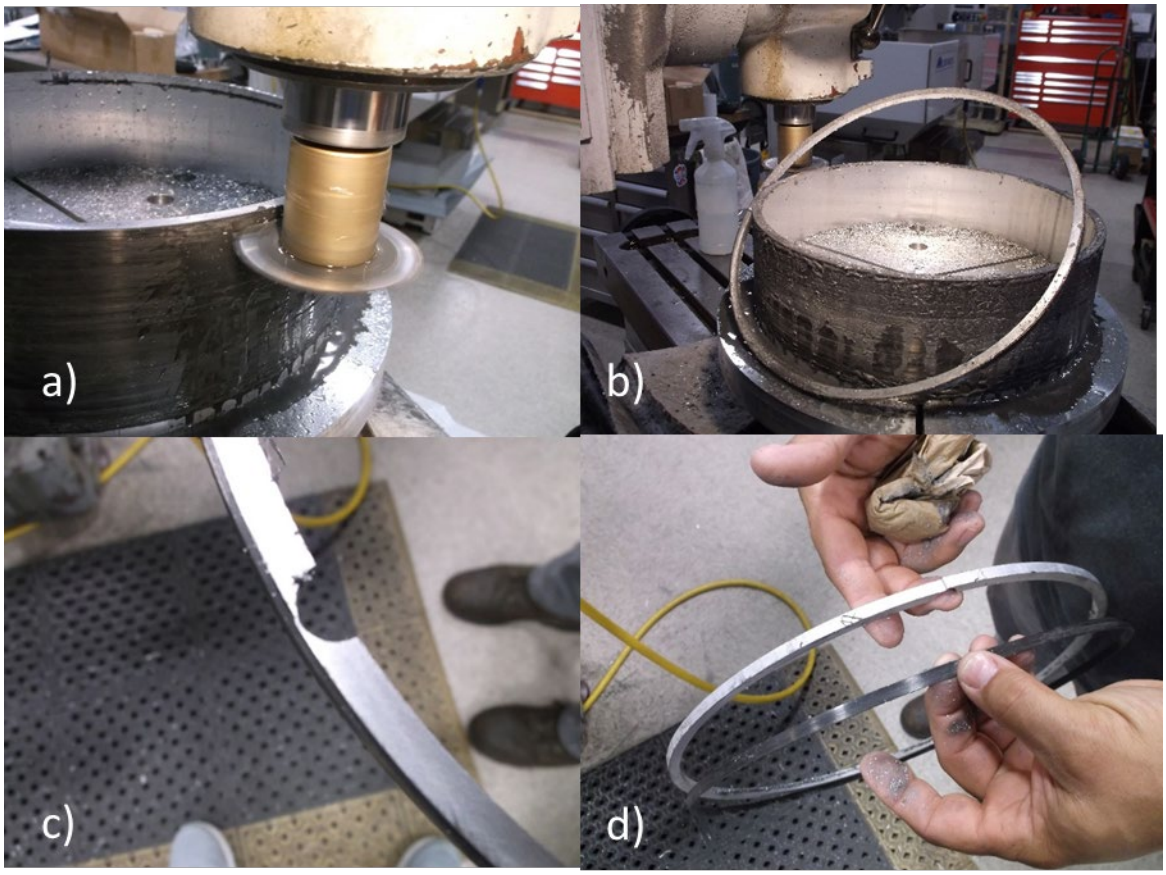


Figure 61. Removing aluminum liner wall to extract test specimen, including a) cutting cylinder and aluminum mandrel, c) drilling through aluminum substrate, and d) removing composite ring.

.

**ASTM D2344 Short Beam Shear Strength**

For each group of ring tension specimens, one of the rings was machined into short beam shear specimens and tested according to ASTM D2344, as shown in Figure 62. All specimens were dried at 90°C for 16 hours prior to testing at room temperature dry conditions. This test is a typical, quality control test to determine the strength of the fiber-resin interface and the layer to layer consolidation of the thermoplastic tape. All specimens were tested at .05”/minute on an Instron test frame.

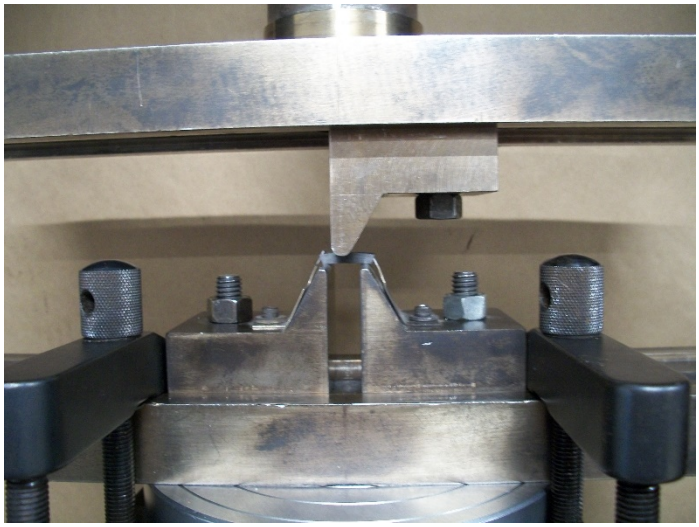

Figure 62. Short beam shear testing setup for curved specimens extracted from rings.

Ring I.D. = 201166-07-11
Support Span = .4976”
ASTM D2344 3 pt. Shear
Support Nose: 0.125 Dia.
Loading Nose: 0.250 Dia.
Material: Mitsubishi Rayon 34-700 12K Carbon Fiber/36D75L Resin

**ASTM D3171 Physical properties ASTM D3171-15 Standard Test Method for Constituent Content of Composite Materials Procedure B – Matrix Digestion using Sulfuric Acid and Hydrogen Peroxide**

For each group of ring tension specimens, one of the rings was machined into physical property specimens and tested according to ASTM D3171. Fiber, resin, and void content was determined. Specific gravity and density of the composite were also reported. The fiber density used was 1.8 g/cm$^3$, and the resin density used was 1.14 g/cm$^3$. Specimens were thoroughly dried prior to testing via Procedure B (acid digestion). Hydrogen peroxide and sulfuric acid are used to digest away the resin. After rinsing and drying, the remaining fiber is weighed and the physical properties of the composite was reported. The slightly negative value of void content is fairly common for low void content composites. Per ASTM D3171: “Calculation of the void volume assumes that reinforcement density and matrix density

obtained on a lot or material basis are held in the laminate sample. There is a normal variation in reinforcement and matrix densities that is dependent on the constituent material. This assumption used by the void calculation equations is typically minor, changing the void calculation by less than 0.2 %. One indication of this variation is the possibility of obtaining a negative void volume in low-void volume composites. If procedural errors can be ruled out, it is reasonable to believe that constituent density variation is responsible. Negative void content is a physical impossibility, but a possibility in these calculations. It is useful to report negative void contents to assess if constituent density values are incorrect or within a typical range of material variation. The negative void value then sets an upper bound on error of this test method for any material."